

HOMOGENEOUS FLOW CATALYSIS STRATEGIES FOR LAB-SCALE KINETIC  
INVESTIGATION AND REACTION DEVELOPMENT

BY

NICHOLAS MASON WANG

DISSERTATION

Submitted in partial fulfillment of the requirements  
for the degree of Doctor of Philosophy in Chemical Engineering  
in the Graduate College of the  
University of Illinois Urbana-Champaign, 2022

Urbana, Illinois

Doctoral Committee:

Professor Damien S. Guironnet, Chair  
Professor Baron G. Peters  
Professor Steven C. Zimmerman  
Professor Xiao Su

## ABSTRACT

Predicated on vapor-liquid separations, we have developed methodologies to effectively immobilize homogeneous organometallic catalysts within a continuous reactor. Compared to the traditional investigation of these catalysts in a batch system, our advanced analysis under steady-state flow provides chemical insight that is not, otherwise, easily accessible. In this dissertation, we detail the design and implementation of these flow methodologies; and overall, the accumulation of our efforts demonstrates the benefit of coupling engineering and chemistry fundamentals toward the development of meaningful catalytic reactions.

Chapter 1 contains a brief introduction to catalysis in addition to a mini-review of separation technologies used for the continuous processing of homogeneous catalysts. In Chapter 2, we introduce the catalytic ethanol coupling reaction (the Guerbet reaction), and we provide a detailed mechanistic investigation of a homogeneous ruthenium catalyst within a continuously stirred tank reactor. In a second project described in Chapter 3, we develop supported liquid phase catalysts to effectively immobilize two organometallic complexes for study in a packed bed reactor. We begin Chapter 4 with a summary of current polyolefin depolymerization strategies prior to introducing a new chemical depolymerization technique. By implementing tandem catalytic reactions (dehydrogenation, isomerization, and metathesis) we seek to selectively convert polyethylene to monomer (propylene and butene). Chapter 5 contains an extension of our depolymerization efforts to several promising heterogeneous catalysts.

## ACKNOWLEDGMENTS

Graduate school has been full of surprises. I've worked hard, and I've learned a lot (as they say you will). But I have also had a lot more fun than I expected, and I owe my happiness these past several years to my mentors, peers, friends, and family.

First, I would like to thank my advisor, Damien Guironnet. You have always gone above and beyond as my mentor, and I can only appreciate your investment in my growth as an individual and a professional. I know you have high expectations, and I hope to make you proud in my future endeavors. Next, I would like to thank my lab group (those graduated and those current). You all have been one of the brighter parts of my life here, and I will miss seeing you all daily. I am happy to have shared our time, our frustration and failure, and our excitement and success. Your ambitions have been contagious, and I am looking forward to all that you will accomplish. Aside from professional relationships, I also nurtured many lasting friendships during this time (old and new). You all have been the best. You've taught me to be brave and proud. You've shown me how to dance. You've convinced me to change my perspective, and you've pushed me to be more than I thought I could be. To the friends I have made at UIUC, I know we will keep in touch, but I miss you already.

Lastly, I would like to thank my family. To my mum, Otricia, and dad, Joe, you all have never given me any less than 100% of your support, and you have walked every step with me in this lifetime. I love you both, and it is an understatement when I say – I wouldn't be here without you. To my brother, Christopher, I love you dearly, and we should talk more. To my partner Hanna – the love of my life – I hope you will forgive me for the long workdays and the occasional short temper. Even though we will miss many of these individuals, I am looking forward to life after UIUC, and I am excited to continue onwards towards new adventures.

## TABLE OF CONTENTS

<b>Chapter 1: Introduction and Literature Review of Physical Separation Methods for Homogeneous Flow Catalysis</b> .....	1
1.1 Introduction.....	1
1.2 Homogeneous vs Heterogeneous Catalysts .....	1
1.3 Physical Separation Methods for the Application of Homogeneous Catalysts.....	3
1.4 Conclusions and Dissertation Summary .....	8
1.5 References.....	9
<b>Chapter 2: Liquid Immobilized Guerbet Catalyst in a Tank Reactor for Mechanistic Investigation</b> .....	14
2.1 Introduction to the Guerbet Reaction.....	14
2.2 Results and Discussion .....	18
2.3 Summary and Conclusions.....	29
2.4 References.....	30
<b>Chapter 3: Study and Immobilization of Homogeneous Catalysts in a Packed Bed Reactor</b> .....	35
3.1 Introduction.....	35
3.2 Experimental Procedure(s) and Setup .....	37
3.3 Results and Discussion .....	39
3.4 Summary and Conclusions.....	49
3.5 References.....	50
<b>Chapter 4: Tandem Homogeneous Flow Catalysis for Selective Polyethylene Depolymerization</b> .....	54
4.1 Introduction.....	54
4.2 Overview of Polyethylene Recycling Strategies.....	55
4.3 Tandem Catalysts in Flow for Polyethylene Upcycling .....	58
4.4 Reactor Build, Methods, and Calculations.....	59
4.5 Results and Discussion .....	62
4.6 Conclusions and Recommendations .....	78
4.7 References.....	79
<b>Chapter 5: Tandem Heterogeneous Catalysts for Selective Polyethylene Depolymerization</b> .....	85
5.1 Introduction.....	85
5.2 $\text{MoO}_x\text{-SiO}_2$ (Mo-Si) for Polyethylene Depolymerization. ....	85
5.3 $\text{MoO}_x\text{-Al}_2\text{O}_3$ (Mo-Al) for Polyethylene Depolymerization. ....	87
5.4 $\text{ReO}_x\text{-Al}_2\text{O}_3$ (Re-Al) for Polyethylene Depolymerization. ....	92
5.5 Summary of Catalyst Performance for Polyethylene Depolymerization in Continuous Flow. ....	94
5.6 Conclusions and Outlook.....	95

5.7 References.....	96
<b>Appendix A:</b> Liquid Immobilized Guerbet Catalyst in a Tank Reactor for Mechanistic Investigation ....	98
<b>Appendix B:</b> Study and Immobilization of Homogeneous Catalysts in a Packed Bed Reactor .....	115
<b>Appendix C:</b> Tandem Homogeneous Flow Catalysis for Selective Polyethylene Depolymerization .....	126
<b>Appendix D:</b> Tandem Heterogeneous Catalysts for Selective Polyethylene Depolymerization .....	133

## **CHAPTER 1: Introduction and Literature Review of Physical Separation Methods for Homogeneous Flow Catalysis**

### **1.1 Introduction**

The overarching theme of this dissertation is the use of continuous reactor systems for the study and development of homogeneously catalyzed reactions. Conventionally, homogeneous catalysts are studied in closed batch vessels. But this mode of operation makes a detailed investigation of kinetics and mechanisms quite tedious, especially when considering multi-phase reaction components under elevated temperatures or pressures. As an alternative to a classical batch setup, a flow reactor offers several advantages including facile and precise control over the reaction residence time, superior mixing and temperature regulation, and improved chemical processing safety.<sup>1,2</sup> Inspired by industrial applications of homogeneous catalysts, we have developed methodologies for the immobilization of organometallics within continuous reactors. By demonstrating the benefit of coupling engineering and chemistry fundamentals, we aim to encourage the adoption of advanced strategies for the investigation of homogeneous catalysts. Prior to an in-depth discussion of our work, a general introduction to catalysis and a brief review of flow technologies will be covered.

### **1.2 Homogeneous vs Heterogeneous Catalysts**

A catalyst is any substance that increases the rate of a chemical reaction without itself being consumed, and these materials can be broadly classified into three major groups: heterogeneous, homogeneous, and enzymatic. Heterogeneous catalysts perform reactions at or near an interface between phases. In contrast to heterogeneous catalysts, the homogeneous counterparts perform reactions within a single phase.<sup>3,4</sup> Biocatalysts (enzymes) are naturally occurring substances which drive biological reactions. Enzymes can be either homogenous or heterogeneous in nature where

they oftentimes consist of an active metal center ligated by proteins. They are known to exhibit high activity and selectivity but can be rapidly deactivated under non-physiological reaction conditions.<sup>1</sup>

In comparison to heterogeneous systems, homogeneous catalysts offer a few exclusive advantages. First, the dispersion of molecules within a single-phase allows for (1) relatively high catalytic activity and (2) kinetic control over reactions since diffusion of substrate to the catalyst occurs rapidly without interference from a phase boundary. Second, homogeneous catalysts also have well-defined reaction sites in comparison to heterogeneous catalysts, which require careful characterization of many surface-active species. Lastly, the active site of a homogeneous catalyst can be designed with molecular precision, providing a scaffold to precisely tune chemical reactivity and selectivity.<sup>5-7</sup> Overall, these advantages simplify the mechanistic investigation of a homogeneous catalyst.

Despite these benefits, homogeneous catalysts have found limited applications within the industry, accounting for only 10-15% of the catalyst market share.<sup>8,9</sup> One of the key contributing factors to their lack of industrial use lies in the difficult recovery of these precious materials after the chemical reaction.<sup>5,10</sup> In response to this challenge, academics have extensively studied the immobilization of homogeneous catalysts onto a solid support since this technique allows for ease of product separation and reuse of the material. However, this strategy requires complex synthetic modification of the catalyst, which usually reduces activity and selectivity. Thus, these developments have been insufficient for industrial application.<sup>11</sup> Instead, current commercial strategies for homogeneous catalyst recovery are based upon physical separations (vapor-liquid or liquid-liquid separations) that do not require chemical alterations to the catalyst. Alternatively, if the activity of the catalyst is sufficiently high no recovery processes are employed.<sup>12</sup> In the context

of our developments, these physical separation methods served as our inspiration for the investigation of organometallics under continuous flow. To provide additional background, we include a non-comprehensive review of these strategies. Key examples of pertinent technology are discussed in detail.

### **1.3 Physical Separation Methods for the Application of Homogeneous Catalysts**

*Liquid – Liquid Separation.* Liquid-liquid separation is a method to separate products and catalysts based upon their relative solubility in two immiscible liquids, generally water and an organic solvent. A selection of examples will be used to showcase the implementation of this strategy on a commercial and academic scale.

Hydroformylation, also known as the oxo synthesis, is an olefin and carbon monoxide coupling reaction that produces aldehydes in the presence of hydrogen. The process was discovered in 1938 by Ruhrchemie.<sup>13</sup> The most common olefin starting material is propene which is converted to butyraldehyde. The aldehyde product is mostly used as a raw material for plasticizers and detergents. Industrially, the reaction is catalyzed by either cobalt or rhodium catalysts at elevated temperatures (140-200°C) and pressures (50-300 bar).<sup>14</sup> To alleviate the cost of the catalyst, “two-phase technology” was developed to recover the expensive catalytic material. Commercialized in the Ruhrchemie/Rhône-Poulenc process, a water-soluble rhodium complex with polar SO<sub>3</sub>Na groups on the phosphine ligands was employed.<sup>15</sup> In this design, aldehyde products accumulate forming an organic phase, which is separated from the aqueous layer containing the catalyst (**Figure 1.1**). This method effectively retains the homogeneous catalyst within the setup during a continuous reaction.





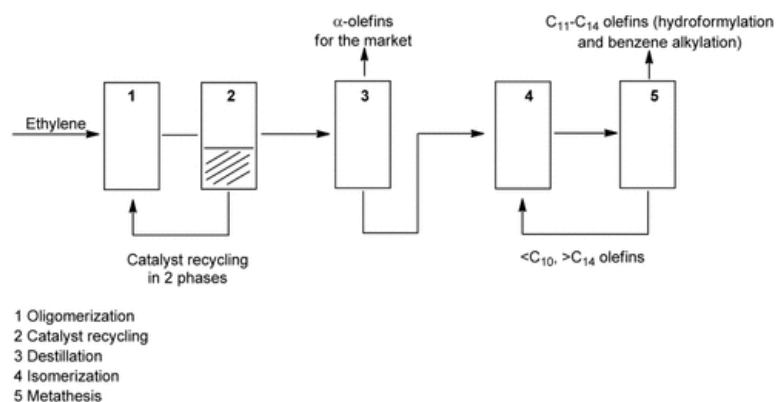


**Figure 1.2.** Simplified Schematic of The Shell Higher Olefin Process for  $\alpha$ -olefin Production (Source: Keim, 2013).<sup>16</sup>

In addition to aqueous and organic solvents, many non-traditional solvents have been used for liquid-liquid catalyst separations. Some unique examples include the use of fluoruous compounds, supercritical fluids (compressed gasses above their critical temperature, SCF), and ionic liquids. These alternative solvents have not yet found wide-spread applicability on an industrial scale.

Catalysts are made soluble in fluoruous solvents by attaching fluorinated ligands. The fluoruous bi-phasic mixture has the advantage of temperature dependent phase behaviour where the fluoruous solvent mixes with organic compounds only under elevated temperatures (catalytic conditions) but separates at room temperature, allowing for decantation of the desired product.<sup>18</sup> Thus far, fluoruous solvents have been successfully employed for a number of homogeneous reactions in literature including hydroformylation, Suzuki-Miyaura reactions, and etc.<sup>10,19</sup>

Pioneering work for homogeneous catalysis in SCFs began in the early 1900s by Ipatiev; however, until the mid-1990s little research in the field was reported.<sup>20</sup> Today, many homogeneously catalysed reactions have been studied in SCFs such as carbon dioxide, water, ethylene, and etc.<sup>21</sup> In these high-pressure systems, SCFs are used to dissolve homogeneous catalysts for reaction. Afterwards, the solvent (SCF) can be easily removed by decompression to a gas; however, the remaining product-catalyst solution, oftentimes, remains in the same phase.<sup>10,19</sup>

The first reports of ionic liquids being used as a fluid reaction medium appeared in 1986 for Friedel-Crafts acylation, and its application as a solvent has since been extended to numerous catalytic reactions (e.g. carbonylation, hydroformylation, etc).<sup>22</sup> These liquid salts have extremely low vapor pressures and remain condensed at elevated temperatures. The numerous combinations of cation and anion create a wide range of physical and chemical solvent characteristics, which offer a route to control solvent-solute interactions. In the context of catalysis, polar catalysts are often solvated within the ionic medium. The poor solubility of organic molecules into the ionic-liquid phase allows for simple decanting to separate chemical products from the catalyst.<sup>10,19</sup>

*Vapor – Liquid Separation.* Another industrially relevant strategy is vapor-liquid separation. By extracting volatile products from a non-volatile reaction mixture, one can separate and recover high value catalytic material from a liquid reaction stream.

One specific example of this strategy is the carbonylation of methanol to acetic acid. Discovered by Monsanto in 1966, a rhodium in combination with an iodide co-catalyst was shown to be highly selective for methanol production (<99%) under relatively mild conditions (30-60 bar pressure and 150-200°C).<sup>23</sup> In 1996 the introduction of the “Cativa” technology by BP Chemicals incorporated the use of iridium (promoted by iodine) rather than rhodium as a catalyst for methanol carbonylation where increased catalyst stability and reactivity provided a significant reduction in production costs.<sup>24–26</sup> In both of these designs, the catalyst material is recovered in the flowing bottoms fraction for recirculation, while the volatile product is continuously removed via distillation (**Figure 1.3**).

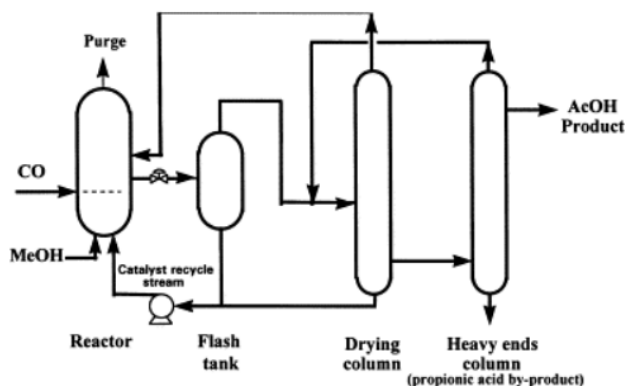


**Figure 1.3.** Simplified Schematic of Monsanto/Cativa Process for Acetic Acid Production (Source: Reuben, 1988).<sup>13</sup>

Another notable development is the Wacker process for acetaldehyde production from ethylene which was first developed in 1959 by researchers at the Wacker Consortium for Industrial Electrochemistry in Munich. In a two-step process, gaseous reagents, ethylene and oxygen, are bubbled into an aqueous  $\text{PdCl}_2$  catalyst solution held at 10 bar and 100-110°C.<sup>27</sup> The resulting product mixture is flashed to isolate the product, and the remaining catalyst solution is regenerated with air prior to recycle (Figure 1.4). In contrast to the Monsanto/Cativa processes, the Wacker system suffered from poor selectivity (significant by-product formation in the presence of water). Therefore, an extraction combined with distillation (reactive distillation) was employed to purify the product while retaining the catalyst in the reactor under continuous conditions.<sup>28</sup>

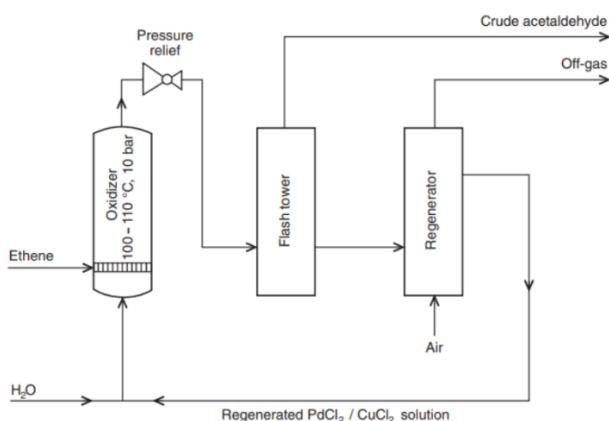


**Figure 1.4.** Schematic of Wacker process for Acetaldehyde Production (Source: Hagen, 2006).<sup>14</sup>

*Alternative Strategies.* Although not industrially relevant, a homogeneous catalyst can also be immobilized for flow applications in a supported liquid phase. The origin for this technology dates

back to 1939 in pioneering work by Acres et al. and Rony.<sup>29,30</sup> In this system, a homogeneous catalyst is solvated in a thin film of liquid which is adsorbed into the pores of a porous inorganic support to afford a supported liquid phase catalyst (SLPC). The simple implementation of physisorption makes this technique much easier to prepare compared to immobilization via chemical bonding. Furthermore, since the molecular structure of the catalyst remains intact so does the catalyst's reactivity. Under continuous flow, the products diffuse out of the stationary phase into the continuous stream while the catalyst remains immobilized. Similar to a conventional heterogeneous catalyst, a SLPC can be used in a plug flow reactor with either liquid or gaseous feeds. Since the technique's inception a variety of solvents have been employed in the synthesis of SLPCs including water, organics, polymers, and ionic liquids. These catalysts have also been used for a variety of reactions such as the Heck reaction, hydroformylation, gas-shift reaction, hydrosilylation, and hydrogenation.<sup>31–38</sup>

## **1.4 Conclusions and Dissertation Summary**

*Application of Flow Strategies for Kinetic and Mechanistic Investigations.* The examples discussed, thus far, have shown the successful immobilization of homogeneous catalysts under continuous flow through the thoughtful engineering of multi-phase reaction systems, and it is this engineering spirit that served as the foundation of our work. Aside from scalability, these strategies can also be used for fundamental investigations. By extending these developments to lab-scale flow devices, one creates an opportunity for transient and steady-state analysis of a homogeneous catalyst's kinetics – unique data that is not easily accessed in a traditional non-continuous setup. In this work, we apply these innovative techniques to enrich our molecular understanding of meaningful catalytic reactions.

*Dissertation Summary.* The remainder of this dissertation will describe the implementation of advanced reactor systems for the study of homogeneous (and some heterogeneous) catalysts under continuous conditions. In Chapter 2, we introduce the catalytic ethanol coupling reaction (the Guerbet reaction), and we provide a detailed mechanistic investigation of a homogeneous ruthenium catalyst within a continuously stirred tank reactor (CSTR). In a second project described in Chapter 3, we develop supported liquid phase catalysts (SLPC) to effectively immobilize two organometallic complexes for study in a packed bed reactor (PBR). In Chapter 4, we explore a tandem catalytic reaction cascade (dehydrogenation, isomerization, and metathesis) for the selective depolymerization of commodity polyethylene to monomer (propylene and butadiene). We begin this chapter with a summary of current polyolefin depolymerization strategies to introduce our novel approach. Afterwards, we report on our systematic investigation of two homogeneous catalysts. Chapter 5 contains an extension of our depolymerization efforts to various promising heterogeneous catalysts.

## 1.5 References

- (1) Wiles, C.; Watts, P. Continuous Flow Reactors: A Perspective. *Green Chem.* **2012**, *14* (1), 38–54.
- (2) Baxendale, I. R. The Integration of Flow Reactors into Synthetic Organic Chemistry. *J. Chem. Technol. Biotechnol.* **2013**, *88* (4), 519–552.
- (3) Laidler, K. J. *The IUPAC Compendium of Chemical Terminology*; Gold, V., Ed.; International Union of Pure and Applied Chemistry (IUPAC): Research Triangle Park, NC, 2019.
- (4) Bertini, I. *Inorganic and Bio-Inorganic Chemistry*, Vol. 2.; EOLSS Publishers Company Limited, 2009.

- (5) Keim, W. Nickel: An Element with Wide Application in Industrial Homogeneous Catalysis. *Angew. Chemie Int. Ed. English* **1990**, 29 (3), 235–244.
- (6) Cornils, B.; Herrmann, W. A. Concepts in Homogeneous Catalysis: The Industrial View. *J. Catal.* **2003**, 216 (1–2), 23–31.
- (7) Cornils, B.; Herrmann, W. A. (Wolfgang A. .; Beller, M.; Paciello, R. *Applied Homogeneous Catalysis with Organometallic Compounds*; Cornils, B., Herrmann, W. A., Beller, M., Paciello, R., Eds.; Wiley, 2017.
- (8) Sun, Y.-P. *Supercritical Fluid Technology in Materials Science and Engineering*; Taylor & Francis, 2006.
- (9) Bravo-Suárez, J. J.; Chaudhari, R. V.; Subramaniam, B. Design of Heterogeneous Catalysts for Fuels and Chemicals Processing: An Overview. *ACS Symp. Ser.* **2013**, 1132, 3–68.
- (10) Cole-Hamilton, D. J. Homogeneous Catalysis - New Approaches to Catalyst Separation, Recovery, and Recycling. *Science* (80-. ). **2003**, 299 (5613), 1702–1706.
- (11) Hübner, S.; de Vries, J. G.; Farina, V. Why Does Industry Not Use Immobilized Transition Metal Complexes as Catalysts? *Adv. Synth. Catal.* **2016**, 358 (1), 3–25.
- (12) Falbe, J.; Bahrmann, H. Homogeneous Catalysis-Industrial Applications. *J. Chem. Educ.* **1984**, 61 (11), 961.
- (13) Beller, M.; Cornils, B.; Frohning, C. D.; Kohlpaintner, C. W. Progress in Hydroformylation and Carbonylation. *J. Mol. Catal. A. Chem.* **1995**, 104 (1), 17–85.
- (14) Hagen, J. *Industrial Catalysis: A Practical Approach: Second Edition*; Wiley-VCH Verlag GmbH & Co. KGaA, 2006.
- (15) Bach, H.; Bahrmann, H.; Gick, W.; Konkol, W.; Wiebus, E. Wissenschaftliche

- Forschungsarbeit. *Angew. Chemie Int. Ed.* **6**(11), 951–952. **1967**, 59 (11), 883–884.
- (16) Keim, W. Oligomerization of Ethylene to  $\alpha$ -Olefins: Discovery and Development of the Shell Higher Olefin Process (SHOP). *Angew. Chemie - Int. Ed.* **2013**, 52 (48), 12492–12496.
- (17) Reuben, B.; Wittcoff, H. Real World of Industrial Chemistry - The SHOP Process: An Example of Industrial Creativity. *J. Chem. Educ.* **1988**, 65 (7), 605–607.
- (18) Nakamura, H.; Usui, T.; Kuroda, H.; Ryu, I.; Matsubara, H.; Yasuda, S.; Curran, D. P. Fluorous Solvent as a New Phase-Screen Medium between Reagents and Reactants in the Bromination and Chlorination of Alcohols. *Org. Lett.* **2003**, 5 (8), 1167–1169.
- (19) Vural Gürsel, I.; Noël, T.; Wang, Q.; Hessel, V. Separation/Recycling Methods for Homogeneous Transition Metal Catalysts in Continuous Flow. *Green Chem.* **2015**, 17 (4), 2012–2026.
- (20) Erkey, C. Homogeneous Catalysis in Supercritical Fluids. *Supercrit. Fluid Sci. Technol.* **2011**, 1 (1 E), 161–209.
- (21) Jessop, P. G. Homogeneous Catalysis Using Supercritical Fluids: Recent Trends and Systems Studied. *J. Supercrit. Fluids* **2006**, 38 (2), 211–231.
- (22) Pârvulescu, V. I.; Hardacre, C. Catalysis in Ionic Liquids. *Chem. Rev.* **2007**, 107 (6), 2615–2665.
- (23) Paulik, F. E.; Roth, J. F. Novel Catalysts for the Low-Pressure Carbonylation of Methanol to Acetic Acid. *Chem. Commun.* **1968**, 11 (24), 2427.
- (24) Sunley, G. J.; Watson, D. J. High Productivity Methanol Carbonylation Catalysis Using Iridium. The Cativa™ Process for the Manufacture of Acetic Acid. *Catal. Today* **2000**, 58 (4), 293–307.



- (25) Thomas, C. M.; Süß-Fink, G. Ligand Effects in the Rhodium-Catalyzed Carbonylation of Methanol. *Coord. Chem. Rev.* **2003**, *243* (2003), 125–142.
- (26) Zoeller, J. R. Eastman Chemical Company's "Chemicals from Coal" Program: The First Quarter Century. *Catal. Today* **2009**, *140*, 118–126.
- (27) Parkins, A. W. Recent Developments in Platinum Group Metal Catalysts in the Petrochemical Industry. In *Studies in Inorganic Chemistry*; Elsevier B.V., 1991; Vol. 11, pp 106–123.
- (28) Budiman, A. W.; Nam, J. S.; Park, J. H.; Mukti, R. I.; Chang, T. S.; Bae, J. W.; Choi, M. J. Review of Acetic Acid Synthesis from Various Feedstocks Through Different Catalytic Processes. *Catal. Surv. from Asia* **2016**, *20* (3), 173–193.
- (29) Rony, P. R. Supported Liquid-Phase Catalysts. *Chem. Eng. Sci.* **1968**, *23* (9), 1021–1034.
- (30) Acres, G. J. K.; Bond, G. C.; Cooper, B. J.; Dawson, J. A. The Use of Supported Solutions of Rhodium Trichloride for Homogeneous Catalysis. *J. Catal.* **1966**, *6* (1), 139–141.
- (31) Zhao, F.; Fujita, S.; Arai, M. Developments and Applications of Supported Liquid Phase Catalysts. *Curr. Org. Chem.* **2006**, *10* (13), 1681–1695.
- (32) Riisager, A.; Fehrmann, R.; Haumann, M.; Wasserscheid, P. Supported Ionic Liquid Phase (SILP) Catalysis: An Innovative Concept for Homogeneous Catalysis in Continuous Fixed-Bed Reactors. *Eur. J. Inorg. Chem.* **2006**, *2006* (4), 695–706.
- (33) Mehnert, C. P.; Cook, R. A.; Dispenziere, N. C.; Afeworki, M. Supported Ionic Liquid Catalysis - A New Concept for Homogeneous Hydroformylation Catalysis. *J. Am. Chem. Soc.* **2002**, *124* (44), 12932–12933.
- (34) Letisha, N.; Friedrich, H. B.; Alisa, G.; Pheladi, M. The Effect of Ionic Liquid on Alumina Supported Copper Catalysts for the Competitive Hydrogenation of Octanal in the Presence

- of Octene. *Appl. Catal. A Gen.* **2018**, 562 (November 2017), 37–48.
- (35) Zhang, M.; Ettelaie, R.; Yan, T.; Zhang, S.; Cheng, F.; Binks, B. P.; Yang, H. Ionic Liquid Droplet Microreactor for Catalysis Reactions Not at Equilibrium. *J. Am. Chem. Soc.* **2017**, 139 (48), 17387–17396.
- (36) Peng, J.; Li, J.; Bai, Y.; Qiu, H.; Jiang, K.; Jiang, J.; Lai, G. Ionic Liquid (Molten Salt): Thermoregulated Catalyst Support for Catalytic Hydrosilylation Process. *Catal. Commun.* **2008**, 9 (13), 2236–2238.
- (37) Kukawka, R.; Pawlowska-Zygarowicz, A.; Dzialkowska, J.; Pietrowski, M.; Maciejewski, H.; Bica, K.; Smiglak, M. Highly Effective Supported Ionic Liquid-Phase (SILP) Catalysts: Characterization and Application to the Hydrosilylation Reaction. *ACS Sustain. Chem. Eng.* **2019**, 7 (5), 4699–4706.
- (38) Brünig, J.; Csendes, Z.; Weber, S.; Gorgas, N.; Bittner, R. W.; Limbeck, A.; Bica, K.; Hoffmann, H.; Kirchner, K. Chemoselective Supported Ionic-Liquid-Phase (SILP) Aldehyde Hydrogenation Catalyzed by an Fe(II) PNP Pincer Complex. *ACS Catal.* **2018**, 8 (2), 1048–1051.

## **Chapter 2: Liquid Immobilized Guerbet Catalyst in a Tank Reactor for Mechanistic Investigation**

### **2.1 Introduction to the Guerbet Reaction**

Interest in alternative energy solutions within the transportation sector is motivated by the limited supply of fossil fuels, and one approach to mitigate the use of non-renewables has been the adoption of bio-based fuel additives, such as bio ethanol. Despite successful adoption and implementation of bio-ethanol fuel, several inherent properties limit its broader application including low energy density, water absorption, and high corrosivity.<sup>1</sup> These limitations can be resolved by the implementation of higher alcohols with superior fuel characteristics, such as butanol.<sup>2,3</sup> Because the properties of butanol are quite similar to that of gasoline, the molecule has received considerable attention in recent decades as a potential petroleum replacement, but the production of bio-butanol has remained a technical challenge.

Large-scale synthesis of butanol from bio-feedstocks is performed predominantly via ABE (acetone, butanol, and ethanol) fermentation; however, the process suffers from low yields and poor selectivity.<sup>4</sup> One potential alternative to fermentation processes is the catalytic self-condensation of ethanol also known as the Guerbet reaction.<sup>1,5-7</sup> This chemistry offers an attractive synthetic route to convert the widely available bio-ethanol into advanced biofuels, such as bio-butanol. But the selective conversion of ethanol to butanol has not been trivial since the starting material and product have the same chemical functionality; thus, butanol and other higher alcohols are also susceptible to condensation. To ensure that butanol remains the sole product of the coupling reaction, a highly selective Guerbet catalyst must be employed. The need for precise control over the molecular weight

\*Portions of this chapter are adapted from: (1) Wang, N. M.; Dillon, S.; Guironnet, D. Mechanistic Investigations on a Homogeneous Ruthenium Guerbet Catalyst in a Flow Reactor. *React. Chem. Eng.* 2022. DOI: 10.1039/d1re00551k

distribution opens an opportunity for the application of homogeneous catalysts which are known for their well-defined structures and tunable selectivity.<sup>8–10</sup>

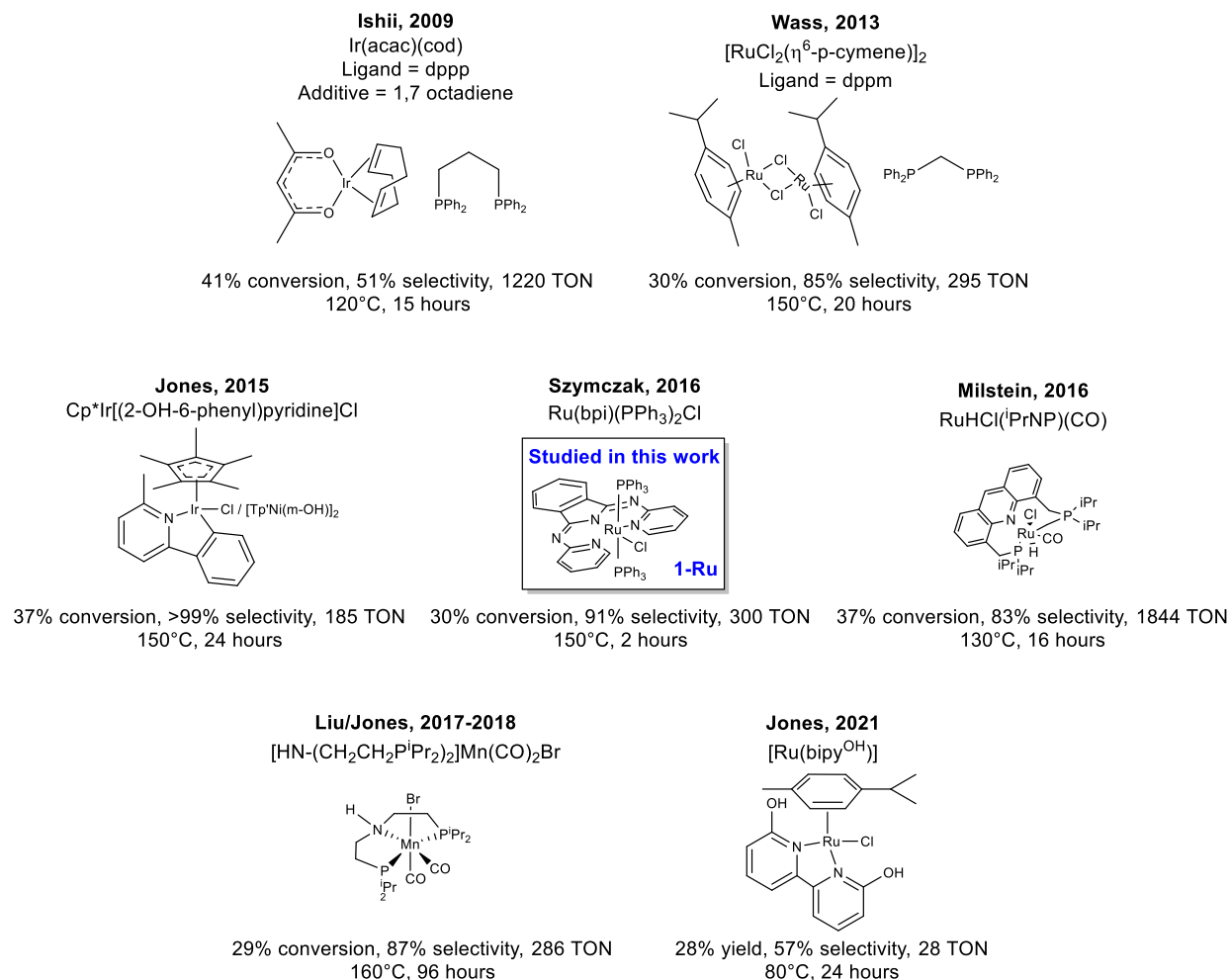
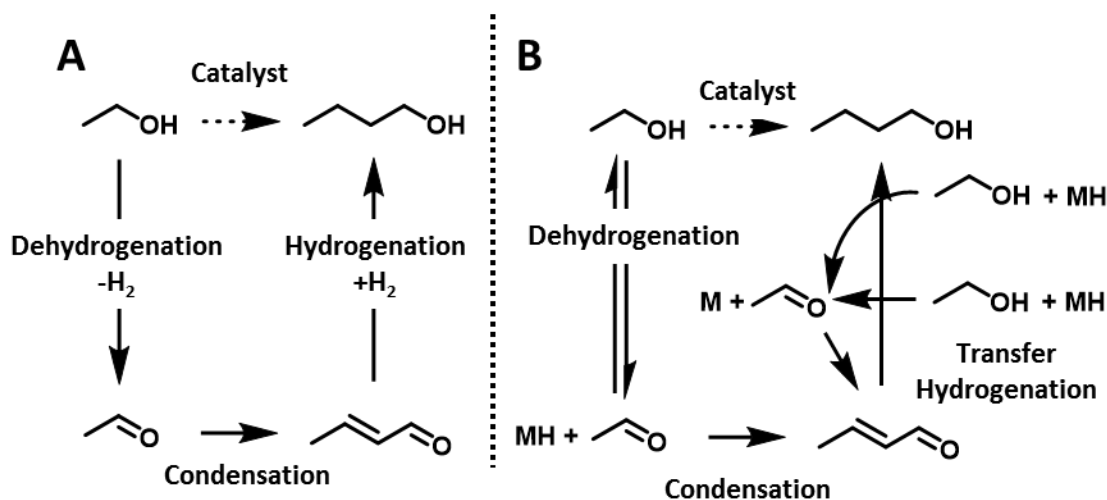


**Figure 2.1.** Summary of recent developments in homogeneous Guerbet catalysis.

In recent years, a series of homogeneous organometallic catalysts have been reported to convert ethanol to 1-butanol with some selectivity (**Figure 2.1**).<sup>11–19</sup> However, the fundamentals of this selectivity are not yet fully understood, and this gap in knowledge motivated us to investigate the reaction mechanism of one of the most selective homogeneous catalysts (**1-Ru, Figure 2.1**).<sup>14</sup> The Guerbet mechanism is commonly accepted to proceed through three key steps: dehydrogenation of an alcohol to an aldehyde; aldol condensation of the unsaturated intermediate; and hydrogenation of the aldol product to higher alcohol (**Scheme 2.1A**). Notably, previous work

showed that bis(pyridylimino)-isoindolate Ru(II) complexes, such as **1-Ru**, can reversibly hydrogenate acetophenone using molecular hydrogen or isopropyl alcohol as a hydrogen substitute.<sup>20,21</sup> However, the mechanism of **1-Ru** has not been investigated for the Guerbet reaction, and the precise pathway for the (de)hydrogenation reaction remains unclear. To better understand the mechanism of **1-Ru** for the Guerbet reaction, we independently investigated key reaction steps. To that end, we constructed a flow reactor setup that allowed us to analyze the catalyst's activity under quasi-steady-state conditions without altering its chemical structure. Ethanol conversion to butanol was monitored for hours on stream where stable activity, up to 10 hours, was achieved. After establishing that the catalysis is not mass transfer limited, a detailed study on the reaction mechanism was performed. First, we established that this catalyst does not present any selectivity for 1-butanol formation under our reaction conditions by comparing our catalytic results to those of a random step-growth model. Second, we determined that **1-Ru** predominantly operates through a transfer hydrogenation pathway and that  $\beta$ -hydride elimination is the rate-limiting step of the reaction (**Scheme 2.1B**).



**Scheme 2.1.** (A) describes the commonly proposed Guerbet mechanism which proceeds through the reaction of molecular hydrogen. (B) describes the Guerbet mechanism which proceeds via transfer hydrogenation “M” represents a metal catalyst.

To study **1-Ru** under flow conditions, we developed an immobilization strategy that maintains **1-Ru** in a reactor while continuously feeding and extracting reagents and products. The most common approach to catalyst immobilization involves anchoring of the catalyst onto a macroscopic support.<sup>22,23</sup> While this strategy successfully immobilizes the catalyst, it requires modification of the ligand structure which can alter the reactivity of the catalyst and can be synthetically intensive.<sup>24</sup> Modeling after industrial processes that use homogeneous catalysts in continuous flow reactors (e.g. Shell Higher Olefin, *Ruhrchemie/Rhône-Poulenc*, and Monsanto/Cativa processes), we opted to implement a methodology which relies on thermodynamic equilibrium to separate the volatile reaction components from the non-volatile catalyst.<sup>25–27</sup> This technique is advantageous as it does not require chemical modification of the catalyst and is applicable to any homogeneous catalyst. In our approach, the catalyst is dissolved in a non-volatile solvent and heated in a continuously stirred tank reactor (CSTR, **Figure 2.2**). Volatile substrates are then continuously fed into the system where they react with the catalyst in the condensed phase. The unreacted substrates, reaction intermediates, and products are evaporated and swept by a carrier gas to an in-line gas chromatograph for analysis (see the Reactor Setup and Equipment Section in Appendix A for more detail). The outlet stream is open to the atmosphere.

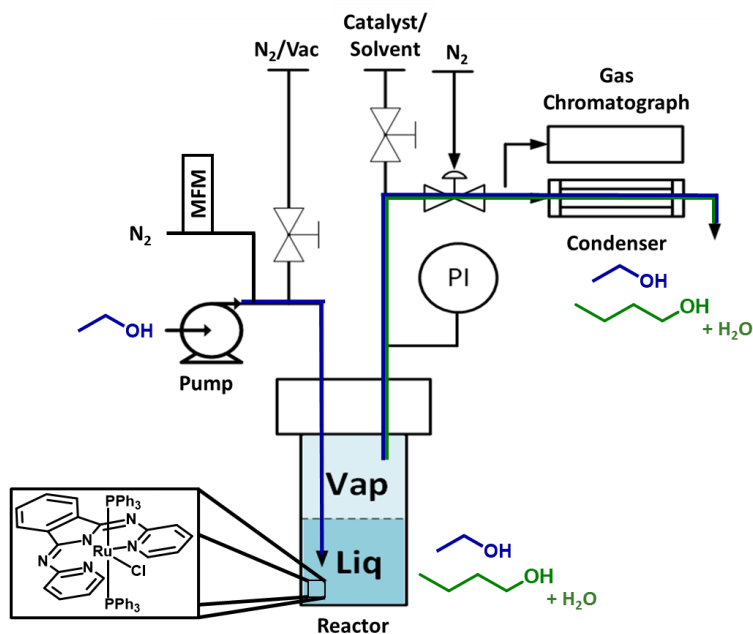


**Figure 2.2.** Schematic for Continuous Stirred Tank Reactor Design

## 2.2 Results and Discussion

*Material Compatibility.* The immobilization of our catalyst through a vapor-liquid equilibrium (VLE) required the implementation of a non-volatile liquid phase, which led us to investigate polymers as solvents.<sup>28,29</sup> We first probed the impact of various polymers on the activity of **1-Ru** for ethanol condensation reactions performed in batch (**Table 2.1**), and due to the large amount of co-catalyst (sodium ethoxide) needed to activate **1-Ru** we initially focused on hydroxyl containing polymers. The presence of hydroxyl groups proved to be detrimental to the catalysis where a notable decrease in activity ( $\text{TON, mol}_{\text{butanol}} \text{ mol}_{\text{cat}}^{-1}$ ) was observed upon the addition of polyvinyl phenol and polyvinyl alcohol. The decrease in activity was rationalized by the increased acidity of the reaction mixture and the protonation of the co-catalyst. These observations led us to select a low molecular weight polyethylene glycol (PEG, MW = 500 g/mol) to serve as the reaction solvent. PEG was thought to be a good solvent because of its strong affinity for alkali ions which would presumably allow us to solubilize a large amount of co-catalyst.<sup>30</sup> The stability of **1-Ru** in

PEG was further established in a series of ethanol coupling experiments performed in batch, in which stable catalytic activity was observed for up to 10 hours (**Figure A2**). Moreover, NMR analysis of a PEG-**1-Ru** mixture heated to 120°C for 30 minutes also showed no change in the  $^{31}\text{P}$  resonance of the ruthenium complex (**Figure A3**). Thus, the combination of these experiments validated that PEG was compatible with **1-Ru**.

**Table 2.1.** Batch condensation of ethanol to butanol by **1-Ru** in the presence of polymers <sup>a</sup>

Entry	Additive	TON ( $n_{\text{C4}}/n_{\text{cat}}$ )
1	Control	145
2	Poly-vinyl phenol	25
3	Poly-vinyl alcohol	100
4	PEG	150

<sup>a</sup>All reactions were carried out for 4 hours at 150°C in 0.4 mL of EtOH with the addition of 50 mg EtONa, 3.5 mg of **1-Ru**, and a known quantity of toluene (internal standard). For reactions loaded with polymer, 100 mg of material was introduced to the reaction mixture. Low ethanol conversions (<5 mol%) were maintained, and butanol was the only detected product from the reaction. TON is defined as the moles of butanol produced per mole of catalyst ( $n_{\text{C4}}/n_{\text{cat}}$ ).

**Table 2.2.** Standard operating conditions for ethanol condensation reactions in the CSTR<sup>a</sup>

<sup>a</sup>Ethanol conversion for flow coupling is kept below 5 mol% to ensure quasi-steady-state kinetics

PEG	5.33 mL
EtONa	386 mM
<b>1-Ru</b>	0.66 mM
N <sub>2</sub>	8.4 mL/min (g)
EtOH	1.25 $\mu\text{L}/\text{min}$ (l)
Pressure	16 psi
Residence time	35 s
Temperature	120°C

*Ethanol Coupling in the CSTR.* The CSTR was loaded with a polymer-catalyst solution which consisted of PEG, sodium ethoxide, and **1-Ru**. The reaction mixture was heated using a hotplate, whereafter liquid ethanol and nitrogen carrier gas were continuously fed into the heated mixture (**Table 2.2**). The pressure was kept constant, and the vapor-phase effluent was directed to an in-line gas chromatograph equipped with an FID detector for analysis. In this study, the ethanol



conversion was kept low (below 5 mol%) to ensure a quasi-steady-state condition and to reduce the formation rate of higher alcohols. Acetaldehyde, butanol, 2-ethyl-butanol, and hexanol were identified as the major products exiting the reactor (see **Figure 2.3** for the product distribution and **Figure A4** for the mass balance). Over the course of a 10-hour reaction, butanol formation underwent multiple phases as it gradually increased for the first 2 hours reaching a maximum TOF ( $\text{mol}_{\text{product}} \text{mol}_{\text{cat}}^{-1} \text{h}^{-1}$ ) of  $6 \text{ h}^{-1}$  before decreasing and steadying at  $4 \text{ h}^{-1}$  after 4 hours. The decrease in butanol formation rate coincides with the increased formation rate of  $\text{C}_6$  products, TOF of  $1 \text{ h}^{-1}$ , and the disappearance of acetaldehyde (see Appendix A for sample rate calculations). After several hours on stream, the rate of evaporation and catalysis converged to produce a steady reaction profile. The initial non-monotonic rate of butanol formation was attributed to transient reaction kinetics (see Appendix A for qualitative kinetic modeling).

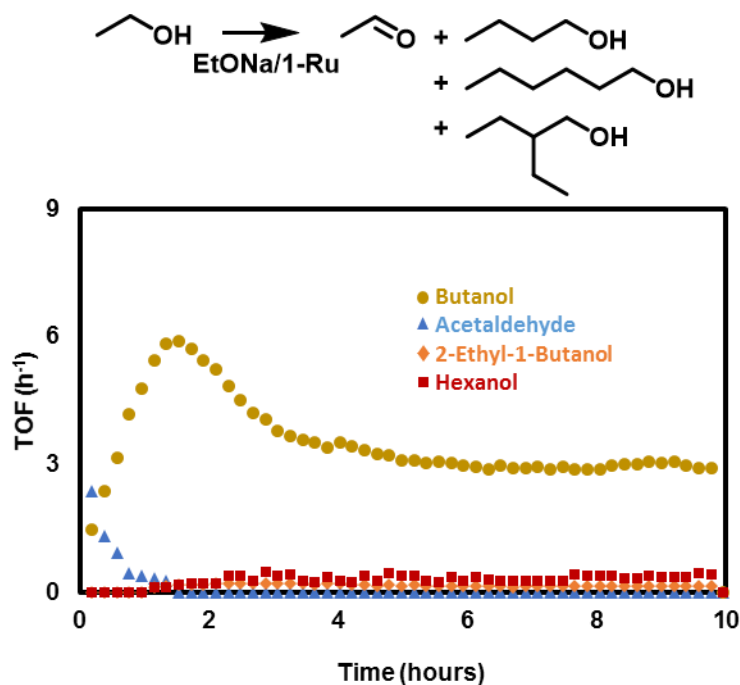


**Figure 2.3.** Product rate profile for ethanol coupling reaction. TOF is defined as the moles of product formed per time per mole of catalyst.

Further analysis of the product distribution also provided valuable insights regarding the selectivity and reaction mechanism of **1-Ru**. First, we compared our experimental  $\text{C}_4/\text{C}_6$  product ratio ( $\text{C}_4/\text{C}_6$

= 4) to a prediction calculated using a random step-growth condensation model based on Flory's equal-reactivity principle ( $C_4/C_6 = 40$ , see Appendix A for Calculations) at equal conversion (2.5mol%). The higher ratio of  $C_6$  in our experiment led us to conclude that **1-Ru** does not exhibit any selectivity for ethanol coupling under our reaction conditions.<sup>31</sup> Our conclusion is in direct contrast to prior reports of the catalyst, and this discrepancy can be, in-part, attributed to the definition of selectivity. Under low conversion conditions, the catalyst is flooded with ethanol as the predominant substrate, which creates an inherent bias for the reaction of ethanol (butanol formation) over butanol reaction, producing a false sense of selectivity. We decouple the effect of conversion by comparing the product ratios ( $C_4/C_6$ ) between a step-growth prediction and our experimental data at identical conversions, which provides a more accurate description of catalytic selectivity.

Second, the absence of unsaturated  $C_4$  intermediates suggests a fast hydrogenation step relative to aldol condensation. This observation was particularly surprising when considering the short residence times (35 s – reaction vol./vol. flow) and the low substrate concentrations. This low substrate concentration is especially true for hydrogen gas due to its higher volatility. Presumably, hydrogen vaporization would result in a non-stoichiometric reaction that would promote the formation of unsaturated intermediates. However, we did not detect unsaturated  $C_4$  and  $C_6$  molecules in the product stream, which suggested that molecular hydrogen does not play a significant role in the hydrogenation reaction. This conclusion led us to postulate that a transfer hydrogenation reaction is the primary mechanism for the hydrogenation step. Prior to probing our mechanistic hypothesis, it is most important to demonstrate that the reaction performed in the CSTR is not mass transfer limited.

*Mass Transfer Studies.* Two potential mass transfer limitations should be considered. First, the transport of ethanol from the bubbles at the inlet to the polymer, and second, the transport of ethanol from the polymer to the head space of the reactor. Mass transfer between the ethanol bubbles and the solvent was studied by varying the PEG loading while maintaining a constant substrate flowrate, co-catalyst concentration, and ethanol partial pressure ( $P_{\text{EtOH}} = 0.4$  psi). A stainless-steel dip-tube is used to deliver ethanol into the cylindrical reactor. By varying the PEG loadings (5.3 – 8 mL), we alter the length of the diffusion path from the inlet of the tube to the surface of the polymer (1.2 mm – 6.7 mm). Despite varying the diffusion path, the cumulative turnovers over 10 hours of catalysis for these experiments remained constant ( $60 \pm 6$  TON), suggesting that the rate of mass transfer is rapid in comparison to the Guerbet reaction (**Table 2.3**). In addition, we also varied the concentration of **1-Ru** (0.66 - 0.33 mM) and no change in catalytic rate was observed, providing further confirmation that the concentration of ethanol is constant throughout the liquid phase. Next, mass transfer effects between the liquid phase and the headspace were probed by varying the stir-bar's rate of rotation. An increase in rotation rate creates a vortex with a larger surface area. For a mass transfer limited system, a surface area increase would consequently accelerate the rate of mass transfer and the rate of product formation. However, no enhancement to the alcohol formation rate was observed while periodically increasing the rate of rotation (500-1000 RPM) during a 10-hour experiment, suggesting that transport between phases is rapid and not rate-limiting (**Figure A6**).

**Table 2.3.** Condensation of ethanol to butanol by **1-Ru** in the CSTR at different residence times<sup>a</sup>

PEG (mL)	Ru (mM)	Residence Time (s)	TON ( $[\text{n}_{\text{C4}}+\text{n}_{\text{C6}}]/\text{n}_{\text{cat}}$ )
5.33	0.66	35	60±6 <sup>b</sup>
6.67	0.66	44	58
6.67	0.50	44	65
6.67	0.33	44	67
8.0	0.66	53	53

<sup>a</sup>EtOH and N<sub>2</sub> are fed into the reactor at 1.25  $\mu\text{L}/\text{min}$  (l) and 8.4 mL/min (g) respectively at 120°C and a pressure of 16 psi ( $P_{\text{EtOH}} = 0.4$  psi). The concentration of sodium ethoxide was held constant at 330 mM for each experiment. <sup>b</sup>Standard deviation was calculated by averaging over three experiments using identical reactor loadings. Butanol, hexanol and 2-ethyl butanol were the predominant products from the reaction. Accordingly, TON is defined as the moles of products formed per mole of catalyst ( $[\text{n}_{\text{C4}}+\text{n}_{\text{C6}}]/\text{n}_{\text{cat}}$ ) after 10 hours of reaction time.

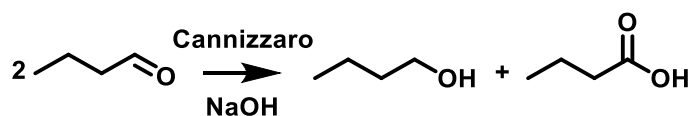
**Table 2.4.** Standard operating conditions for C<sub>4</sub> hydrogenation reactions in the CSTR

PEG	5.33 mL
EtONa	386 mM
<b>1-Ru</b>	1.12 mM
He	100 mL/min (g)
<sup>i</sup> PrOH	20 $\mu\text{L}/\text{min}$ (l)
Unsaturated C <sub>4</sub>	1 mol% in <sup>i</sup> PrOH
Pressure	16 psi
Residence time	0.05 s
Temperature	120°C

*Hydrogenation of unsaturated molecules.* To probe our hypothesis that the reaction proceeds predominantly through a transfer hydrogenation mechanism we performed a series of hydrogenations on unsaturated C<sub>4</sub> intermediates in the presence of a hydrogen donor, isopropyl alcohol (**Table 2.4**). Dilute mixtures of unsaturated C<sub>4</sub> intermediate in isopropyl alcohol were continuously fed as a liquid into the heated CSTR which contained a polymer-catalyst mixture. Helium carrier gas was used to sweep the vapor-phase effluent to the in-line gas chromatograph for analysis of the reaction progress.

We first studied the transfer hydrogenation of butyraldehyde in the presence of excess isopropyl alcohol. In this experiment, we observed an initial butanol formation rate of 26 h<sup>-1</sup> which gradually decayed over 3 hours (**Figure 2.4** and **Figure A14**). Further examination of the product

distribution showed a high conversion of butyraldehyde to butanol (59.5 mol%, **Table 2.5**). Notably, however, 30.6 mol% of the substrate fed into the reactor was unaccounted for in the gas-phase mass balance. The missing substrate was attributed to the formation of low volatility products via aldol condensation and the commonly reported base-catalyzed Cannizzaro disproportionation reaction (**Scheme 2.2**).<sup>32,33</sup> The low volatility products were identified in batch experiments by performing the cross condensation of butyraldehyde and acetaldehyde catalyzed by sodium ethoxide in the absence of **1-Ru** at 120°C (**Table A1**). In particular, the acidic products from the Cannizzaro reaction (acetic and butyric acid) will consume the co-catalyst to form non-reactive sodium salts. Under our flow reactor conditions, the acids (formed continuously in-situ) react quickly with the high concentration of sodium ethoxide which is consistent with the observed decay in catalyst activity.



**Scheme 2.2.** Cannizzaro disproportionation reaction of butyraldehyde.

Acetone was also detected in the gaseous product stream during the butyraldehyde transfer hydrogenation reaction with an average TOF of 18 h<sup>-1</sup> over 3 hours (~1 mol% conversion of isopropyl alcohol). Comparing rates of acetone and butanol formation (**Table 2.5** and **Figure A17**) we noted that the ratio of rates was near unity ( $R_{\text{Butanol}}/R_{\text{Acetone}}=1.1$ ). This observation provided additional evidence for a transfer hydrogenation pathway, since at least one molecule of acetone was produced for each unsaturated bond that was hydrogenated. The slightly faster rate of butanol formation was attributed to the Cannizzaro reaction.

### Transfer Hydrogenation

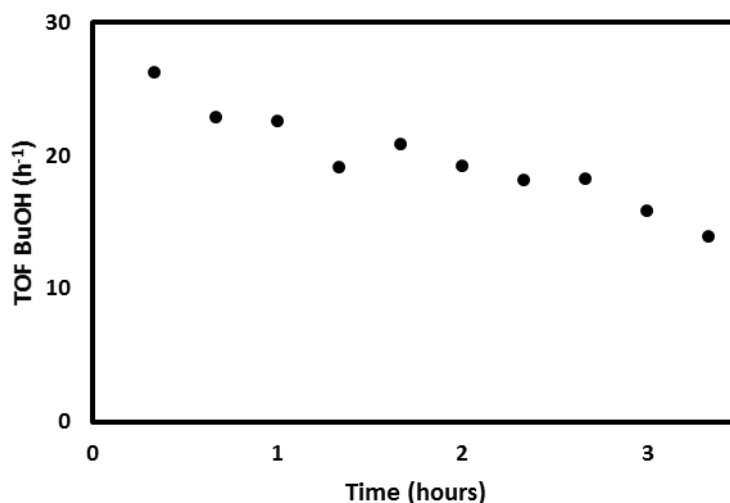
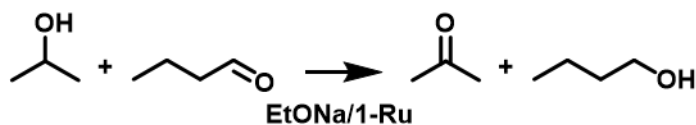


**Figure 2.4.** Butanol formation rate reported over time for the transfer hydrogenation of butyraldehyde.

**Table 2.5.** Summary of Transfer Hydrogenation Reactions<sup>a</sup>

Substrate		Butyraldehyde	Crotyl Alcohol	Crotonaldehyde
Products (mol%)	Butyraldehyde	9.9	n.d.	2.2
	Crotyl Alcohol	n.d.	57.9	1.2
	Crotonaldehyde	n.d.	n.d.	1.5
	Butanol	59.5	37.8	16.2
	Missing C <sub>4</sub>	30.6	4.3	78.9
Rate (h <sup>-1</sup> )	R <sub>Butanol</sub>	20	13	12
	R <sub>Acetone</sub>	18	25	16
	R <sub>Butanol</sub> /R <sub>Acetone</sub>	1.1	0.5	0.8

<sup>a</sup>The table depicts the distribution of intermediates detected at the reactor outlet for transfer hydrogenation reactions while employing different hydrogenation substrates. The formation rate of butanol and acetone are also compared. Note, the conversion of <sup>i</sup>PrOH does not exceed 2 mol% for all experiments, and the reported data were aggregated by averaging the product formation rates over 3 hours of flow catalysis. Rate is defined as the moles of product formed per time per mole of catalyst. Refer to **Figure A14 – A20** for the gaseous product profiles and for the comparison of acetone and butanol formation rates over time.

Next, we studied the transfer hydrogenation of crotyl alcohol (**Figure 2.5**) where we observed a moderate conversion of the substrate to butanol (37.8 mol%) and an average butanol formation rate of  $13\text{ h}^{-1}$  over 3 hours (**Table 2.5 and Figure A15**). Compared to the rate of butyraldehyde hydrogenation, the hydrogenation of crotyl alcohol was slower, suggesting that C=C bonds are more difficult to hydrogenate than C=O bonds. Furthermore, the gas-phase mass balance for crotyl alcohol hydrogenation was well-accounted, where 95.7 mol% of the initial feed was either converted to butanol or unreacted. Other unsaturated C<sub>4</sub> intermediates apart from unreacted substrate were not detected (<0.001 mol% conversion). We postulate that the missing substrate (4.3 mol%) is indicative of butanol dehydrogenation to butyraldehyde which subsequently condenses to form low volatility C<sub>8</sub> products. Nonetheless, a well-accounted mass balance was consistent with the inability of crotyl alcohol to react via aldol-condensation or Cannizzaro reactions. Moreover, a comparison of the butanol and acetone formation rates revealed that more acetone was being formed than butanol ( $R_{\text{Butanol}}/R_{\text{Acetone}}=0.5$ , **Table 2.5 and Figure A18**). Thus, in addition to transfer hydrogenation **1-Ru** was also presumably dehydrogenating isopropyl alcohol to yield hydrogen gas and acetone, which was confirmed by reacting isopropyl alcohol with **1-Ru** and sodium ethoxide in the flow system (**Figure A20**). In this control reaction, isopropyl alcohol conversion remained below 2 mol%, and acetone was formed at an average TOF of  $34\text{ h}^{-1}$  over 3 hours. This reactivity was consistent with the ability of bis(pyridylimino)isoindolate Ru(II) catalysts to perform the dehydrogenation of secondary alcohols.<sup>20,21</sup> Although these experiments provided evidence for the formation of hydrogen gas during the Guerbet reaction, a thermodynamic analysis (see Appendix A for CHEMCAD simulation) of hydrogen solubility in PEG under our reaction conditions revealed that the concentration of hydrogen would be at least three orders of magnitude lower than that of the alcohol substrates. These low concentrations

strongly suggest that the hydrogenation of unsaturated intermediates through molecular hydrogen is negligible.

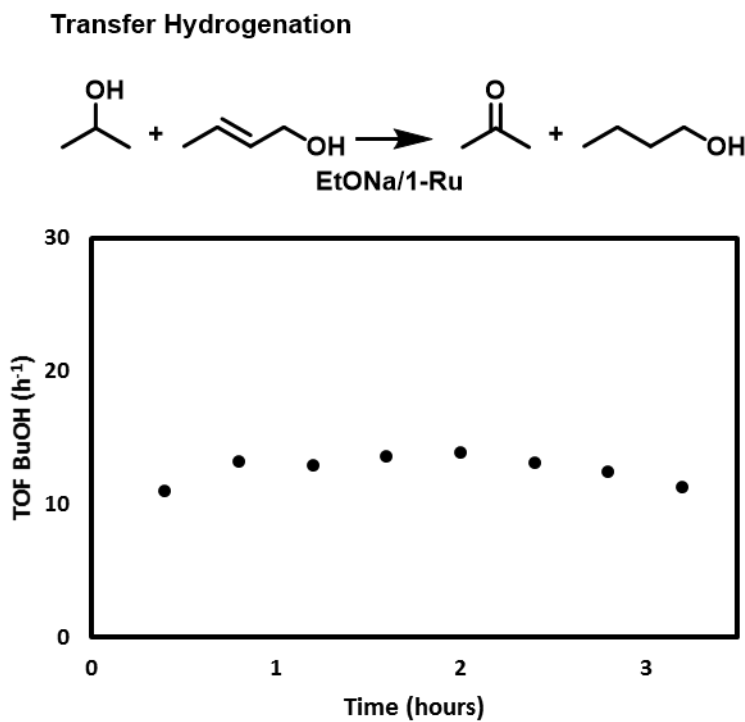


**Figure 2.5.** Butanol formation rate reported over time for the transfer hydrogenation of crotyl alcohol.

Finally, the hydrogenation of crotonaldehyde was investigated where we observed an average butanol formation rate of 12 h<sup>-1</sup> over 3 hours (**Figure 2.6 and Figure A16**). This turnover rate for butanol formation corresponds to two cycles of hydrogenation. Thus, the hydrogenation rate of crotonaldehyde appears comparable to crotyl alcohol despite the low conversion of crotonaldehyde to butanol (16.2 mol%, **Table 2.5**). Only traces of unsaturated intermediates were detected during catalysis (1-2 mol%). Crotonaldehyde was also subject to side-reactions in the presence of sodium ethoxide as evidenced by poor closure of the mass balance where 78.9 mol% of the starting



material was unaccounted for in the gas phase. Correspondingly, the acetone and butanol formation rates were less than unity ( $R_{\text{Butanol}}/R_{\text{Acetone}} = 0.8$ , **Table 2.5** and **Figure A19**).

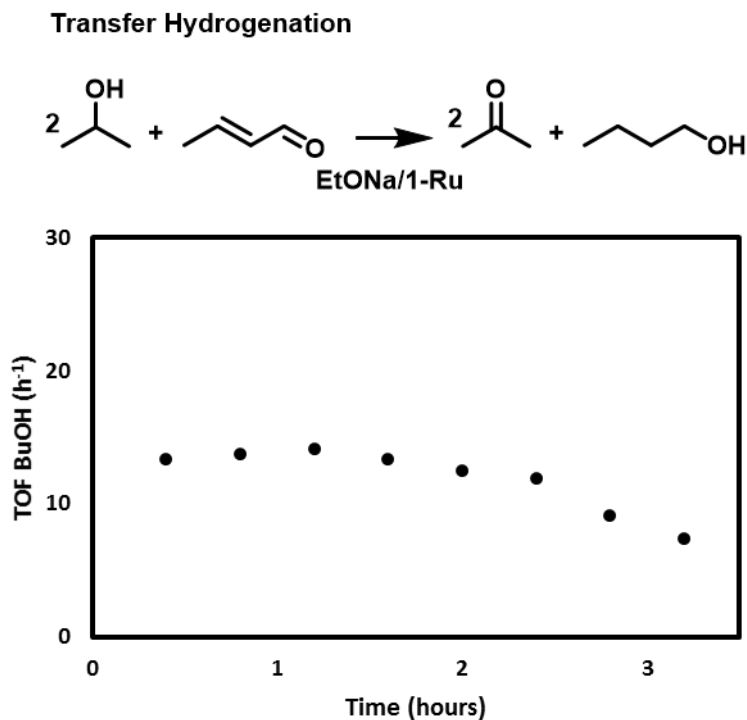


**Figure 2.6.** Butanol formation rate reported over time for the transfer hydrogenation of crotonaldehyde.

*Reaction mechanism.* Through our investigations we have provided evidence that the hydrogenation step of the Guerbet reaction mediated by **1-Ru** proceeds predominantly through a transfer hydrogenation mechanism. The absence of detectable unsaturated C<sub>4+</sub> products during ethanol coupling reactions suggests that transfer hydrogenation is fast. This furthermore implies that condensation must be similarly fast, otherwise no C<sub>6</sub> products would be formed. Overall, these observations point to  $\beta$ -hydride elimination of the ruthenium alkoxy species as the rate-limiting step of the mechanism.<sup>34</sup> It is worth noting that the hydrogenation rate of unsaturated C<sub>4</sub> in the presence of isopropyl alcohol (**Table 2.5**) was faster than the butanol formation rate reported for the Guerbet reaction (**Figure 2.3**). This difference in rate is consistent with the higher reactivity of a secondary alcohol which would more readily undergo  $\beta$ -hydride elimination in comparison to

ethanol. A reaction mechanism involving two cycles, one for the monounsaturated and one for the di-unsaturated product is drawn in **Figure 2.7**. Each cycle includes a transfer hydrogenation reaction and a  $\beta$ -hydride elimination step. Finally, we demonstrated that the hydrogenation of unsaturated intermediates through molecular hydrogen is unlikely due to the fast rate of transfer hydrogenation and the low solubility of hydrogen under our reaction conditions. The high concentration of alcohol in a batch reaction would also favor hydrogenation through hydrogen transfer over molecular hydrogen.

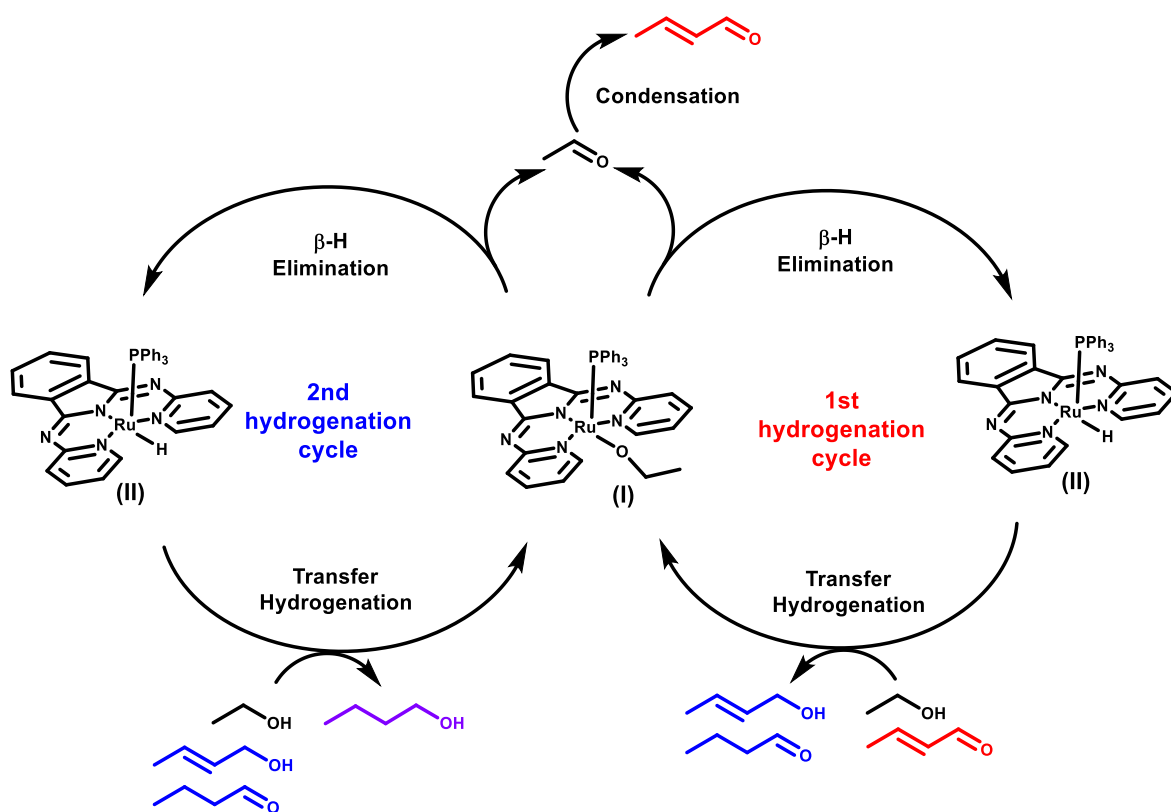


**Figure 2.7.** Simplified Guerbet Mechanism Mediated by **1-Ru**.

## 2.3 Summary and Conclusions

Through the development of a flow reactor set-up involving a simple immobilization strategy, we have gained mechanistic insights into the ethanol self-condensation reaction catalyzed by a homogeneous ruthenium catalyst (**1-Ru**). The methodology allowed us to monitor the reaction progress at steady state for hours. The technique consists of dissolving the catalyst in a non-volatile

solvent (a polymer) and leveraging VLE to continuously remove reagents and products of the reaction. The composition of the vapor stream exiting the reaction mixture is analyzed using an in-line GC. This technique for catalyst immobilization is particularly powerful as it does not require the modification of the catalyst; and thus, any homogeneous Guerbet catalyst could be used. Stable butanol production was achieved in the reactor for more than 12 hours. By comparing the composition of our product mixture to a prediction from a step-growth polymerization model, we demonstrated that **1-Ru** does not exhibit any selectivity toward butanol formation under our reaction conditions. We also showcased that the hydrogenation step follows a transfer hydrogenation mechanism and that  $\beta$ -hydride elimination of the ruthenium alkoxy is the rate-limiting step of the reaction. Finally, we established that molecular hydrogen, while potentially formed during the reaction, does not participate in the hydrogenation reaction. This combination of reactor engineering and mechanistic insight will help develop next generation catalysts with the goal of identifying catalytic systems that offer high selectivity for ethanol condensation.

## 2.4 References

- (1) Ramey, D. E. Butanol : The Other Alternative Fuel. *Agric. Biofuels Technol. Sustain. Profitab.* **2007**, 85, 137.
- (2) Trindade, W. R. da S.; Santos, R. G. dos. Review on the Characteristics of Butanol, Its Production and Use as Fuel in Internal Combustion Engines. *Renew. Sustain. Energy Rev.* **2017**, 69 (October 2015), 642–651.
- (3) Pfromm, P. H.; Amanor-Boadu, V.; Nelson, R.; Vadhani, P.; Madl, R. Bio-Butanol vs. Bio-Ethanol: A Technical and Economic Assessment for Corn and Switchgrass Fermented by Yeast or *Clostridium Acetobutylicum*. *Biomass and Bioenergy* **2010**, 34 (4), 515–524.
- (4) Green, E. M. Fermentative Production of Butanol-the Industrial Perspective. *Curr. Opin.*

- Biotechnol.* **2011**, 22 (3), 337–343.
- (5) Guerbet, M. Action de l'alcool Amylique de Fermentation Sur Son Dérivé Sodé. *C. R. Acad. Sci. Paris* **1899**, 128, 511, 1002.
- (6) Bankar, S. B.; Survase, S. A.; Ojamo, H.; Granström, T. Biobutanol: The Outlook of an Academic and Industrialist. *RSC Adv.* **2013**, 3 (47), 24734–24757.
- (7) Dürre, P. Biobutanol: An Attractive Biofuel. *Biotechnol. J.* **2007**, 2 (12), 1525–1534.
- (8) Petrus, L.; Noordermeer, M. A. Biomass to Biofuels, a Chemical Perspective. *Green Chem.* **2006**, 8 (10), 861–867.
- (9) Alonso, D. M.; Bond, J. Q.; Dumesic, J. A. Catalytic Conversion of Biomass to Biofuels. *Green Chem.* **2010**, 12 (9), 1493–1513.
- (10) Hagen, J. *Industrial Catalysis: A Practical Approach: Second Edition*; Wiley-VCH Verlag GmbH & Co. KGaA, 2006.
- (11) Matsu-Ura, T.; Sakaguchi, S.; Obora, Y.; Ishii, Y. Guerbet Reaction of Primary Alcohols Leading to  $\beta$ -Alkylated Dimer Alcohols Catalyzed by Iridium Complexes. *J. Org. Chem.* **2006**, 71 (21), 8306–8308.
- (12) Dowson, G. R. M.; Haddow, M. F.; Lee, J.; Wingad, R. L.; Wass, D. F. Catalytic Conversion of Ethanol into an Advanced Biofuel: Unprecedented Selectivity for n-Butanol. *Angew. Chemie - Int. Ed.* **2013**, 52 (34), 9005–9008.
- (13) Xie, Y.; Ben-David, Y.; Shimon, L. J. W.; Milstein, D. Highly Efficient Process for Production of Biofuel from Ethanol Catalyzed by Ruthenium Pincer Complexes. *J. Am. Chem. Soc.* **2016**, 138 (29), 9077–9080.
- (14) Tseng, K. N. T.; Lin, S.; Kampf, J. W.; Szymczak, N. K. Upgrading Ethanol to 1-Butanol with a Homogeneous Air-Stable Ruthenium Catalyst. *Chem. Commun.* **2016**, 52 (14),

2901–2904.

- (15) Kulkarni, N. V.; Brennessel, W. W.; Jones, W. D. Catalytic Upgrading of Ethanol to N-Butanol via Manganese-Mediated Guerbet Reaction. *ACS Catal.* **2018**, 8 (2), 997–1002.
- (16) Fu, S.; Shao, Z.; Wang, Y.; Liu, Q. Manganese-Catalyzed Upgrading of Ethanol into 1-Butanol. *J. Am. Chem. Soc.* **2017**, 139 (34), 11941–11948.
- (17) Chakraborty, S.; Piszal, P. E.; Hayes, C. E.; Baker, R. T.; Jones, W. D. Highly Selective Formation of N-Butanol from Ethanol through the Guerbet Process: A Tandem Catalytic Approach. *J. Am. Chem. Soc.* **2015**, 137 (45), 14264–14267.
- (18) Aitchison, H.; Wingad, R. L.; Wass, D. F. Homogeneous Ethanol to Butanol Catalysis - Guerbet Renewed. *ACS Catal.* **2016**, 6 (10), 7125–7132.
- (19) Dibenedetto, T. A.; Jones, W. D. Upgrading of Ethanol to N-Butanol via a Ruthenium Catalyst in Aqueous Solution. *Organometallics* **2021**, 40 (12), 1884–1888.
- (20) Tseng, K. N. T.; Kampf, J. W.; Szymczak, N. K. Base-Free, Acceptorless, and Chemoselective Alcohol Dehydrogenation Catalyzed by an Amide-Derived NNN - Ruthenium(II) Hydride Complex. *Organometallics* **2013**, 32 (7), 2046–2049.
- (21) Tseng, K. N. T.; Kampf, J. W.; Szymczak, N. K. Mechanism of N,N,N-Amide Ruthenium(II) Hydride Mediated Acceptorless Alcohol Dehydrogenation: Inner-Sphere  $\beta$ -H Elimination versus Outer-Sphere Bifunctional Metal-Ligand Cooperativity. *ACS Catal.* **2015**, 5 (9), 5468–5485.
- (22) Li, C.; Liu, Y. *Bridging Heterogeneous and Homogeneous Catalysis: Concepts, Strategies, and Applications*; Can, L., Yan, L., Eds.; Wiley-VCH Verlag GmbH & Co. KGaA: Weinheim, Germany, 2014; Vol. 9783527335.
- (23) Haynes, A. *Concepts of Modern Catalysis and Kinetics*; Wiley-VCH, 2005; Vol. 2005.

- (24) Hübner, S.; de Vries, J. G.; Farina, V. Why Does Industry Not Use Immobilized Transition Metal Complexes as Catalysts? *Adv. Synth. Catal.* **2016**, 358 (1), 3–25.
- (25) Keim, W. Oligomerization of Ethylene to  $\alpha$ -Olefins: Discovery and Development of the Shell Higher Olefin Process (SHOP). *Angew. Chemie - Int. Ed.* **2013**, 52 (48), 12492–12496.
- (26) Kohlpaintner, C. W.; Fischer, R. W.; Cornils, B. Aqueous Biphasic Catalysis: Ruhrchemie/Rhône-Poulenc Oxo Process. *Appl. Catal. A Gen.* **2001**, 221 (1–2), 219–225.
- (27) Sunley, G. J.; Watson, D. J. High Productivity Methanol Carbonylation Catalysis Using Iridium. The Cativa™ Process for the Manufacture of Acetic Acid. *Catal. Today* **2000**, 58 (4), 293–307.
- (28) Harrell, M. L.; Malinski, T.; Torres-López, C.; Gonzalez, K.; Suriboot, J.; Bergbreiter, D. E. Alternatives for Conventional Alkane Solvents. *J. Am. Chem. Soc.* **2016**, 138 (44), 14650–14657.
- (29) Clarke, C. J.; Tu, W. C.; Levers, O.; Bröhl, A.; Hallett, J. P. Green and Sustainable Solvents in Chemical Processes. *Chem. Rev.* **2018**, 118 (2), 747–800.
- (30) Trimble, H. M. Solubilities of Salts in Ethylene Glycol and in Its Mixtures with Water. *Ind. Eng. Chem.* **1931**, 23 (2), 165–167.
- (31) Flory, P. J. Fundamental Principles of Condensation Polymerization. *Chem. Rev.* **1946**, 39 (1), 137–197.
- (32) Cannizzaro, S. Ueber Den Der Benzoësäure Entsprechenden Alkohol. *Justus Liebigs Ann. Chem.* **1853**, 88 (1), 129–130.
- (33) Tishchenko, V. T. On the Effect of Aluminium Alkoxides on Aldehydes. Ester Condensation, as a New Kind of Aldehyde Condensation. *J. Russ. Phys.-Chem. Soc.* **1906**,

38, 355.

- (34) Gabriëls, D.; Hernández, W. Y.; Sels, B.; Van Der Voort, P.; Verberckmoes, A. Review of Catalytic Systems and Thermodynamics for the Guerbet Condensation Reaction and Challenges for Biomass Valorization. *Catal. Sci. Technol.* **2015**, 5 (8), 3876–3902.

## CHAPTER 3: Study and Immobilization of Homogeneous Catalysts in a Packed Bed

### Reactor

#### 3.1 Introduction

Homogeneous catalysts are traditionally maintained within a flow setup through their immobilization onto macroscopic supports. To do so, the organic ligand is modified to include a tethering group, which is used to anchor the organometallic complex.<sup>1</sup> Other approaches include the incorporation of organometallics within metal-organic frameworks or the use of polymeric ligands.<sup>2-6</sup> All these methods are synthetically complex, and the ligand modification, oftentimes, has negative effects on the performance of the catalyst.<sup>7-10</sup> Thus, there is a need for the development of alternative immobilization strategies that do not require modification of the ligand structure, and one such methodology is the supported liquid phase catalyst (SLPC).

In this strategy, a homogeneous catalyst is dissolved in a small quantity of reaction solvent that is spread onto an inorganic support to afford a catalytic reaction film.<sup>11-21</sup> The resulting solid material (the SLPC) is compatible with continuous packed-bed operation similar to conventional heterogeneous catalysts. As this technique relies on physical absorption, no modification of the catalyst's chemical structure is required, and the simplicity of this approach served as our inspiration. Thus, we were interested in extending the SLPC strategy to new chemistries by immobilizing an ethanol coupling (Guerbet reaction) catalyst (**1-Ru**, **Figure 3.1**) and a hydrogenation catalyst (**2-Ir**, **Figure 3.1**).<sup>22</sup> By using a low-volatility polymer solvent in the formulation of our SLPC, we retain the molecular catalyst within a packed bed reactor (PBR) at constant concentration while under a continuous flow of gaseous substrate. The substrates diffuse into the solvent layer to react while unreacted substrate and product diffuse out.



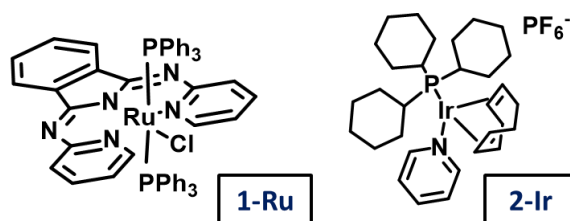
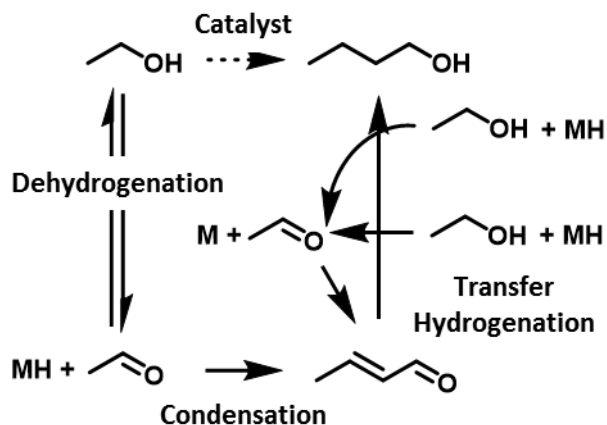


**Figure 3.1.** Homogeneous catalysts studied in this work.

In this chapter, we detail the immobilization and study of organometallic catalysts within a PBR. In comparison to more recently popularized SLPC solvents such as ionic liquids, our use of a non-volatile polymer to coat inorganic particles offers a few advantages. First, polymers can be specifically designed to have a low inhibitory effect on an organometallic catalyst. Second, the wide array of polymer compositions, structures, and functionalities allow for fine-tuning of polarity which can affect the reaction process. We decided to perform a case study on the Guerbet reaction (**Scheme 3.1**) to establish the SLPC methodology. This reaction is ideal for our process since the components of the ethanol coupling chemistry are volatile under the reaction conditions. Through a series of kinetic experiments, we demonstrate that the ethanol coupling reaction can be performed in continuous flow within a regime that is not mass transfer limited. The absence of mass transfer is critical for performing kinetic investigations. After the Guerbet case study, we used our SLPC technique to immobilize Crabtree's catalyst (**2-Ir**) for the hydrogenation of 1-hexene under flow conditions.



**Scheme 3.1.** Previously Proposed Mechanism for the Guerbet reaction mediated by **1-Ru**.

### 3.2 Experimental Procedure(s) and Setup

*SLPC Synthesis.* The synthesis of the SLPC was performed under an inert atmosphere using a wet-impregnation technique. For the immobilization of **1-Ru**, basic alumina ( $\text{Al}_2\text{O}_3$ ) is first dried in a heated oven ( $150^\circ\text{C}$ ). Afterwards, basic  $\text{Al}_2\text{O}_3$  is taken and stirred with sodium ethoxide ( $\text{EtONa}$ , co-catalyst) in ethanol for 1 hour. This material is dried under vacuum to remove any trapped ethanol. The co-catalyst serves two functions: (1) as a condensation catalyst and (2) as an activator/initiator for the ruthenium complex.<sup>23</sup> Sole  $\text{EtONa}$  does not catalyze the (de)hydrogenation reaction, but both  $\text{EtONa}$  and **1-Ru** are required for (de)hydrogenation to proceed.<sup>26</sup> Next, the alumina supported  $\text{EtONa}$  is mixed in a solution of diethyl ether ( $\text{Et}_2\text{O}$ ) with PEG and the desired quantity of **1-Ru** for 1 hour. Additional ligand (triphenylphosphine,  $\text{PPh}_3$ ) can also be added in the prior step. This resulting solution is dried under vacuum to remove the solvent, affording the SLPC.  $\text{Et}_2\text{O}$  was used as solvent as it dissolves, simultaneously, the catalyst and polymer without dissolving  $\text{EtONa}$ . This resulting slurry is dried under vacuum to remove the solvent, affording the SLPC. For the immobilization of **2-Ir**, the catalyst was heterogenized onto neutral  $\text{Al}_2\text{O}_3$  in a single wet impregnation step using dichloromethane as the solvent. See the Supporting Information for additional detail on the SLPC synthesis.

*Reactor Design and Build.* We used a homemade PBR system equipped with a syringe pump for the delivery of liquid substrate and a mass flow meter for the delivery of nitrogen (carrier gas). A cylindrical glass reactor containing the SLPC is loaded into a stainless-steel tube which is heated using an oven with controlled temperature. The reactor pressure is maintained at ca. 1 atmosphere, and the gaseous product flow is analysed using an in-line gas chromatograph equipped with an FID detector (**Figure 3.2**). For hydrogenation reactions at room temperature, the syringe pump was removed, and 1-hexene was fed into the PBR by saturating a nitrogen gas stream whose delivery was controlled by a mass flow meter. This setup ensures that there is no condensation of 1-hexene in the reactor. The flowrate of hexene was determined gravimetrically. A second mass flowmeter was installed to control the co-feed of hydrogen gas. This mixed feed was then flown over the catalyst bed. See Appendix B for additional details on equipment and reactor design.

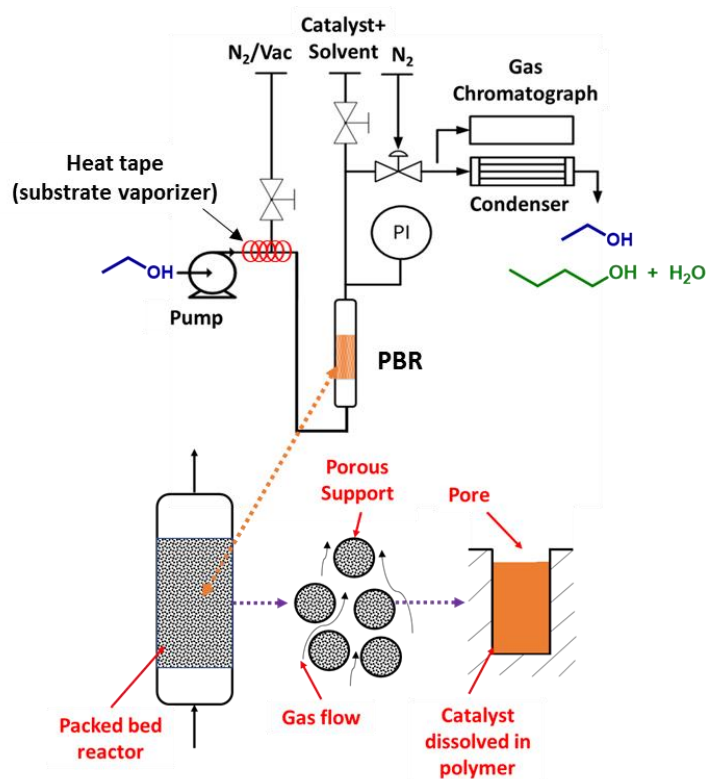


**Figure 3.2.** Schematic of PBR design and SLPC methodology.

### 3.3 Results and Discussion

*Material Compatibility with 1-Ru.* In Chapter 2, we had investigated the steady-state flow kinetics of **1-Ru** using a continuously stirred tank reactor (CSTR). Within this prior work, polyethylene glycol (PEG) was shown to be inert toward **1-Ru** under elevated reaction conditions. Moreover, additives with high acidity were shown to negatively affect catalytic activity.<sup>23</sup> Thus, to develop the SLPC containing **1-Ru**, we selected PEG (MW~500 g/mol) as the liquid non-volatile reaction phase and basic Al<sub>2</sub>O<sub>3</sub> as the inorganic support (silica was shown to inhibit the reaction see Appendix B for details). To ensure **1-Ru** was compatible with basic Al<sub>2</sub>O<sub>3</sub>, we performed a series of ethanol coupling batch experiments that showed stable catalytic activity in the presence of the additive (**Figure B3**). Moreover, infrared (IR) spectroscopy revealed that characteristic stretches (1450 – 1600 cm<sup>-1</sup>) of the complexed isoindoline functionality present in **1-Ru** remained intact after impregnation of the catalyst onto the support (**Figure B4**).<sup>24</sup> This spectroscopic data suggested that the catalyst structure remained unchanged when absorbed onto alumina. Furthermore, a control IR spectrum of the bis(pyridylimino)isoindoline ligand was also collected that showed a characteristic N-H stretch for the non-deprotonated ligand located between 1600-1650 cm<sup>-1</sup>.<sup>24</sup> No peaks in this window were observed for the alumina supported **1-Ru**, validating that the ligand remained bound to the metal center upon deposition. The addition of a PEG layer onto the support obscured these characteristic **1-Ru** IR signals, which prevented the spectroscopic characterization of the fully formulated SLPC. Finally, an extraction experiment was performed by placing the SLPC into a solution of benzene (**Figure B6**), and an NMR analysis of the solution revealed no change in the <sup>31</sup>P resonance of the heterogenized and extracted ruthenium catalyst. Thus, the combination of these experiments validated that the immobilization procedure does not alter the chemical structure of **1-Ru**.

**Table 3.1.** SLPC formulation and standard operating conditions for the study of **1-Ru**

<u>Catalyst Composition</u>	
Alumina	84.3wt%
PEG	7wt%
EtONa	7wt%
<b>1-Ru</b>	1.7wt%
<u>Reactor Conditions</u>	
N <sub>2</sub> (g)	8 mL/min
EtOH (l)	4 $\mu$ L/min
Pressure	16 psi
Residence time	0.64 s
Temperature	120°C

*Ethanol Coupling Reaction in the PBR.* The residence time for the ethanol coupling reaction was kept short to maintain conversions below 5 mol% (see Appendix B for sample calculations). In this first experiment (see **Table 3.1** for reaction conditions), butanol was identified as the major product of the reaction reaching a maximum TOF ( $\text{mol}_{\text{product}} \text{mol}_{\text{1-Ru}}^{-1} \text{h}^{-1}$ ) of  $45 \text{ h}^{-1}$  which corresponds to 3 mol% conversion of ethanol. Its formation continued for numerous hours (**Figure 3.3**). In addition to butanol, trace quantities of butanal and crotonaldehyde were detected ( $>0.01 \text{ mol}\%$ ). Throughout the reaction, ca. 99 mol% of the substrate fed into the reactor was accounted for by the summation of these products and unreacted ethanol (near-quantitative closure of the mass balance). A control experiment was also performed by removing PEG from the SLPC formulation. In this experiment, the formation of butanol was not detected (**Figure 3.3**), confirming that the reaction occurred within the polymer film and not on the support surface. However, in contrast to the stability observed in batch and CSTR experiments (**Figure B3**), the catalyst activity decayed rapidly and reproducibly during the first hour of the reaction in the PBR (88% decay of the maximum conversion rate).

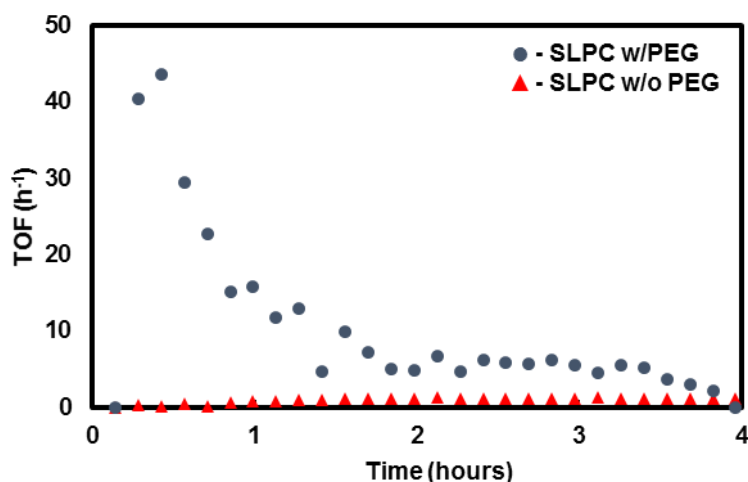


**Figure 3.3.** EtOH and N<sub>2</sub> are fed into the reactor at 4  $\mu\text{L}/\text{min}$  (l) and 8 mL/min (g) respectively at 120°C and a pressure of 16 psi ( $P_{\text{EtOH}} = 1.4$  psi). Circles (blue) indicate the activity of the SLPC in the presence of polymer (100 mg of SLPC, 7wt% base, 7wt% PEG, 1.7wt% **1-Ru**). Triangles (red) indicate the activity of an identical catalyst, but in the absence of polymer

*PBR Mass Transfer Studies.* To use the SLPC methodology to investigate the kinetics of a homogeneous catalyst, it is critical to establish that the reaction proceeds in a non-mass transfer limited regime. The mass transfer study discussed below is based upon the Koros-Nowak and Madon-Boudart criteria.<sup>25,26</sup>

First, we addressed intraparticle mass transfer considerations by performing catalysis with different concentrations of **1-Ru** in the polymer film. In the absence of mass transfer, the catalyst activity should be invariant to its concentration. This also implies that conversion should scale linearly with **1-Ru** loading. We synthesized three batches of SLPC with varying ruthenium loadings (0.34, 0.25, and 0.19wt%), keeping the quantity of base and PEG constant (7wt% base and 7wt% PEG). The cumulative conversions obtained over 3 hours were calculated (see Appendix B for sample calculations), and the conversion of the reaction was observed to scale linearly with the molar ruthenium loading (**Figure 3.4**). Additionally, when changing the concentration of **1-Ru** in our material, we saw no change in the turnover frequency per mol of metal (**Figure 3.5**). These observations establish that intraparticle mass transfer limitations are negligible under the reaction conditions studied.

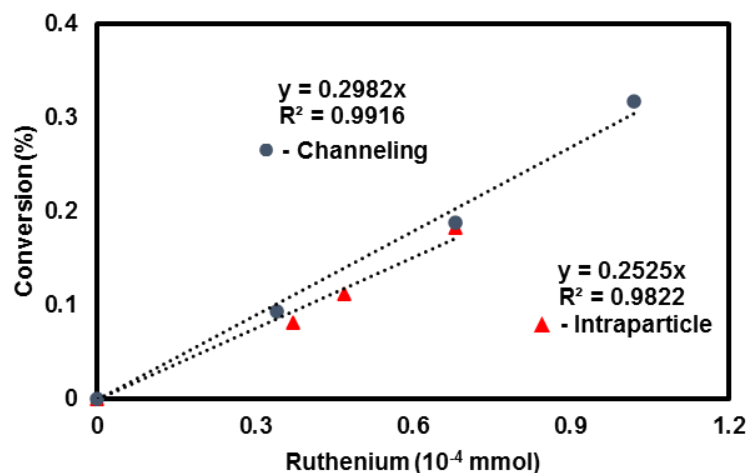


**Figure 3.4.** EtOH and N<sub>2</sub> are fed into the reactor at 4  $\mu\text{L}/\text{min}$  (l) and 8 mL/min (g) respectively at 120° and a pressure of 16 psi ( $P_{\text{EtOH}} = 1.4$  psi). Circles (blue) show the data obtained while varying the total quantity of SLPC while maintaining a constant composition: 100, 200, and 300 mg (7wt% base, 7wt% PEG and 0.34wt% **1-Ru**). Triangles (red) show data obtained while varying the concentration of catalyst material within three different batches: 200 mg SLPC with 0.34, 0.25, and 0.19wt% **1-Ru** (7wt% base, 7wt% PEG).

Second, we probed for inhomogeneous contacting between the gaseous reagent stream and the inorganic particles (channeling effects). To accomplish this task, we varied the overall quantity of SLPC (100, 200, and 300 mg) while maintaining a constant composition. The cumulative conversion over 2.5 hours of reaction time were calculated and plotted against the **1-Ru** content (**Figure 3.4**). A linear and nearly identical scaling to that of our intraparticle studies was observed suggesting that the catalyst bed has uniform contacting with the reagent.

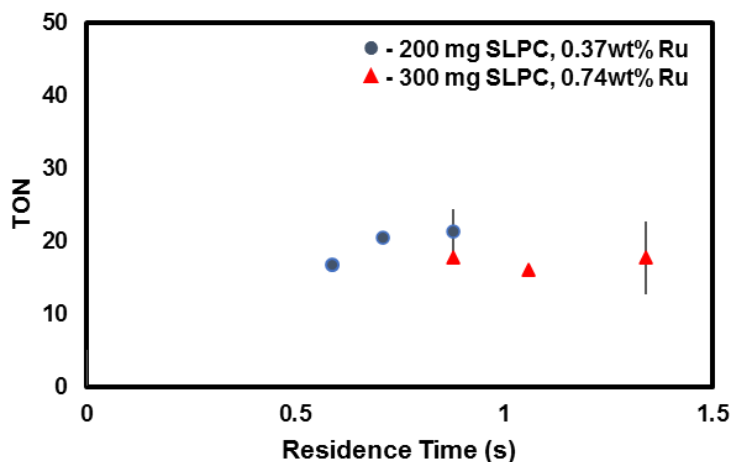


**Figure 3.5.** The plot depicts total turnovers over 2.5 hours of reaction time vs residence time over the bed at 120°C and 16 psi. N<sub>2</sub> (g) flowrates were varied between 8 – 12 mL/min. EtOH (g) flowrates were varied between 2.2 – 3.3 mL/min. The partial pressure of EtOH was held constant at 3.5 psi. Two sets of experiments were conducted with

**Figure 3.5 (cont.)** varied catalyst composition and quantity. Circles (blue) show data obtained using 200 mg of SLPC (7.4wt% PEG, 7.4wt% base, and 0.37wt% **1-Ru**). Triangles (red) show data obtained using 300 mg of SLPC (7.4wt% PEG, 7.4wt% base, and 0.74wt% **1-Ru**). Standard deviations are reported based on 3 repeat experiments for a single batch of SLPC.

Finally, we tested for interparticle mass transfer effects by varying the residence time. This was achieved by changing the ethanol and nitrogen flow rates while maintaining a constant ethanol partial pressure. In the absence of mass transfer limitations, the reagent flowrate should not affect the catalyst's activity ( $\text{TON, mol}_{\text{product}} \text{ mol}_{\text{1-Ru}}^{-1}$ ). This is showcased in **Figure 3.5**, where a constant TON of 18 is calculated regardless of residence time changes. The reported errors for the TON are, however, relatively large ( $\pm 3.5$  TON). This large fluctuation was attributed to the rapid catalyst decay in the PBR (**Figure 3.3**). Nonetheless, our systematic analysis revealed that the SLPC containing **1-Ru** was not limited by particle transport phenomena; and thus, the technique can be used to investigate the kinetics of the catalyst.

*Stabilization of 1-Ru.* The discrepancy in 1-Ru stability between our batch, CSTR and PBR experiments led us to investigate the fundamental differences between these setups. First, we lowered the reaction temperature in the PBR based on the possibility that the reaction mixture was held at a lower temperature in batch than recorded because only measurements of the bath temperature were noted. However, even reactions performed at 90°C in the PBR resulted in almost complete catalyst deactivation after 2 hours on stream (**Figure B10**). Second, we considered the effect of the continuous evaporation of volatile products in the PBR as opposed to their accumulation in batch. We performed a series of experiments, cofeeding water (by-product of the aldol condensation) and acetaldehyde (product of ethanol dehydrogenation) into the PBR to compensate for their evaporation. Co-feeding 1 mol% H<sub>2</sub>O in ethanol accelerated catalyst deactivation (**Figure 3.6**) in the PBR. Feeding an acetaldehyde-ethanol mixture increased the butanol formation rate. A 1 mol%



acetaldehyde feed doubled the reaction rate from 45 to 95 TOF h<sup>-1</sup>; and a 15 mol% acetaldehyde feed resulted in a rate of 111 TOF h<sup>-1</sup> (**Figure 3.7**). The increased rate is not only consistent with a faster rate of aldol condensation (caused by the higher acetaldehyde concentration) but also with a faster rate of the subsequent hydrogenation reaction. However, the decay in activity was comparable to the deactivation observed when using ethanol as the sole substrate. Interestingly, no unsaturated C<sub>4</sub> molecules were detected with a 1 mol% acetaldehyde feed. At an acetaldehyde concentration of 15 mol%, we observed the formation of C<sub>4</sub> unsaturated condensation intermediates, including butanal and crotonaldehyde which reached maximum rates of 39 and 9 TOF h<sup>-1</sup>, respectively (see **Figure B11** for rate profile and mass balance). Only trace quantities of crotyl alcohol were detected in the vapor phase (>0.01 mol%). In our prior study of **1-Ru**, we determined that the hydrogenation of unsaturated C=C bonds is slower than the hydrogenation of C=O bonds.<sup>23</sup> Thus, if the acetaldehyde coupling product, crotonaldehyde, were to undergo partial hydrogenation, we expected the rate of crotyl alcohol to be faster than butanal. Observing the opposite trend in the PBR, we attributed the relatively high rate of butanal formation to butanol dehydrogenation. Moreover, the low concentration of unsaturated C<sub>4</sub> intermediates (>0.7 mol%) was consistent with our report of a rapid transfer hydrogenation step in comparison to aldol condensation.<sup>23</sup> Under a high concentration of transfer agent (ethanol), C<sub>4</sub> intermediates are quickly converted to butanol.

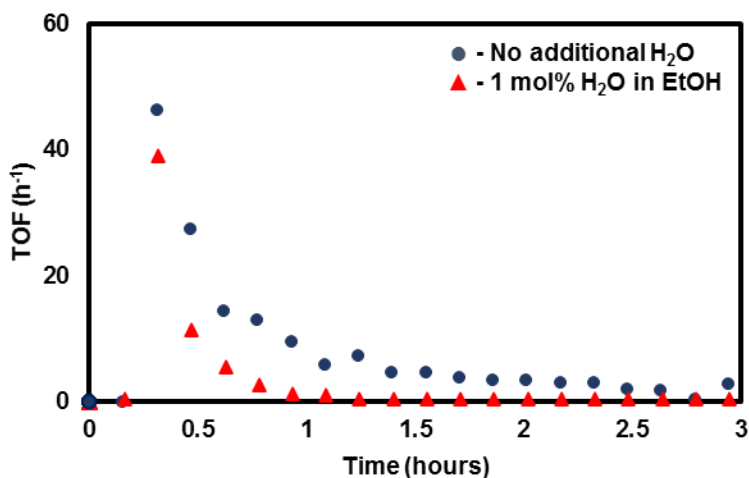


**Figure 3.6.** An EtOH/H<sub>2</sub>O mixture and N<sub>2</sub> are fed into the reactor at 4  $\mu$ L/min (l) and 8 mL/min (g) respectively at 120°C and a pressure of 16 psi ( $P_{\text{EtOH}} = 1.4$  psi). Circles (blue) indicate the activity of the SLPC (200 mg of SLPC, 7wt% base, 7wt% PEG, 0.68wt% **1-Ru**) in the absence of water. Triangles (red) indicate the activity of an identical catalyst, but in the presence of a water-ethanol feed (1 mol% water in ethanol).

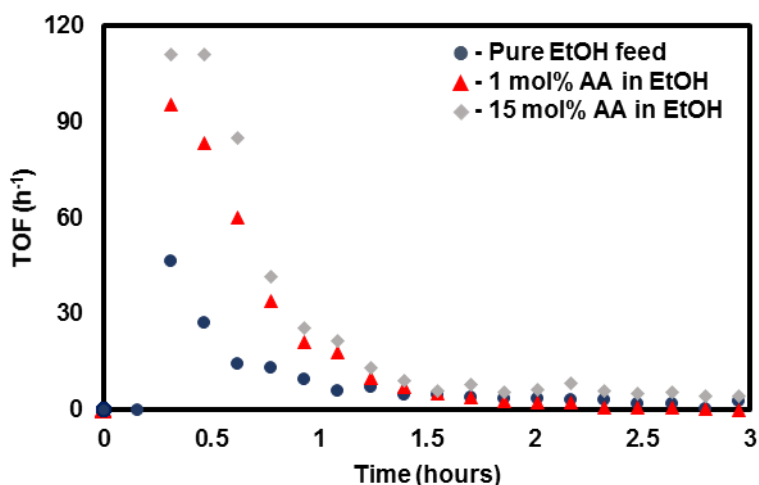


**Figure 3.7.** EtOH and N<sub>2</sub> are fed into the reactor at 4  $\mu$ L/min (l) and 8 mL/min (g) respectively at 120°C and a pressure of 16 psi. Circles (blue) indicate the activity of the SLPC (200 mg of SLPC, 7wt% base, 7wt% PEG, 0.68wt% **1-Ru**) in the absence of acetaldehyde. Triangles (red) indicate the activity of an identical catalyst, but in the presence of an acetaldehyde-ethanol feed (1 mol% acetaldehyde in ethanol). Diamonds (grey) indicate the activity in the presence of a feed that is 15 mol% acetaldehyde.

Next, we attempted to stabilize **1-Ru** through the addition of PPh<sub>3</sub> (via wet impregnation, see SLPC Synthesis section above). A SLPC containing 0.1wt% PPh<sub>3</sub> showed slower catalyst deactivation where only 42% of the maximum rate had decayed after 2 hours (**Figure 3.8**). However, this stability coincided with a decrease in butanol formation rate. Further increasing the PPh<sub>3</sub> loading to 0.46wt%, drastically decreased the rate of butanol formation (an average of 0.29 TOF h<sup>-1</sup>) while

only modestly improving stability (38% decay after 2 hours). The low TOF was rationalized by the competition for coordination to the ruthenium center between  $\text{PPh}_3$  and the substrate. The same decrease in activity was observed in batch experiments when using a high concentration of  $\text{PPh}_3$  (Figure B12).

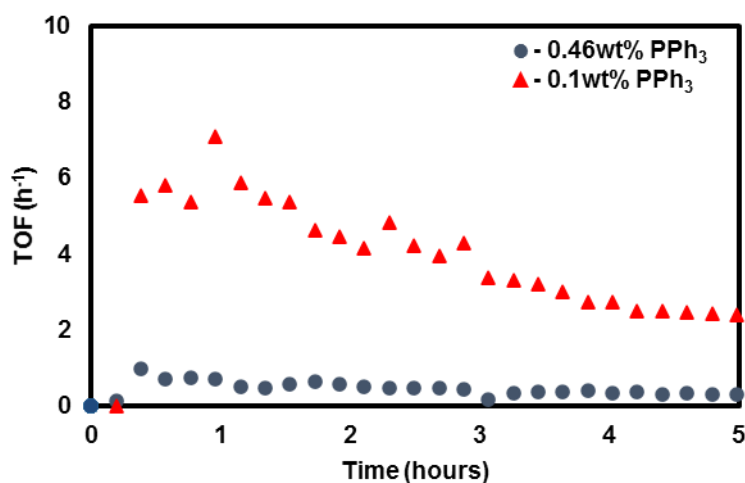


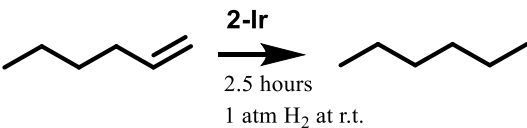
**Figure 3.8.** The plot depicts the catalyst activity against reaction time. Nitrogen and ethanol were fed at 8 mL/min and 1.25  $\mu\text{L}/\text{min}$ , respectively, into the reactor held at 120°C and 16 psi. The feed was vaporized and flown over the SLPC (300 mg SLPC, 7.4wt% base, 7.4wt% PEG and 0.36wt% **1-Ru** and various  $\text{PPh}_3$  loadings).

These failed attempts to enhance the catalytic stability of **1-Ru** in the PBR led us to compare the reaction conditions across reactor systems. Examining our reactions performed in PEG, the ethanol concentration in the polymer solution and the ratio of co-catalyst to **1-Ru** were comparable in our batch, PBR, and CSTR setups.<sup>27</sup> However, the ruthenium loading in the PBR was nearly 100 times more concentrated. We hypothesize that the deactivation of **1-Ru** is dependent on its concentration, which could explain the deactivation of **1-Ru** seen in the PBR. This conclusion is also consistent with bimolecular decomposition pathways of pincer catalysts.<sup>28</sup>

*Material Compatibility with 2-Ir.* To showcase the universality of the SLPC approach, we performed a second chemical reaction using our PBR. Specifically, we selected Crabtree's catalyst (**2-Ir**) for the hydrogenation of 1-hexene to hexane.<sup>29</sup> We first probed the catalyst's compatibility with different ingredients for the heterogenization in batch experiments

(**Table 3.2**). Acidic supports (acidic alumina and silica) were shown to be detrimental to the catalytic activity, which is consistent with the known catalyst's sensitivity to acidic protons.<sup>30</sup> We selected neutral Al<sub>2</sub>O<sub>3</sub> as the solid support, since **2-Ir** exhibited the highest activity in the presence of this additive (1030 TON, 46% conversion). **2-Ir**'s sensitivity to acidic protons led us to implement a dimethyl ether PEG (MW ~ 500 g/mol) as the polymer solvent. In batch experiments, we observed a significant increase in activity in the presence of polymer in comparison to our control (control 960 TON, PEG 2160 TON). The low activity in our control experiment is due to the poor solubility of **2-Ir** in neat hexene. In contrast, **2-Ir** was fully soluble in a PEG/hexene mixture (consistent with higher activity, 95% hexene conversion after 2 hours). Ultimately, this experiment showcased that PEG did not deactivate **2-Ir**.

**Table 3.2.** Batch hydrogenation of 1-hexene to hexane by **2-Ir** in the presence of various additives<sup>a</sup>



Entry	Additive	TON
1	Control	960
2	Basic Alumina	1000
3	Neutral Alumina	1030
4	Acidic Alumina	400
5	Silica	770
6	PEG	2160

<sup>a</sup>All reactions were carried out at room temperature in 0.74 mL of 1-hexene using 2 mg of **2-Ir** under 1 atm H<sub>2</sub>. For reactions with additives, either 1000 mg of polymer or 200 mg of support was added to the batch reactor.

**Table 3.3.** SLPC formulation and standard operating conditions for the study of **2-Ir**

<u>Catalyst Composition</u>	
Alumina	90.31wt%
PEG	9wt%
<b>2-Ir</b>	0.69wt%
<u>Reactor Conditions</u>	
N <sub>2</sub> (g)	9 mL/min
H <sub>2</sub> (g)	2 mL/min
1-hexene (g)	0.12 mL/min
Pressure	17 psi
Residence time	2.2 s
Temperature	r.t.

*Olefin hydrogenation in the PBR.* After formulating a SLPC containing **2-Ir** (via wet impregnation, see SLPC Synthesis section above), we used the catalyst to hydrogenate 1-hexene in our homemade PBR. The reaction residence time was kept short (2.2 s) to maintain low conversions. Standard operating conditions are described in **Table 3.3**. A mixed feed of gaseous 1-hexene and hydrogen diluted by a nitrogen carrier gas was flown over a SLPC containing 0.69wt% **2-Ir** at room temperature. Hexane formation was observed with a maximum TOF ( $\text{mol}_{\text{product}} \text{mol}^{-1}_{\text{2-Ir}} \text{h}^{-1}$ ) of  $\sim 140 \text{ h}^{-1}$  (7 mol% conversion) reached after 5 min on stream (**Figure 3.9**). See Appendix B for rate calculations. The activity of the catalyst decayed rapidly (89% decay in rate after 2 hours). However, this rapid deactivation is not attributed to the immobilization strategy as the instability of **2-Ir** is well established in the literature.<sup>29,30</sup> In this experiment, we showcased the conversion of 1-hexane to 1-hexene using **2-Ir** within a supported particle, accomplishing our primary goal. To provide a more detailed kinetic analysis on **2-Ir**, one must reassess transport limitations – an analysis not performed in this work – because **2-Ir** has a different intrinsic rate than **1-Ru**. Nonetheless, the successful hydrogenation reaction has demonstrated the flexibility of the SLPC approach to any homogeneously catalyzed reaction with volatile reagents and products.

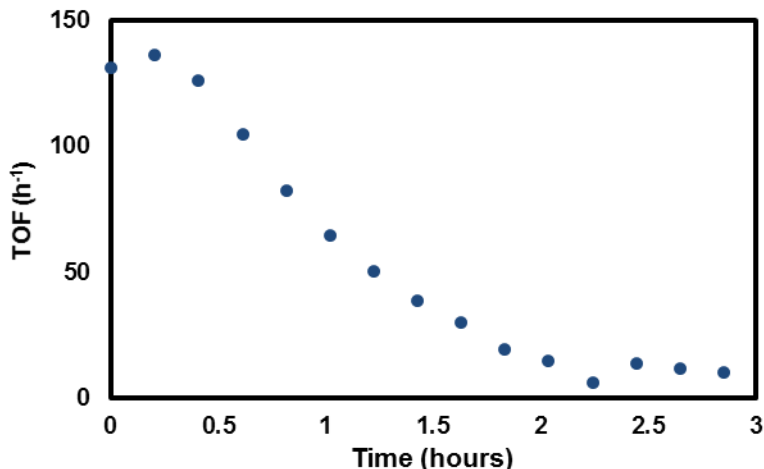


**Figure 3.9.** The plot depicts the rate of hexane production against reaction time. A mixed vapor of N<sub>2</sub>, H<sub>2</sub> and 1-hexene (9 mL/min, 2 mL/min and 0.12 mL/min respectively) are flown over the SLPC (300 mg Al<sub>2</sub>O<sub>3</sub>, 9wt% PEG, and 0.69wt% **2-Ir**) at room temperature.

### 3.4 Summary and Conclusions

Our application of the SLPC methodology to immobilize homogeneous organometallic catalysts has permitted the continuous study of **1-Ru** and **2-Ir** in a PBR. The technique involves solvating the catalyst within a non-volatile solvent (PEG) which is subsequently absorbed into a porous inorganic support. In a first case study, we showed that the SLPC immobilization components did not alter the chemical structure of **1-Ru**. However, significant decay in catalytic rate was observed during ethanol coupling experiments in flow. The primary cause of catalyst deactivation is neither temperature decomposition nor the selective evaporation of key reaction intermediates. The addition of excess ligand (PPh<sub>3</sub>) to the SLPC formulation containing **1-Ru** modestly improves the stability of catalyst at the expense of catalytic activity (ligand-substrate competition). We hypothesize that **1-Ru** instability is due to high catalyst concentration within the polymer coating. Moreover, we also extended the SLPC methodology to the hydrogenation of 1-hexene where the catalyst was shown to be active for multiple hours on stream. Our implementation of this technique serves to inspire the adoption of advanced reactor engineering strategies for the study of homogeneous catalysts.

### 3.5 References

- (1) Li, C.; Liu, Y. *Bridging Heterogeneous and Homogeneous Catalysis*; Can, L., Yan, L., Eds.; Wiley-VCH Verlag GmbH & Co. KGaA: Weinheim, Germany, 2014.
- (2) García-García, P.; Müller, M.; Corma, A. MOF Catalysis in Relation to Their Homogeneous Counterparts and Conventional Solid Catalysts. *Chem. Sci.* **2014**, 5 (8), 2979.
- (3) Yang, D.; Gates, B. C. Catalysis by Metal Organic Frameworks: Perspective and Suggestions for Future Research. *ACS Catal.* **2019**, 9 (3), 1779–1798.
- (4) Lee, J.; Farha, O. K.; Roberts, J.; Scheidt, K. A.; Nguyen, S. T.; Hupp, J. T. Metal–organic Framework Materials as Catalysts. *Chem. Soc. Rev.* **2009**, 38 (5), 1450.
- (5) Genna, D. T.; Wong-Foy, A. G.; Matzger, A. J.; Sanford, M. S. Heterogenization of Homogeneous Catalysts in Metal–Organic Frameworks via Cation Exchange. *J. Am. Chem. Soc.* **2013**, 135 (29), 10586–10589.
- (6) Chauvin, Y.; Commereuc, D.; Dawans, F. *Polymer Supported Catalysis*, 5th ed.; Pergamon Press: France, Rueil-Malmaison-Cedex, 1977.
- (7) Hübner, S.; de Vries, J. G.; Farina, V. Why Does Industry Not Use Immobilized Transition Metal Complexes as Catalysts? *Adv. Synth. Catal.* **2016**, 358 (1), 3–25.
- (8) Jones, C. W. On the Stability and Recyclability of Supported Metal–Ligand Complex Catalysts: Myths, Misconceptions and Critical Research Needs. *Top. Catal.* **2010**, 53 (13–14), 942–952.
- (9) Hintermair, U.; Franciò, G.; Leitner, W. Continuous Flow Organometallic Catalysis: New Wind in Old Sails. *Chem. Commun.* **2011**, 47 (13), 3691–3701.
- (10) Cole-Hamilton, D. J. Homogeneous Catalysis--New Approaches to Catalyst Separation,

- Recovery, and Recycling. *Science* (80-. ). **2003**, 299 (5613), 1702–1706.
- (11) Zhao, F.; Fujita, S.; Arai, M. Developments and Applications of Supported Liquid Phase Catalysts. *Curr. Org. Chem.* **2006**, 10 (13), 1681–1695.
  - (12) Tundo, P.; Perosa, A. Multiphasic Heterogeneous Catalysis Mediated by Catalyst-Philic Liquid Phases. *Chem. Soc. Rev.* **2007**, 36 (3), 532–550.
  - (13) Yasuda, T.; Uchiage, E.; Fujitani, T.; Tominaga, K. ichi; Nishida, M. Reverse Water Gas Shift Reaction Using Supported Ionic Liquid Phase Catalysts. *Appl. Catal. B Environ.* **2018**, 232 (March), 299–305.
  - (14) Riisager, A.; Fehrmann, R.; Haumann, M.; Wasserscheid, P. Supported Ionic Liquid Phase (SILP) Catalysis: An Innovative Concept for Homogeneous Catalysis in Continuous Fixed-Bed Reactors. *Eur. J. Inorg. Chem.* **2006**, 2006 (4), 695–706.
  - (15) Mehnert, C. P.; Mozeleski, E. J.; Cook, R. A. Supported Ionic Liquid Catalysis Investigated for Hydrogenation Reactions. *Chem. Commun.* **2002**, No. 24, 3010–3011.
  - (16) Naicker, L.; Friedrich, H. B.; Govender, A.; Mohlala, P. The Effect of Ionic Liquid on Alumina Supported Copper Catalysts for the Competitive Hydrogenation of Octanal in the Presence of Octene. *Appl. Catal. A Gen.* **2018**, 562 (November 2017), 37–48.
  - (17) Zhang, M.; Ettelaie, R.; Yan, T.; Zhang, S.; Cheng, F.; Binks, B. P.; Yang, H. Ionic Liquid Droplet Microreactor for Catalysis Reactions Not at Equilibrium. *J. Am. Chem. Soc.* **2017**, 139 (48), 17387–17396.
  - (18) Peng, J.; Li, J.; Bai, Y.; Qiu, H.; Jiang, K.; Jiang, J.; Lai, G. Ionic Liquid (Molten Salt): Thermoregulated Catalyst Support for Catalytic Hydrosilylation Process. *Catal. Commun.* **2008**, 9 (13), 2236–2238.
  - (19) Kukawka, R.; Pawlowska-Zygarowicz, A.; Dzialkowska, J.; Pietrowski, M.; Maciejewski,



- H.; Bica, K.; Smiglak, M. Highly Effective Supported Ionic Liquid-Phase (SILP) Catalysts: Characterization and Application to the Hydrosilylation Reaction. *ACS Sustain. Chem. Eng.* **2019**, 7 (5), 4699–4706.
- (20) Brünig, J.; Csendes, Z.; Weber, S.; Gorgas, N.; Bittner, R. W.; Limbeck, A.; Bica, K.; Hoffmann, H.; Kirchner, K. Chemoselective Supported Ionic-Liquid-Phase (SILP) Aldehyde Hydrogenation Catalyzed by an Fe(II) PNP Pincer Complex. *ACS Catal.* **2018**, 8 (2), 1048–1051.
- (21) Hatanaka, M.; Yasuda, T.; Uchiage, E.; Nishida, M.; Tominaga, K. Continuous Gas-Phase Hydroformylation of Propene with CO<sub>2</sub> Using SILP Catalysts. *ACS Sustain. Chem. Eng.* **2021**, 9 (35), 11674–11680.
- (22) Tseng, K.-N. T.; Lin, S.; Kampf, J. W.; Szymczak, N. K. Upgrading Ethanol to 1-Butanol with a Homogeneous Air-Stable Ruthenium Catalyst. *Chem. Commun.* **2016**, 52 (14), 2901–2904.
- (23) Wang, N. M.; Dillon, S.; Guironnet, D. Mechanistic Investigations on a Homogeneous Ruthenium Guerbet Catalyst in a Flow Reactor. *React. Chem. Eng.* **2022**.
- (24) Gagne, R. R.; Marks, D. N. Ruthenium Complexes of 1,3-Bis (2-Pyridylimino) Isoindolines as Alcohol Oxidation Catalysts. *Inorg. Chem.* **1984**, 23 (1), 65–74.
- (25) Koros, R. M.; Nowak, E. J. A Diagnostic Test of the Kinetic Regime in a Packed Bed Reactor. *Chem. Eng. Sci.* **1967**, 22, 31916.
- (26) Madon, R. J.; Boudart, M. Experimental Criterion for the Absence of Artifacts in the Measurement of Rates of Heterogeneous Catalytic Reactions. *Ind. Eng. Chem. Fundam.* **1982**, 21 (4), 438–447.
- (27) For Batch Reactions, the [EtOH] in PEG Is 0.87 M. This Value Was Calculated Using

Initial Substrate Loadings. Under Flow in Our PBR and CSTR, the [EtOH] Is ca. 0.25 M. This Value Was Determined by Simulating the VLE for a PEG/EtOH Mixture in CHEMCAD(SRK).

- (28) Choi, J.; MacArthur, A. H. R.; Brookhart, M.; Goldman, A. S. Dehydrogenation and Related Reactions Catalyzed by Iridium Pincer Complexes. *Chem. Rev.* **2011**, *111* (3), 1761–1779.
- (29) Crabtree, R. Iridium Compounds in Catalysis. *Acc. Chem. Res.* **1979**, *12* (9), 331–337.
- (30) Xu, Y.; Mingos, D. M. P.; Brown, J. M. Crabtree's Catalyst Revisited; Ligand Effects on Stability and Durability. *Chem. Commun.* **2008**, *44* (2), 199–201.

## CHAPTER 4: Tandem Homogeneous Flow Catalysis for Selective Polyethylene

### Depolymerization

#### 4.1 Introduction

Plastic pollution poses one of the most pressing environmental challenges in our generation. Currently, only 30% of all plastic ever produced is in active use, and the remaining 70% amounts to nearly 6300 million metric tons of waste. Of this waste, approximately 12% has been incinerated, 9% has been recycled, but an overwhelming 79% has been gathered in landfills or other surroundings.<sup>1</sup> Undoubtedly, this enormous quantity of non-biodegradable material has had detrimental effects on our ecosystems, wildlife, and well-being.<sup>2-5</sup> Considering the projected increase in polymer production (12000 million metric tons by 2050),<sup>1</sup> we must develop and adopt new strategies to address the ever-growing quantity of plastic waste.

Polyolefins (polypropylene - PP and polyethylene - PE) accounted for almost 50% of the polymer production worldwide in 2018, and their extensive application in single-use products only exacerbates our current conundrum (**Figure 4.1**).<sup>6</sup> As one of the largest contributors to plastic waste, polyolefins are the primary focus of the research developments in this dissertation. Specifically, within this chapter, we discuss the implementation of three tandem catalytic reactions for the selective chemical depolymerization of polyethylene to monomer (propylene and butadiene). To further contextualize our work, we provide an overview of polyethylene recycling strategies. These recycling efforts can be broadly divided into three approaches: mechanical, energy recovery, and chemical.<sup>7,8</sup>

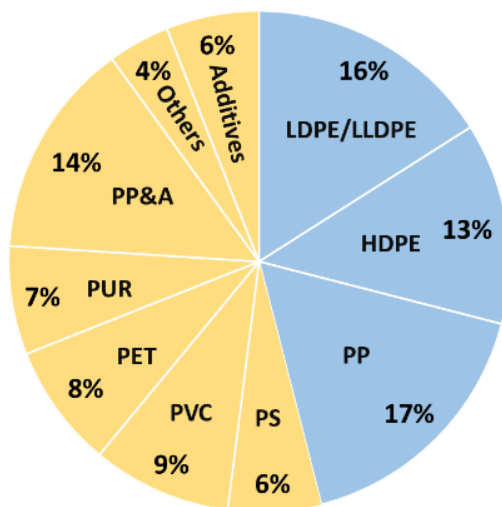


**Figure 4.1.** Breakdown of polymer production worldwide. Blue shaded portions depict the fraction dedicated to polyolefins (Source: Geyer 2017).<sup>1</sup>

## 4.2 Overview of Polyethylene Recycling Strategies

*Mechanical Recycling.* Mechanical recycling is only effective for thermoplastics (PP, PE, etc.). This process begins with the collection of polymers from municipal waste. Afterward, the polymers must be separated from contaminants and segregated according to the resin type; this requires sophisticated identification systems (e.g., spectroscopy, density-based separations, imaging, etc.) in addition to physical separations (sorting, washing, etc.).<sup>9</sup> After collection and sorting, the isolated polymer is compounded and pelletized.<sup>7</sup> Generally, this step is performed using either a twin- or single-screw extruder and a granulator to yield the recycled polymer product. However, thermo-mechanical degradation during reprocessing and impurities within the recycled plastic results in a material with lesser properties when compared to virgin polymer (downcycling).<sup>10</sup> Overall, this approach extends the lifetime of polymer materials for a relatively short duration at a low cost, but the production of new virgin plastics remains a necessity.

*Energy Recovery.* Another approach to recycling is energy recovery (e.g., waste incineration), and the goal of this strategy is two-fold: (1) reduction in the volume of solid waste and (2) generation of energy from exothermic combustion. This method is quite successful in volume reduction;

however, it is challenged by the release of greenhouse gasses and toxins in addition to the formation of residual ash.<sup>7,11-14</sup> To achieve the second goal, many of these systems are designed to recover energy in the form of heat (steam/electricity); however, the energy benefit does not fully compensate for the initial input required in the production of virgin plastic.<sup>15</sup> Overall, this strategy has clear benefits to landfilling, but it remains a non-sustainable operation.

*Chemical Recycling.* The final method, chemical recycling, aims to transform a finished plastic product into new raw material, ideally, of higher value (upcycling). In this section of the review, we discuss several chemical recycling approaches including industrially applied strategies and recently developed technologies from academic literature.

*Chemical Recycling (Commercial Strategies).* Pyrolysis is one chemical recycling strategy that has found some commercial success.<sup>7</sup> Pyrolysis (i.e., partial combustion followed by cracking) of polymer mixtures (including PE, PP, PS, PET and etc.) predominantly converts the long polymer chains into pyrolysis oil under elevated temperatures (ca. 350-600°C).<sup>7</sup> The composition of the product oil includes a mixture of shorter-chained aliphatic hydrocarbons and aromatics that are usually recovered as a liquid or semi-solid fraction.<sup>16</sup> This complex mixture arises from random C-C scission and aromatization of the polymer fragments, and it does not have direct applications without additional treatment. As a hydrocarbon product, it can be processed similarly to crude oil, allowing us to reuse current infrastructure. The separated product fractions can be used as fuel or further converted to new chemicals.<sup>17,18</sup>

Gasification is another strategy that has been employed on an industrial scale.<sup>7,19</sup> Under elevated temperatures (ca. 600-850°C) in the presence of oxygen (often air but occasionally pure O<sub>2</sub>), gasification predominantly converts polymer to syngas (CO, and H<sub>2</sub>),<sup>11</sup> which is commonly used as a building block to synthesize new value-added products such as methanol, ammonia, etc.<sup>20,21</sup>

Gasification is challenged by high energy inputs and the formation of particulate impurities (ash, char, etc.). Thus, extensive cleaning of the product stream is necessary prior to downstream processing.<sup>22,23</sup>

*Chemical Recycling (New Technologies in the Polyolefin Sphere)*. In addition to commercialized strategies, new approaches to polyethylene depolymerization have been reported in academic literature, and one example is hydrogenolysis. Hydrogenolysis involves (mostly) random C-C scission of polymer chains in the presence of H<sub>2</sub> to produce a mixture of alkanes.<sup>24–28</sup> Notably, the catalysts reported, thus far, have shown some preference for the cleavage of terminal C-C bonds to form methane. To address the inherently low-value of the alkane product, hydrogenolysis has also been coupled with aromatization to produce higher-valued long-chained alkyl aromatics.<sup>29</sup> As a whole, these methods are effective at degrading polyethylene into shorter-chained products, but control over the molecular weight distribution (MWD) remains a technical challenge.

One final strategy of discussion within this review is tandem dehydrogenation, isomerization, and cross metathesis. This methodology is based upon a catalytic cross alkane metathesis process initially developed by the Goldman and Huang groups.<sup>30–32</sup> A dehydrogenation catalyst is used to introduce an olefinic group to an n-alkane and to a polyethylene chain. Whereafter, the functionalized molecules undergo a series of tandem isomerization and metathesis reactions which redistribute the olefins while also exchanging their alkene fragments. In this cascade reaction, the polymer distribution is averaged with the shorter n-alkene to produce a new distribution with a reduced molecular weight. This strategy was employed to effectively shift the MWD of polyethylene towards lighter products within the range of fuels and waxes.<sup>33,34</sup> But similar to hydrogenolysis, there is limited control over reaction selectivity.

*Summary.* Thus far, we have discussed several recycling strategies, and each of these techniques has its benefits and challenges. Realistically, a holistic approach to polymer recycling is necessary to address plastic waste as a single solution does not yet exist. But, in comparison to other technologies, chemical upcycling of plastic waste offers an opportunity to significantly alter the linear life cycle of plastics. Allured by the plausibility of true recycling circularity, the work in this dissertation is solely focused on the development of a new selective chemical depolymerization strategy that yields a monomer necessary to produce commodity plastics. Currently, many chemical recycling methods suffer from poor selectivity (except for gasification). Their mechanisms proceed through random scission, and in the context of polymer distributions, random scission of a high dispersity starting material will invariably lead to a product with a similarly wide distribution. Thus, selectively forming and isolating monomer products from chemical depolymerization becomes non-trivial. Our work seeks to directly address this limitation, and herein, we disclose the development of three tandem catalytic reactions for the selective upcycling of polyethylene to monomer (propylene and butadiene).

### **4.3 Tandem Catalysts in Flow for Polyethylene Upcycling**

Our polyethylene upcycling strategy involves a catalytic reaction cascade that consists of: (1) transfer dehydrogenation to introduce unsaturation ( $C=C$ ) in the polymer backbone; (2) ethenolysis to perform  $C=C$  scission; and (3) isomerization of vinyl-terminated polymer fragments to internal olefins and subsequent ethenolysis (**Figure 4.2**). By reacting polyethylene with an excess of ethylene, we drive the reaction equilibrium to selectively produce propylene and butadiene as the predominant and desired products. Thus far, this strategy has only been explored via simulation. Within this modeling effort, a set of differential equations are derived describing the tandem isomerization and metathesis of functionalized PE (100 units long) under excess

ethylene. The authors disclose a numerical and analytical solution of these equations, which model the progressive decrease in the polymer MWD as a function of time. After complete depolymerization of the polymer, propylene is produced as the sole product.<sup>35</sup> In this dissertation, we seek to develop this strategy via lab-scale experimentation.

In a pioneering study, we built off of our group's existing expertise on homogeneous Grubbs' metathesis catalysts.<sup>36</sup> These catalysts were implemented in conjunction with various isomerization and dehydrogenation catalysts to provide proof of concept experimentation (conversion of polyethylene into propylene) and to generate an understanding of the tandem reaction kinetics. The work in this dissertation is predominantly focused on the development of the tandem metathesis and isomerization reactions, and throughout this chapter, the tandem application of these reactions will be referred to as "depolymerization".

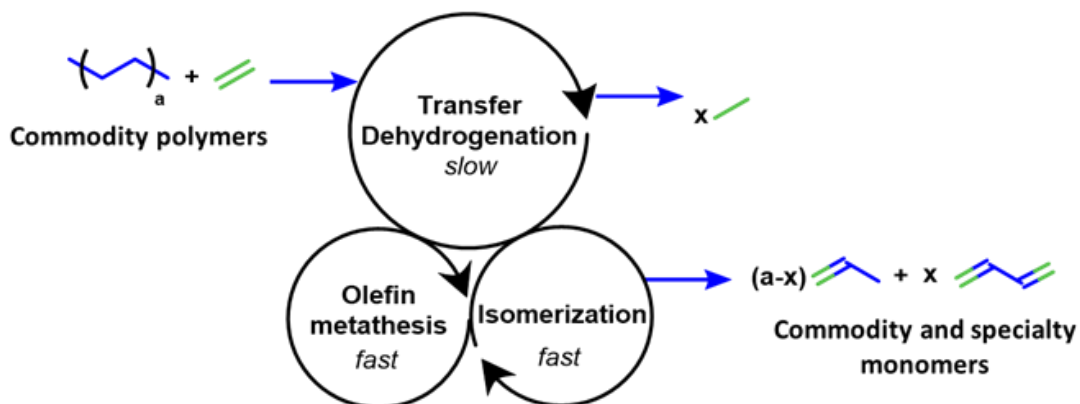


**Figure 4.2.** Tandem catalysis strategy for polyolefin depolymerization.

#### 4.4 Reactor Build, Methods, and Calculations

*Flow Reactor Design and Build.* Compared to a traditional batch reactor, the use of a flow device for the development of this chemistry offers a few advantages. First, a replenishing flow of ethylene allows us to maintain a high concentration ethylene relative to polymer. Second, if provided a stable catalytic system, the continuous removal of short olefin products from the reaction mixture helps drive the equilibrium-limited cascade toward the complete consumption of





*Calculation of Gaseous Molar Flows Using our Flow Device.* Gaseous molar flow rates are calculated using ethylene as the internal standard whose delivery is controlled using a mass flow controller. Ethylene is flown in excess (thus  $\dot{n}_T \sim \dot{n}_{C2}$ ) and its conversion is kept low (>7 mol%) to ensure an accurate estimation of product formation rates. The mole fraction for a species of interest ( $x_{Ci}$ ) can be calculated using the GC output ( $A_i$ ) and tabulated GC response factors (method of internal standards, for RFs see **Appendix C**) using the equation below (**Equation 4.1**). Multiplying the mole fraction by the molar ethylene feed rate provides an estimation of product formation ( $\dot{n}_{Ci}$ , **Equation 4.2**). These response factors are identical for flow and batch experiments.

$$x_{Ci} = \frac{\left[ \left( \frac{A_{Ci}}{A_{C2}} \right) \left( \frac{RF_{C2}}{RF_{Ci}} \right) \right]}{\sum \left[ \left( \frac{A_i}{A_{C2}} \right) \left( \frac{RF_{C2}}{RF_{Ci}} \right) \right]}$$

**Equation 4.1.** Gaseous mole fraction of hydrocarbon species ( $x_{Ci}$ ).

$$\dot{n}_{Ci} = \dot{n}_T x_{Ci} = \dot{n}_{C2} x_{Ci}$$

**Equation 4.2.** Molar flowrate of hydrocarbon species  $\dot{n}_{Ci}$  using ethylene (fed in excess) as an internal standard.

*Estimating Polymer Conversion Using Flow Data.* Integrating the molar flowrate ( $\dot{n}_{Ci}$ ) of each species using the trapezoidal rule within a flow reaction profile (see **Equation 4.3**) affords the total moles of product formed ( $n_{Ci}$ ) for a given experiment. This cumulative quantity is then compared to the initial polymer loading ( $m_{PE,o}$ ) to estimate polyethylene conversion by mass. Aside from the first molecule of olefin product formed (the 1<sup>st</sup> cleavage event), the olefins produced theoretically contain two carbons from ethylene; thus, a weighting factor is introduced that conservatively estimates the mass conversion of PE (see **Equation 4.4**).

$$n_{ci} = \int \dot{n}_{ci} = \Sigma \left( \left( \frac{1}{2} \right) (\dot{n}_{ci} |_{t} + \dot{n}_{ci} |_{t+\delta}) \delta \right)$$

$\vdots$   
Rate at time  $t$ 
 $\vdots$   
Rate at time  $t+\delta$ 
 $\vdots$   
Timestep (sampling)

**Equation 4.3.** Cumulative olefin formation is calculated using the trapezoidal rule described above.

$$WT\% = \frac{\Sigma \left( 100 \left( \frac{i-2}{i} \right) n_{ci} MW_{ci} \right)}{m_{PE,o}}$$

$\vdots$   
Initial PE loading
 $\vdots$   
Weighting factor

**Equation 4.4.** Conservative estimate of polymer consumption by weight, assuming each molecule of olefin formed contains two carbons from ethylene. "i" represents of the number of carbon units within the olefin.

*Selectivity Calculations.* Selectivity is determined by calculating the ratio of cumulative propylene formed to the sum of other volatile olefin products ( $S_{C3}$ , **Equation 4.5**). This value can be averaged over reaction time "t" or evaluated for each individual timepoint within a continuous flow experiment. This calculation for selectivity only considers extracted gaseous products from the continuous reactor.

$$S_{C3} = \frac{\dot{n}_{C3}}{\Sigma \dot{n}_{Ci}}$$

**Equation 4.5.** Selectivity for propylene that only considers the extracted gaseous products.

## 4.5 Results and Discussion

*Tandem Homogeneous Catalysts in Batch.* Prior to the implementation of the flow reactor, we first established compatibility between a pair of homogeneous catalysts in batch reactions. Specifically, a bis-cyclic alkyl amino carbene ruthenium Grubbs metathesis catalyst (**Ultracat**) known for its rapid ethenolysis activity was used in conjunction with a ruthenium phosphine isomerization

catalyst (**2-Ru**,  $\text{Ru}[\text{PPh}_3]_3[\text{CO}][\text{Cl}]\text{H}$ ).<sup>37,38</sup> **Ultracat** was purchased commercially and **2-Ru** was synthesized according to literature procedure (refer to **Appendix C**).<sup>39</sup>

Using these molecular catalysts as handles to tune the relative reaction rates, we studied tandem isomerization and metathesis using 1-decene as a model substrate (refer to **Appendix C** for reaction conditions). In a first set of batch experiments, we probed for compatibility between the two catalysts (**Figure C3**). The self-metathesis of 1-decene mediated by **Ultracat** approached a maximum conversion (ca. 80 %) after 1.5 hours of reaction time with or without the addition of the **2-Ru**. The matching conversion rates suggested that the isomerization catalyst did not inhibit the metathesis catalyst. To assess whether alkene substrates were isomerized, the liquid products distribution was analyzed by GC after 3 hours of reaction time (**Figure C4**). In the absence of **2-Ru**, the predominant species produced were the 1-decene self-metathesis products, octadecene and ethylene.  $\text{C}_{18}$  accounted for 90 mol% of the condensed phase (volatile products were not collected) where the remaining balance consisted of  $\text{C}_{16}$  (0.5 mol%),  $\text{C}_{17}$  (2 mol%), and unreacted starting material (7.5 mol%). In contrast, upon the addition of **2-Ru** we observed increased formation of  $\text{C}_{16}$  (3 mol%) and  $\text{C}_{17}$  (21 mol%) products relative to  $\text{C}_{18}$  (65 mol%), suggesting that some of the starting material had been isomerized. To better visualize the evolution of the product distribution, we report the liquid composition of the reaction as a function of time (**Figure 4.4**). Under standard tandem catalytic conditions, a 1 mL aliquot of the reaction mixture is sampled every 0.5 hours as indicated by the colored bar graph. From this experimental data, we observe a rapid initial consumption of  $\text{C}_{10}$  (77.5 mol% conversion) within the first 0.5 hours of reaction. Subsequent samples or snapshots of the distribution show slowed consumption of  $\text{C}_{10}$ . Overall, the data depicted a bi-modal distribution of starting material and product that was consistent with a stalled reaction cascade. This conclusion led to two implications. First, it suggested that the reaction was

proceeding with limited isomerization, which could lead to unproductive and reversible self-metathesis reactions. Second, it also implied that the cross-metathesis of two internal olefins was significantly slower than the cross-metathesis of terminal olefins.

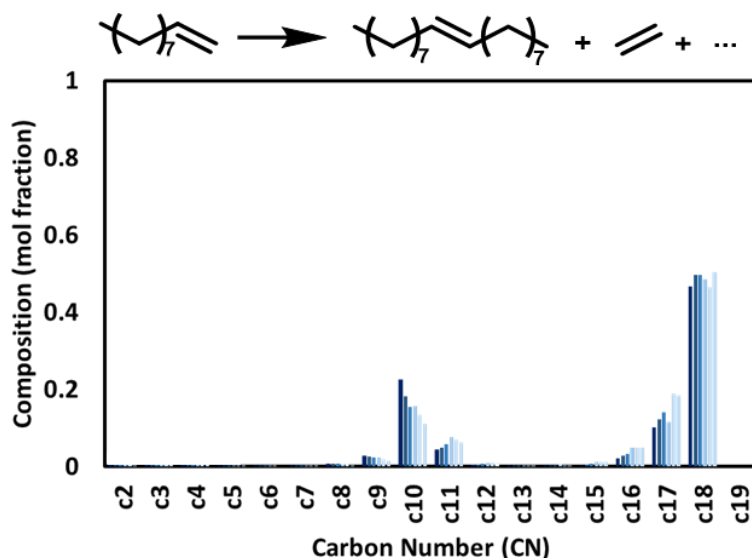


**Figure 4.4.** Products distribution of the condensed phase (volatile products were not collected) for tandem isomerization and metathesis of 1-decene catalyzed by 1.57 mM **Ultracat** and 3.5 mM **2-Ru** in 24 mL of 1-decene. Each colored bar (dark blue to light blue) represents a sample of the reaction mixture taken after an additional 0.5 hours of reaction time.

In attempts to accelerate the isomerization rate relative to metathesis, we decreased the loading of **Ultracat**. By slowing the metathesis reaction, we expected to see increased isomerization of the starting material and thus a broader products distribution. Under otherwise standard conditions, we collected data over time for three reactions with different concentrations of **Ultracat** (**Figure 4.5**, 1.57, 0.39, and 0.098 mM), and we compared the ratio of C<sub>18</sub> to other high molecular weight products ( $C_{18}/[C_{15} + C_{16} + C_{17} + C_{19}]$ ) after 3 hours of reaction time. This value decreased from 2.0 to 0.91 and finally to 0.84 as the loading of the metathesis catalyst was reduced, which showcased increased isomerization of alkene substrates; but despite these improvements, decreasing **Ultracat** loading invariably resulted in a bi-modal distribution of starting material and higher molecular weight product. From this observation, we concluded that our decrease in the

metathesis rate relative to isomerization was only marginally beneficial towards broadening of the product distribution.

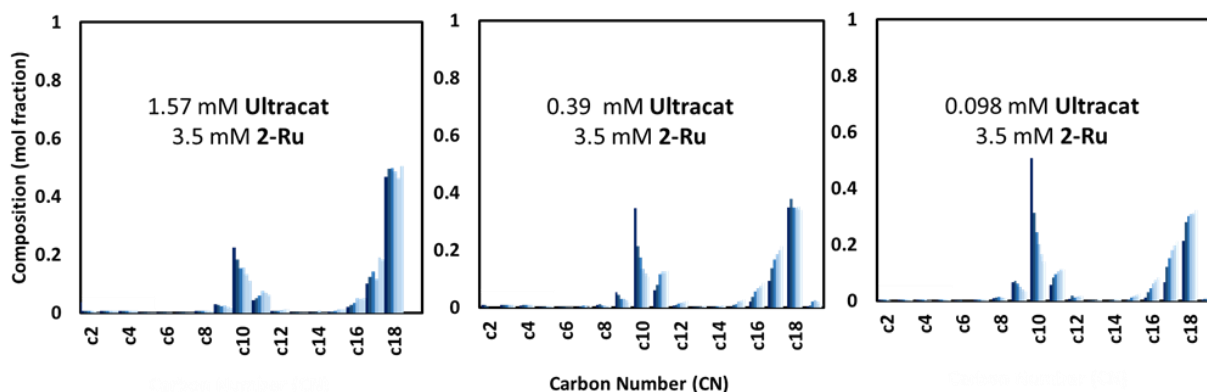


**Figure 4.5.** Products distribution for tandem isomerization and metathesis of 1-decene (24 mL) catalyzed by **Ultracat** (variable concentration) and **2-Ru**. Each colored bar (dark to light) represents a sample of the reaction mixture taken after an additional 0.5 hours of reaction time.

*Tandem Catalysts in Flow.* The rapid metathesis activity observed in the batch experiments provided evidence of **Ultracat**'s compatibility with the isomerization catalyst. Thus, we continued with our developments to establish proof of principle, and we studied the tandem metathesis and isomerization of 1-decene and ethylene using our flow reactor. In this reaction, 6 mL of 1-decene, 0.0016 mM of **Ultracat**, and 0.0075 mM of **2-Ru** were loaded into the CSTR. Afterwards, the reactor vessel is charged with 70 PSI of ethylene at room temperature and heated to 50°C. Under a continuous flow of ethylene gas (15 mmol/h), we automatedly sample the system's gaseous effluent stream every half hour, and we report light olefin formation over time (**Figure 4.6**). The only detected products of this flow reaction were butene and propylene produced at a maximum rate of 0.1 and 1.1 mmol/h, respectively. The formation of these products demonstrated the successful and selective conversion of model alkene to propylene through the proposed tandem catalytic route. At the maximum conversion rate, the gaseous phase consisted of nearly 10 mol% propylene (89 mol% unreacted ethylene), although the reaction was not stable where activity decayed by 82% after 7 hours on stream. Moreover, GC analysis of the condensed phase revealed

conversion (58 mol%) of 1-decene to C<sub>16</sub>-C<sub>18</sub> products, showcasing that metathesis of terminal olefins remained rapid in the presence of ethylene.

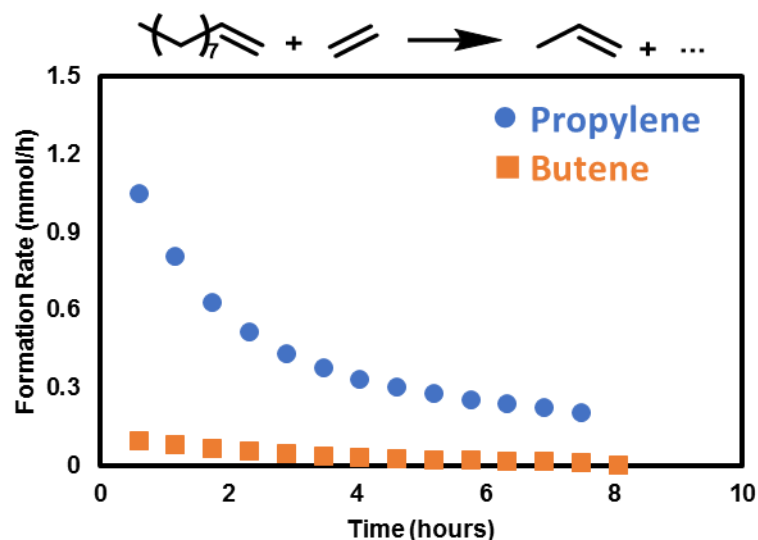


**Figure 4.6.** Continuous flow reactor data depicting the formation rate of olefin products in an ethylene and 1-decene cross-metathesis reaction as a function of time.

After showcasing successful formation of propylene upon the reaction of 1-decene and ethylene, we extended our study to reactions with polyethylene. A low molecular weight olefin-terminated polyethylene (MW~870 g/mol, refer to **Appendix C** for synthetic details) was used as starting material. The low MW increases the concentration of olefinic groups in the polymer chain, and the solution has a lower viscosity.<sup>40</sup> Propylene was here again detected as the predominant product formed at a maximum rate of 0.8 mmol/h while butene and pentene were detected in lesser quantities (**Figure 4.7**, >0.1 mmol/h). Integrating the olefin formation rate over time, we calculated a polyethylene conversion of 2.5wt% (see Reactor Build, Methods, and Calculations section). This result, ultimately, demonstrated our successful application of tandem homogeneous metathesis and isomerization catalysts to form propylene from polyethylene.

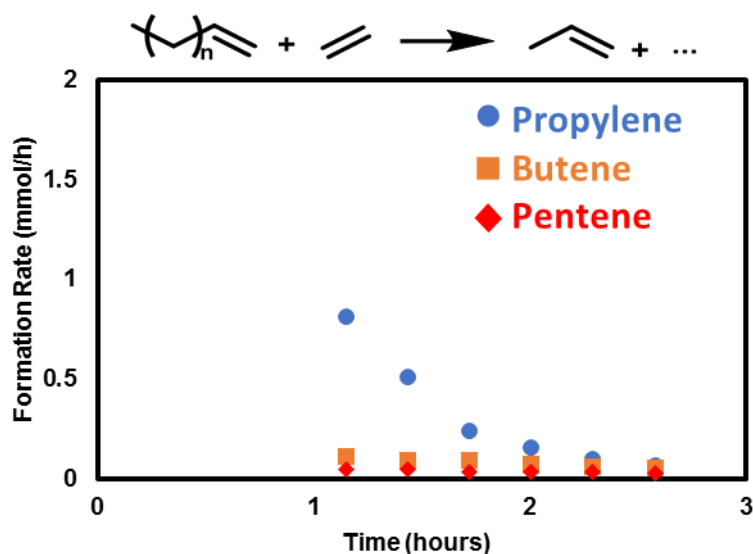


**Figure 4.7.** Continuous flow reactor data depicting the formation rate of olefin products upon tandem metathesis and isomerization of polyethylene. In this experiment, 0.0017 mM of **Ultracat**, 0.0039 mM of **2-Ru**, and 0.2 mM of polyethylene were solvated in 4 mL of Dowtherm A. Ethylene was fed continuously (15 mmol/h) into the flow reactor held at 80 PSI and 90°C while the gaseous effluent stream was analyzed.

*Continuous Addition of **Ultracat**.* Although we successfully formed propylene from polyethylene, the conversion of polymer was low as the rate of desired olefins rapidly decayed during the reaction (**Figure 4.7**). We first suspected that **Ultracat** may be deactivating under our conditions since the catalyst is known to optimally operate within a modest temperature range (40 to 85°C).<sup>38</sup> Thus, to assess the stability of the metathesis catalyst, we installed a syringe pump to deliver a liquid solution of **Ultracat** precisely and continuously into our CSTR. We reacted polyethylene (MW~2000 g/mol) in our flow reactor under a co-flow of ethylene and **Ultracat** (solvated in toluene) to produce propylene and butene at a maximum rate of 0.035 and 0.037 mmol/h, respectively (>1wt% PE conversion, see **Figure 4.8** for reaction conditions). Notably, the olefin formation rate decayed rapidly despite the continuous addition of fresh **Ultracat**. This observation suggested that decomposition of the metathesis catalyst was not the predominant cause of product rate decay. Thus, we turned to an investigation of the isomerization reaction and its impact on the depolymerization.



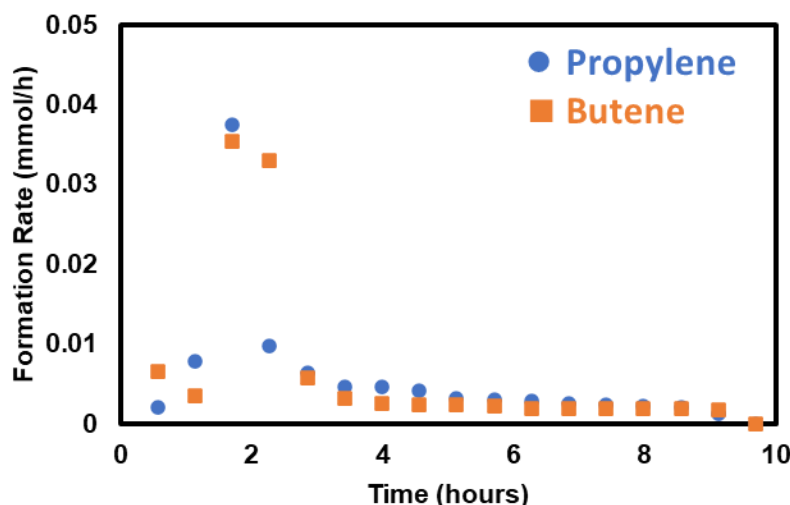


**Figure 4.8.** Continuous flow reactor data depicting the formation rate of olefin products upon tandem metathesis and isomerization of polyethylene. A 0.01 M solution of **Ultracat** in toluene (0.01 mL/min) was co-fed with ethylene (5 mmol/h) into our CSTR setup held at 85°C and 60 PSI. The reactor contained 150 mg of polyethylene.

We augmented the isomerization rate by introducing a heterogeneous dehydrogenation and isomerization catalyst (Pt5wt%-Re5wt%-SiO<sub>2</sub>, **PtRe-Si**) supplied by Dow Chemical. The catalyst was added to the CSTR in addition to polyethylene (MW~2000 g/mol, see **Appendix C** for reaction conditions).<sup>26</sup> Under otherwise identical flow conditions, the batch addition of **PtRe-Si** nearly doubled the yield of propylene from 0.035 to 0.08 mmol (evaluated over the first 4 hours of catalysis, 1wt% PE conversion); however, we continued to observe a decay in product formation rate (**Figure C5**). Further tuning the depolymerization cascade, we decreased the feed rate of **Ultracat** (0.005 mL/min, **Figure C6**) to slow down the metathesis reaction relative to isomerization. Interestingly, despite altering the rate of metathesis, we saw no change to the steady-state propylene production rate (0.0035 mmol/h). This pair of experiments offered two pieces of insight (1) product formation was insensitive to the concentration of metathesis catalyst and (2) augmentations to the isomerization rate (addition of **PtRe-Si**) had increased product yield. Based on these observations, we concluded that the depolymerization cascade was isomerization limited. Thus, we sought to improve the rate and stability of the isomerization reaction. Accordingly, we replaced **PtRe-Si** with **2-Ru** – a faster isomerization catalyst. **2-Ru** was solvated in toluene and

loaded into the CSTR with polyethylene. The tandem metathesis and isomerization reactions were then carried out under standard flow conditions (see **Figure 4.9**). The propylene formation rate reached a maximum of 0.13 mmol/h (2.1wt% PE conversion). Compared to reactions with **PtRe-Si**, the tandem reaction of **Ultracat** and **2-Ru** produced nearly 5 times more propylene over 10 hours of catalysis (0.38 mmol of C<sub>3</sub>). This experiment clearly showed the sensitivity of the depolymerization cascade to changes in isomerization rate.

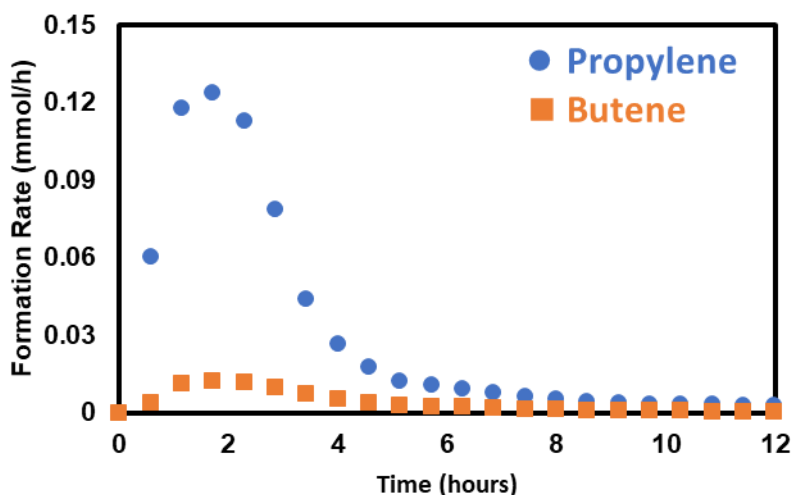


**Figure 4.9.** Continuous flow reactor data depicting the formation rate of olefin products upon tandem metathesis and isomerization of polyethylene. A 0.01 M solution of **Ultracat** in toluene (0.005 mL/min) was co-fed with ethylene (5 mmol/h) into our CSTR setup held at 100°C and 60 PSI. The reactor was initially loaded with 250 mg of polyethylene and 20 mg of **2-Ru** solvated in 2 mL of toluene.

*Continuous Addition of **Ultracat** and **2-Ru**.* Attempting to further mitigate the olefin decay, we continuously fed a fresh feed of isomerization and metathesis catalyst (**2-Ru** and **Ultracat**) into the CSTR containing polyethylene (see **Figure C7** for reaction conditions). In this reaction, propylene and butene were produced as the major products at a maximum rate of 0.15 and 0.025 mmol/h, respectively (1.1wt% PE conversion). Noticeably, the continuous feed **2-Ru** into the reactor did not significantly improve the stability of olefin formation. Moreover, we observed lower olefin formation rates in this experiment as compared to the batch addition of **2-Ru** (**Figure 4.9**). We attributed the low olefin formation rates to the low concentration of active **2-Ru** present in the reactor during the continuous addition. Thus, we sought to increase the concentration of the

isomerization catalyst in the continuous feed. Reproducing the experiment, we fed a catalyst solution that contained a 5-fold molar increase of **2-Ru** (see **Figure 4.10** for reaction conditions). Under these conditions, polyethylene (MW~1000 g/mol) was reacted to form propylene and butene at a maximum formation rate of 0.93 and 0.08 mmol/h, respectively. Pentenes and hexenes were also detected in low quantities (not shown in **Figure 4.10**, ca. 0.01 and 0.001 mmol/h, respectively). The presence of C<sub>5</sub> and C<sub>6</sub> products was consistent with the increased rate of isomerization. More importantly, the augmented rate of isomerization had significantly improved the extent of depolymerization where 19.4wt% of the polymer was converted to propylene at high selectivity (**Figure 4.11**). Of the gaseous olefin products formed, propylene accounted for 94 mol% of the distribution (C<sub>4</sub> products ~ 5 mol% and C<sub>5+</sub> products >1 mol%). The selectivity reported in this work for a single olefin product is unprecedented, showcasing the benefit of our tandem ethenolysis and isomerization strategy for the selective conversion of polymer to monomer.

This set of experiments (see **Figure 4.9**, **Figure 4.10**, and **Figure C7**) also revealed that a reduction in ethylene pressure (from 60 to 14.7 PSI) did not have a significant impact on olefin formation rates. This observation is consistent with an isomerization-limited cascade. Higher reaction pressure increases the concentration of ethylene in the reaction solution, which predominantly affects the rate of ethenolysis – the non-rate-limiting step.

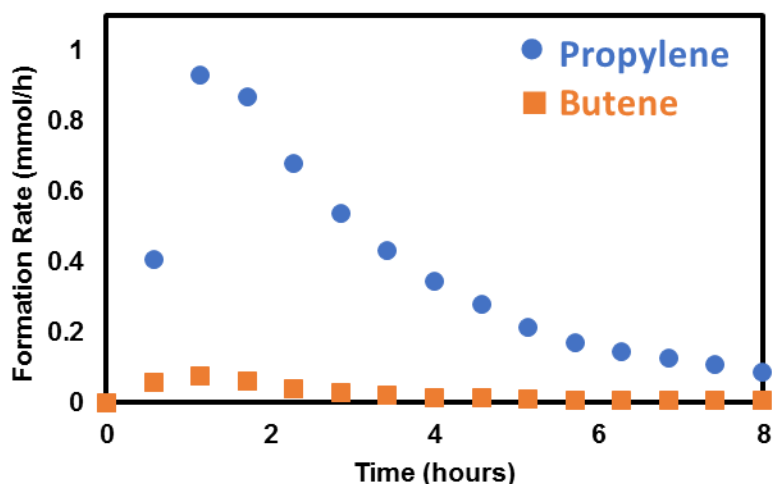


**Figure 4.10.** Continuous flow reactor data depicting the formation rate of olefin products upon tandem metathesis and isomerization of polyethylene. A solution of **Ultracat** (0.01 M) and **2-Ru** (ca. 0.02 M, saturated solution) in toluene (0.01 mL/min) was co-fed with ethylene (5 mmol/h) into our CSTR setup held at 70°C and 14.7 PSI. The reactor was initially loaded with 250 mg of polyethylene.

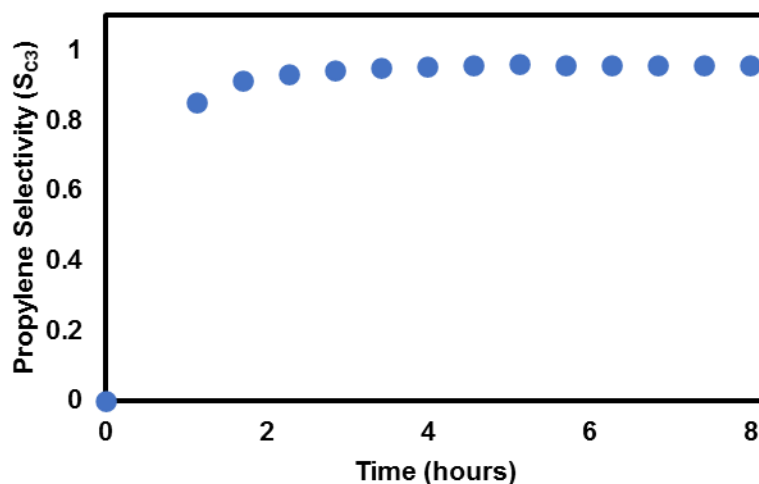
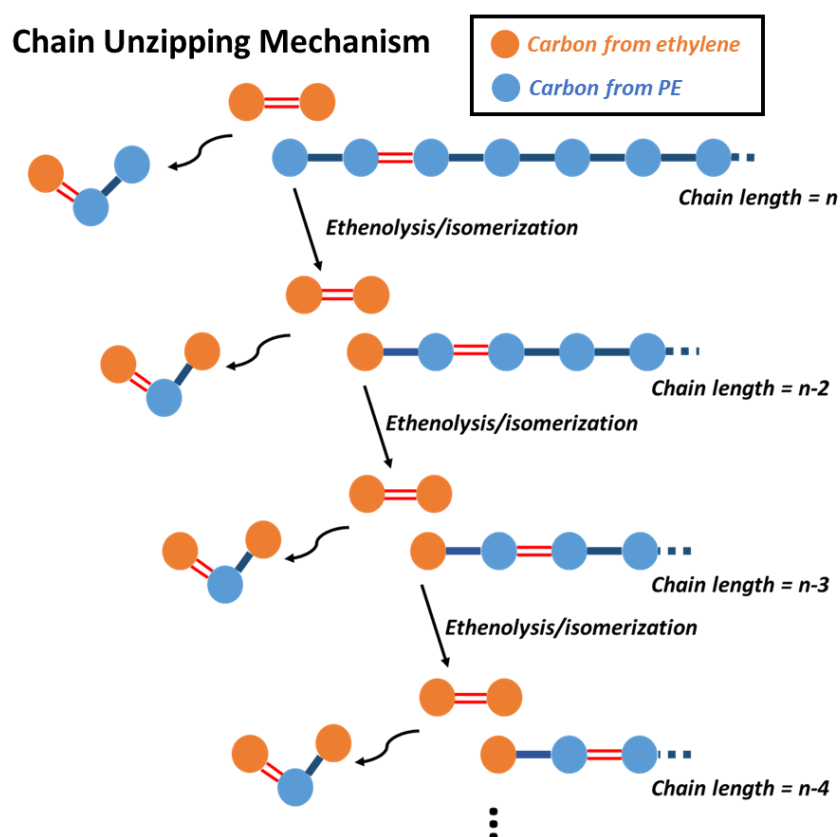


**Figure 4.11.** Selectivity profile for a continuous flow depolymerization reaction performed by **2-Ru** and **Ultracat**. This selectivity only considers the gaseous products exiting the flow reactor, and it is calculated by normalizing propylene formation rate by the cumulative formation rate of all olefin products.

*Mechanistic Insight on the Depolymerization Cascade.* Our investigations revealed an isomerization-limited cascade reaction, and this conclusion has interesting implications on the mechanism of depolymerization. Importantly, our starting polymer material consists of terminally and internally unsaturated polyethylene (40 mol% 1-olefin and 60 mol% 2-olefin, **Table 4.1**). A fast metathesis reaction results in the rapid cleavage of 2-olefin-terminated PE to produce a molecule of propylene in addition to a molecule of 1-olefin-terminated PE. Under isomerization

limited conditions, the subsequent migration of the C=C bond from the 1-olefin position to an interior location is slow, thus, resulting in the accumulation of terminally unsaturated polymer. This balance of metathesis and isomerization leads to the unzipping of the polymer chain upon a productive cleavage event (see **Scheme 4.1**). Based on this mechanistic proposal, we hypothesized that the depletion of 2-olefin-terminated PE (a result of an isomerization-limited reaction cascade) was the predominant cause of the rapid decay in product formation during our depolymerization reactions.



**Scheme 4.1.** Simplified schematic of tandem isomerization and metathesis of unsaturated PE. Under isomerization-limiting conditions PE is depolymerized one carbon at a time.

To better support our hypothesis, we compared the cumulative propylene formation to the initial loading of 2-olefin-terminated PE before reaction (**Table 4.1**, see **Appendix C** for details end-group analysis). Reacting PE with **Ultracat** produced 0.63 propylene units per internally

unsaturated chain. This value is relatively close to unity, and it is consistent with our hypothesis that propylene is predominantly produced from the cleavage of 2-olefin-terminated polymer. As we increase isomerization, either by the addition of **PtRe-Si** or **2-Ru**, this fraction increases to a value greater than unity (a best of ca. 20 units of propylene per chain of PE), which indicates that more propylene has been formed than the initial loading of 2-olefin-terminated polymer. Ultimately, this evidence serves as a quantitative indicator of successful depolymerization via tandem isomerization and metathesis.

In addition to the analysis of propylene formation, we also assessed the quality of the polymer post-reaction. The initial ratio of internal- to terminal olefin end-groups in the starting polymer is 1 to 0.66. Generally, after a depolymerization reaction, the remaining polymer becomes concentrated in terminally unsaturated chains (**Table 4.1**). Moreover, a depolymerization reaction using recycled polymer – now concentrated in terminally unsaturated ends (**Figure C8**) – showed a lower maximum propylene formation rate compared to a reaction with fresh polymer ( $R_{C3,max}$  of 0.07 vs 0.44 mmol/h). These observations are consistent with the depletion of the 2-olefin group after the tandem depolymerization reactions, and they provide additional support for our proposed pathway.

Interestingly, at a high depolymerization extent, which requires a high **2-Ru** loading, this trend had reversed (**Table 4.1**). Instead, we only detected internal olefinic groups in the recovered material, which is consistent with tandem metathesis and isomerization post-depolymerization. Because the catalyst mixture is not immediately quenched, depressurization of the reactor setup (i.e., the removal of ethylene) accompanied by a 2- to 3-hour cooling period leads to (1) isomerization of 1-olefin-terminated PE chains in addition to (2) recombination of PE fragments

via self-metathesis. Each of these reactions contributes to the formation of internally unsaturated chains.

In general, the polymer molecular weight ( $M_N$ ) decreases after the tandem reactions, but the reduction in molecular weight is larger than we would expect considering the depolymerization extent. Further investigation is being performed to better understand the changes to polymer molecular weight.

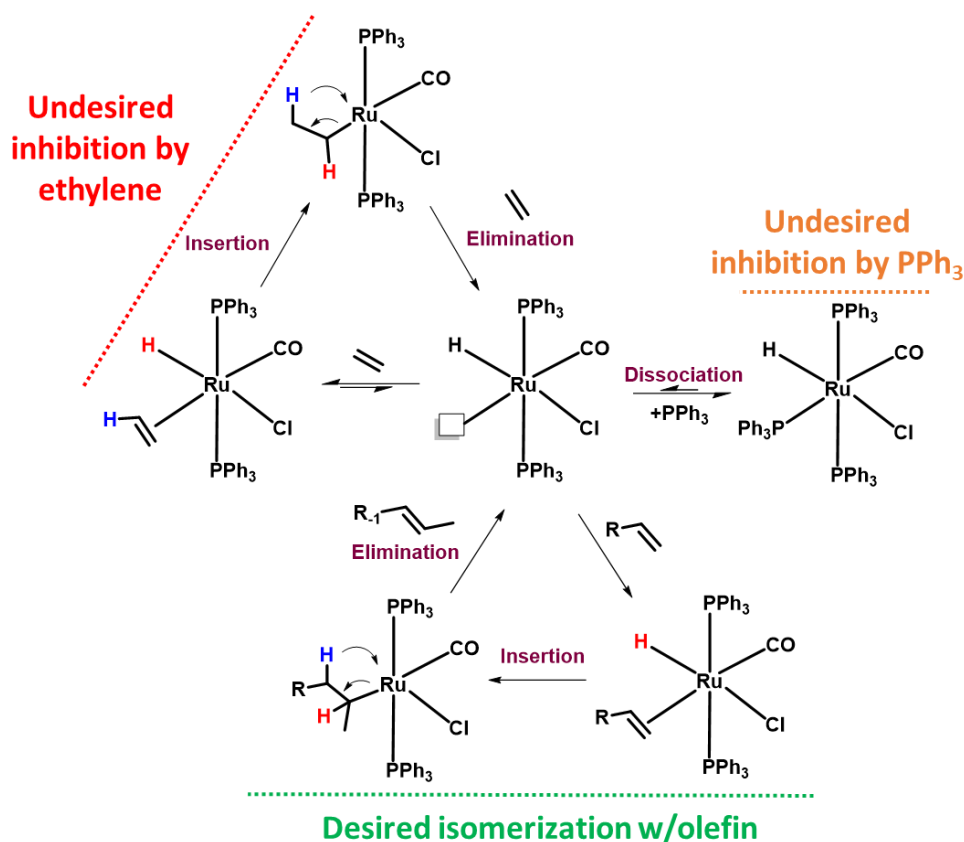
**Table 4.1.** Data summary of tandem depolymerization under a continuous co-flow of **Ultracat** and ethylene.

Catalyst(s) <sup>a</sup>	T/ <sup>o</sup> C	Ethylene P/ $\dot{n}$ (PSI/mmol h <sup>-1</sup> )	PE Conv <sup>b</sup> (wt%)	$n_{C3,tot}/n_{PE,o}$ <sup>c</sup>	Internal to Terminal C=C	$M_N$
Unreacted PE	n/a	n/a	n/a	n/a	1 to 0.66	132.5 $\pm$ 3.5 <sup>d</sup>
<b>Ultracat (F)</b>	85	60/5	>1.0	0.63	Internal n.d.	50
<b>Ultracat (F)</b> <b>PtRe-Si (B)</b>	100	60/5	1.0	1.55	1 to 2.25	92 $\pm$ 8.5 <sup>d</sup>
<b>Ultracat (F)</b> <b>2-Ru (B)</b>	100	60/5	2.1	4.90	1 to 3.81	91.8 $\pm$ 1.1 <sup>d</sup>
<b>Ultracat (F)</b> <sup>e</sup> 0.02 M <b>2-Ru (F)</b>	70	14.7/5	19.4	21.75	Terminal n.d.	86

<sup>a</sup>All PE samples were reprecipitated in methanol prior to analysis. <sup>a</sup>“(F)” and “(B)” denote flow or batch addition of the catalyst. All reactions (unless otherwise noted) were carried out using 250 mg of PE and an **Ultracat** solution with a concentration of 0.01 M. <sup>b</sup>PE conversion is determined by calculating the amount of polymer consumed based upon the gaseous olefin formed (see Reactor Build, Methods, and Calculations section). <sup>c</sup>Total moles of propylene are calculated by integrating area under the curve of the flow profiles over the designated reaction time. This value is divided by the initial molar loading of olefinic polyethylene. Via <sup>1</sup>H NMR the starting PE was determined to be 60 mol% olefin-terminated and 40 mol% vinyl. <sup>d</sup>Standard deviations were determined by performing calculations on two distinct proton resonances via <sup>1</sup>H NMR. <sup>e</sup>A different batch of polyethylene was used for this experiment with the following characteristics – Internal to Terminal = 1 to 0.73 and  $M_N$  = 73.16 $\pm$ 3.6.

*Proposed Route(s) for the Inhibition of 2-Ru.* The decay in catalytic rate led us to assess possible routes of inhibition in our depolymerization reaction. The isomerization catalyst (**2-Ru**) is known to proceed through an insertion-elimination mechanism (**Scheme 4.2**).<sup>41,42</sup> Thus, **2-Ru** can preferably react with ethylene instead of the olefin groups of the polymer. Moreover, the continuous addition of **2-Ru** and its deactivation leads to the accumulation of excess ligand (triphenylphosphine, PPh<sub>3</sub>), which also competes for active sites. Ligand accumulation would

affect both the metathesis and isomerization catalyst. Overall, the reactivity of the isomerization catalyst toward ethylene and a continually increasing concentration of  $\text{PPh}_3$  could contribute to the inhibition in the overall rate of depolymerization.



**Scheme 4.2.** Plausible routes for **2-Ru** inhibition involving ethylene and excess  $\text{PPh}_3$ .

*Tandem Ultracat* and  $[\text{Pd}^{\text{I}}(\mu\text{-Br})^{\text{I}}\text{Bu}_3\text{P}]_2$  (**3-Pd**) for Polyethylene Depolymerization. To alleviate decomposition and inhibition, we employed a palladium isomerization catalyst (purchased commercially  $[\text{Pd}^{\text{I}}(\mu\text{-Br})^{\text{I}}\text{Bu}_3\text{P}]_2$ , **3-Pd**) in conjunction with **Ultracat**.<sup>32,43,44</sup> Extensive modeling efforts have shown that the phosphine ligands on **3-Pd** are not likely released upon formation of the active site (breaking of the dimer), during the catalytic cycle, or even during deactivation.<sup>45</sup> Thus, the use of **3-Pd** as an isomerization catalyst would slow inhibition (and also deactivation) via ligand accumulation. In a final experiment, we continuously fed ethylene and a fresh feed of isomerization and metathesis catalyst (**3-Pd** and **Ultracat**) into the CSTR containing polyethylene



(MW  $\sim$  1000 g/mol, see **Figure 4.12** for reaction conditions). Propylene and butene were produced as the major products at a maximum rate of 3.26 and 0.24 mmol/h, respectively. Pentenes, hexenes, and heptenes were also detected in low quantities (not shown in **Figure 4.12**, ca. 0.02, 0.001, and  $>0.001$  mmol/h, respectively). In this experiment, we attained an even greater extent of depolymerization (29.1wt% conversion of PE) using **3-Pd** as compared to experiments using **2-Ru** (19.4wt% conversion of PE). Under near-identical molar loadings of isomerization and metathesis catalysts, this result indicated that we had performed more productive ethenolysis events per mol of **3-Pd** compared to **2-Ru**. This observation was consistent with an increased rate of isomerization which also led to a decrease in propylene selectivity (**Figure 4.13**). Of the products formed in this reaction, propylene accounted for 78 mol% of the gaseous-products distribution ( $C_4$  products  $\sim$  16.0 mol% and  $C_{5-7}$  products  $\sim$  6 mol%). In an isomerization-limited depolymerization, increasing the isomerization rate leads to more productive cleavage events. However, this comes at the cost of selectivity since faster migration of the double bond from the PE-chain end amplifies the formation of other volatile light-olefins ( $C_{4-7}$ ) in addition to propylene. At this time, further analysis of the polymer samples is currently under investigation.

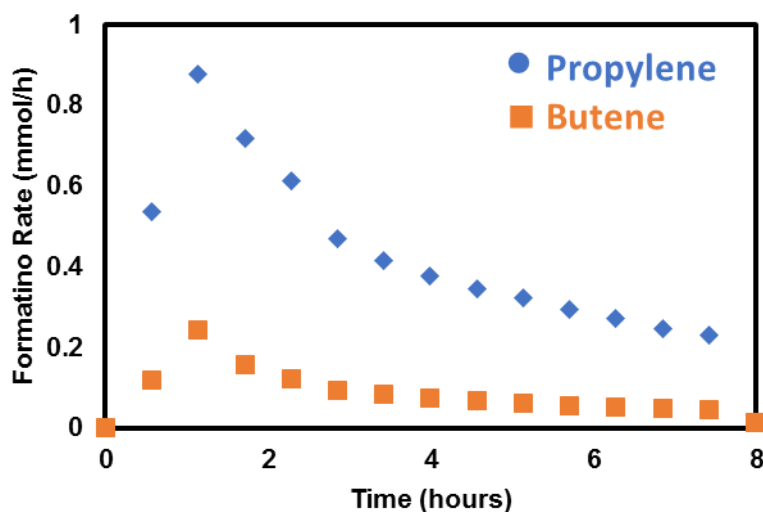


**Figure 4.12.** Continuous flow reactor data depicting the formation rate of olefin products upon tandem metathesis and isomerization of polyethylene. A solution of **Ultracat** (0.01 M) and **3-Pd** (0.01 M) in toluene (0.01 mL/min) was co-

**Figure 4.12 (cont.)** fed with ethylene (25 mmol/h) into our CSTR setup held at 70°C and 14.7 PSI. The reactor was initially loaded with 250 mg of polyethylene.

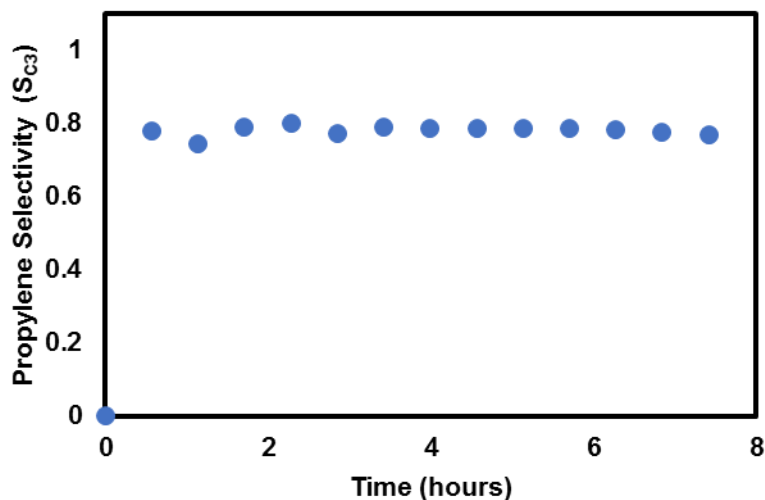


**Figure 4.13.** Selectivity profile for a continuous flow depolymerization reaction performed by **3-Pd** and **Ultracat**. This selectivity only considers the gaseous products exiting the flow reactor, and it is calculated by normalizing propylene formation rate by the cumulative formation rate of all olefin products.

*Gravimetric Measurement of Polyethylene Conversion.* In addition to our theoretical estimate, we also gravimetrically measured polyethylene consumption. After the tandem depolymerization, the residual polymer exists in a liquid mixture of toluene and deactivated catalyst. GC analyses of these toluene mixtures showed no trace of shorter volatile olefins ( $C_2$ - $C_{20}$ ). Thus, we employed two procedures that focused on recovery of the remaining solid polymer.

The first procedure involves precipitation of the polymer into a solution of methanol, which is followed by centrifugation, drying (overnight at 50°C and 38.1 Torr), and weighing of the remaining polymer. Precipitation in methanol extracts the solubilized catalyst from PE (two to three precipitation cycles). However, gravimetric recovery through this method is biased since low molecular weight fractions of the polymer are lost during the process (selective precipitation). This is evident in **Table 4.2 lines 1-4** where the gravimetric measurement of PE consumption greatly exceeds the theoretical conversion based on propylene formation (**Equation 4.4**).

In the second procedure, we directly dry our reaction vessel to remove all volatiles under vacuum (overnight at 50°C and 38.1 Torr); thus, avoiding selective precipitation. By subtracting out the

reactor, stir bar, and catalyst mass from the final weight of the dried reaction vessel, we can calculate (gravimetrically) the consumption of polymer. Using this second procedure, our calculation of PE conversion (**Equation 4.4**, 30.2wt%) agrees well with gravimetric analysis (31.5wt %, see **Table 4.2 line 5**). Agreement between these two measurements further supports our proposed chain-unzipping mechanism where the only products formed in this process are light olefins upon productive ethenolysis.

**Table 4.2.** Theoretical PE consumption vs gravimetric measurement of recovered polymer.

Line	Catalyst(s) <sup>a</sup>	T/°C	Ethylene P/ <i>n</i> (PSI/mmol h <sup>-1</sup> )	PE Conv. (wt%) <sup>b</sup>	Gravimetric Loss (wt%)
1	Ultracat (F)	85	60/5	>1.0	35 <sup>c</sup>
2	Ultracat (F) PtRe-Si (B)	100	60/5	1.0	31 <sup>c</sup>
3	Ultracat (F) 2-Ru (B)	100	60/5	2.1	30 <sup>c</sup>
4	Ultracat (F) 0.02 M 2-Ru (F)	70	14.7/5	19.4	38 <sup>c</sup>
5	Ultracat (F) 0.01 M 3-Pd (F)	70	14.7/25	30.2±3.9 <sup>e</sup>	31.5±3.4 <sup>d,e</sup>

<sup>a</sup>“(F)” denotes a flow addition of the catalyst. All reactions (unless otherwise noted) were carried out using 250 mg of PE and an **Ultracat** solution with a concentration of 0.01 M. <sup>b</sup>PE conversion is determined by calculating the amount of polymer consumed based upon the gaseous olefin formed (see Reactor Build, Methods, and Calculations section). <sup>c</sup>Gravimetric loss is calculated after recovering the polymer via precipitation. <sup>d</sup>Gravimetric loss is calculated after removing all volatiles from the reaction vessel using a vacuum oven. <sup>e</sup>Values and standard deviations are determined by averaging over three experiments.

## 4.6 Conclusions and Recommendations

In this pioneering work, we have provided quantitative evidence of successful PE depolymerization via isomerization and metathesis. Moreover, we have achieved appreciable conversion of PE (up to 30wt%) to highly desired light olefin products with unprecedented selectivity for a single monomer product – propylene (up to 95% selectivity). High selectivity is a direct result of a fast metathesis reaction relative to isomerization, which leads to a chain unzipping

depolymerization mechanism. Ultimately, our detailed mechanistic and kinetic insight on the cascade reactions will aid in the development of forthcoming catalytic systems.

We offer several recommendations for future endeavors on this work. Currently, high loadings of catalyst are necessary to attain any considerable extent of depolymerization (at best ca. 90 mg of Pd +Ru to convert 75 mg of PE); thus, increases to catalytic rate and stability will be crucial in extending this technology to high MW commercial and waste polymer. Moreover, our work has not yet detailed the investigation of a compatible dehydrogenation catalyst. Dehydrogenation of unsaturated polyethylene is a key step to the full realization of our proposed tandem catalysis strategy. These investigations will be challenged by the identification of appropriate conditions for the three tandem catalysts. Furthermore, the interplay of the dehydrogenation kinetics with isomerization and metathesis will have a significant impact on the final products distribution. Deconvoluting the effects of these reactions will be vital to establishing a fundamental understanding of the depolymerization cascade.

#### 4.7 References

- (1) Geyer, R.; Jambeck, J. R.; Law, K. L. Production, Use, and Fate of All Plastics Ever Made. *Sci. Adv.* **2017**, *3* (7), e1700782.
- (2) *Marine Anthropogenic Litter*; Bergmann, M., Gutow, L., Klages, M., Eds.; Springer International Publishing: Cham, 2015.
- (3) Kumar, P. Role of Plastics on Human Health. *Indian J. Pediatr.* **2018**, *85* (5), 384–389.
- (4) Rustagi, N.; Singh, R.; Pradhan, S. Public Health Impact of Plastics: An Overview. *Indian J. Occup. Environ. Med.* **2011**, *15* (3), 100.
- (5) Thompson, R. C.; Moore, C. J.; vom Saal, F. S.; Swan, S. H. Plastics, the Environment and Human Health: Current Consensus and Future Trends. *Philos. Trans. R. Soc. B Biol.*

- Sci.* **2009**, *364* (1526), 2153–2166.
- (6) Yeo, J. C. C.; Muiruri, J. K.; Thitsartarn, W.; Li, Z.; He, C. Recent Advances in the Development of Biodegradable PHB-Based Toughening Materials: Approaches, Advantages and Applications. *Mater. Sci. Eng. C* **2018**, *92* (December), 1092–1116.
  - (7) Jubinville, D.; Esmizadeh, E.; Saikrishnan, S.; Tzoganakis, C.; Mekonnen, T. A Comprehensive Review of Global Production and Recycling Methods of Polyolefin (PO) Based Products and Their Post-Recycling Applications. *Sustain. Mater. Technol.* **2020**, *25*, e00188.
  - (8) Ignatyev, I. A.; Thielemans, W.; Vander Beke, B. Recycling of Polymers: A Review. *ChemSusChem* **2014**, *7* (6), 1579–1593.
  - (9) Ragaert, K.; Delva, L.; Van Geem, K. Mechanical and Chemical Recycling of Solid Plastic Waste. *Waste Manag.* **2017**, *69*, 24–58.
  - (10) Capone, C.; Di Landro, L.; Inzoli, F.; Penco, M.; Sartore, L. Thermal and Mechanical Degradation during Polymer Extrusion Processing. *Polym. Eng. Sci.* **2007**, *47* (11), 1813–1819.
  - (11) Ponzio, A.; Kalisz, S.; Blasiak, W. Effect of Operating Conditions on Tar and Gas Composition in High Temperature Air/Steam Gasification (HTAG) of Plastic Containing Waste. *Fuel Process. Technol.* **2006**, *87* (3), 223–233.
  - (12) Sun, X.; Li, J.; Zhao, X.; Zhu, B.; Zhang, G. A Review on the Management of Municipal Solid Waste Fly Ash in American. *Procedia Environ. Sci.* **2016**, *31*, 535–540.
  - (13) Huang, S. J. Polymer Waste Management–Biodegradation, Incineration, and Recycling. *J. Macromol. Sci. Part A* **1995**, *32* (4), 593–597.
  - (14) Mekhzoum, M.; Benzeid, H.; Rodrigue, D.; Qaiss, A.; Bouhfid, R. Recent Advances in

- Polymer Recycling: A Short Review. *Curr. Org. Synth.* **2017**, *14* (2), 171–185.
- (15) Schwarz, A. E.; Ligthart, T. N.; Godoi Bizarro, D.; De Wild, P.; Vreugdenhil, B.; van Harmelen, T. Plastic Recycling in a Circular Economy; Determining Environmental Performance through an LCA Matrix Model Approach. *Waste Manag.* **2021**, *121*, 331–342.
  - (16) Frączak, D. Chemical Recycling of Polyolefins (PE, PP): Modern Technologies and Products. In *Current Topics in Recycling [Working Title]*; IntechOpen, 2021.
  - (17) Jie, X.; Li, W.; Slocombe, D.; Gao, Y.; Banerjee, I.; Gonzalez-Cortes, S.; Yao, B.; AlMegren, H.; Alshihri, S.; Dilworth, J.; et al. Microwave-Initiated Catalytic Deconstruction of Plastic Waste into Hydrogen and High-Value Carbons. *Nat. Catal.* **2020**, *3* (11), 902–912.
  - (18) Coates, G. W.; Getzler, Y. D. Y. L. Chemical Recycling to Monomer for an Ideal, Circular Polymer Economy. *Nat. Rev. Mater.* **2020**, *5* (7), 501–516.
  - (19) Frączak, D. Chemical Recycling of Polyolefins (PE, PP): Modern Technologies and Products. In *Current Topics in Recycling [Working Title]*; IntechOpen, 2021.
  - (20) da Rosa, A. V.; Ordóñez, J. C. Hydrogen Production. In *Fundamentals of Renewable Energy Processes*; Elsevier, 2022; pp 419–470.
  - (21) Ray, R.; Thorpe, R. A Comparison of Gasification with Pyrolysis for the Recycling of Plastic Containing Wastes. *Int. J. Chem. React. Eng.* **2007**, *5* (1).
  - (22) Mondal, P.; Dang, G. S.; Garg, M. O. Syngas Production through Gasification and Cleanup for Downstream Applications — Recent Developments. *Fuel Process. Technol.* **2011**, *92* (8), 1395–1410.
  - (23) Asadullah, M. Biomass Gasification Gas Cleaning for Downstream Applications: A

- Comparative Critical Review. *Renew. Sustain. Energy Rev.* **2014**, *40*, 118–132.
- (24) Hou, Q.; Zhen, M.; Qian, H.; Nie, Y.; Bai, X.; Xia, T.; Laiq Ur Rehman, M.; Li, Q.; Ju, M. Upcycling and Catalytic Degradation of Plastic Wastes. *Cell Reports Phys. Sci.* **2021**, *2* (8), 100514.
- (25) Rorrer, J. E.; Troyano-Valls, C.; Beckham, G. T.; Román-Leshkov, Y. Hydrogenolysis of Polypropylene and Mixed Polyolefin Plastic Waste over Ru/C to Produce Liquid Alkanes. *ACS Sustain. Chem. Eng.* **2021**, *9* (35), 11661–11666.
- (26) Ertem, S. P.; Onuoha, C. E.; Wang, H.; Hillmyer, M. A.; Reineke, T. M.; Lodge, T. P.; Bates, F. S. Hydrogenolysis of Linear Low-Density Polyethylene during Heterogeneous Catalytic Hydrogen-Deuterium Exchange. *Macromolecules* **2020**.
- (27) Kots, P. A.; Liu, S.; Vance, B. C.; Wang, C.; Sheehan, J. D.; Vlachos, D. G. Polypropylene Plastic Waste Conversion to Lubricants over Ru/TiO<sub>2</sub> Catalysts. *ACS Catal.* **2021**, *11*, 8104–8115.
- (28) Sánchez-Rivera, K. L.; Huber, G. W. Catalytic Hydrogenolysis of Polyolefins into Alkanes. *ACS Cent. Sci.* **2021**, *7* (1), 17–19.
- (29) Zhang, F.; Zeng, M.; Yappert, R. D.; Sun, J.; Lee, Y. H.; LaPointe, A. M.; Peters, B.; Abu-Omar, M. M.; Scott, S. L. Polyethylene Upcycling to Long-Chain Alkylaromatics by Tandem Hydrogenolysis/Aromatization. *Science* (80-. ). **2020**, *370* (6515), 437–441.
- (30) Goldman, A. S.; Roy, A. H.; Huang, Z.; Ahuja, R.; Schinski, W.; Brookhart, M. Catalytic Alkane Metathesis by Tandem Alkane Dehydrogenation-Olefin Metathesis. *Science* (80-. ). **2006**, *312* (5771), 257–261.
- (31) Huang, Z.; Rolfe, E.; Carson, E. C.; Brookhart, M.; Goldman, A. S.; El-Khalafy, S. H.; Roy MacArthur, A. H. Efficient Heterogeneous Dual Catalyst Systems for Alkane

- Metathesis. *Adv. Synth. Catal.* **2010**, 352 (1), 125–135.
- (32) Pollini, J.; Pankau, W. M.; Gooßen, L. J. Isomerizing Olefin Metathesis. *Chem. – A Eur. J.* **2019**, 25 (31), 7416–7425.
- (33) Ellis, L. D.; Orski, S. V.; Kenlaw, G. A.; Norman, A. G.; Beers, K. L.; Román-Leshkov, Y.; Beckham, G. T. Tandem Heterogeneous Catalysis for Polyethylene Depolymerization via an Olefin-Intermediate Process. *ACS Sustain. Chem. Eng.* **2021**, 9 (2), 623–628.
- (34) Jia, X.; Qin, C.; Friedberger, T.; Guan, Z.; Huang, Z. Efficient and Selective Degradation of Polyethylenes into Liquid Fuels and Waxes under Mild Conditions. *Sci. Adv.* **2016**, 2 (6), 1–8.
- (35) Guironnet, D.; Peters, B. Tandem Catalysts for Polyethylene Upcycling: A Simple Kinetic Model. *J. Phys. Chem. A* **2020**, 124 (19), 3935–3942.
- (36) Hyatt, M. G.; Walsh, D. J.; Lord, R. L.; Andino Martinez, J. G.; Guironnet, D. Mechanistic and Kinetic Studies of the Ring Opening Metathesis Polymerization of Norbornenyl Monomers by a Grubbs Third Generation Catalyst. *J. Am. Chem. Soc.* **2019**, 141 (44), 17918–17925.
- (37) Consorti, C. S.; Aydos, G. L. P.; Dupont, J. Tandem Isomerisation-Metathesis Catalytic Processes of Linear Olefins in Ionic Liquid Biphasic System. *Chem. Commun.* **2010**, 46 (47), 9058–9060.
- (38) Gawin, R.; Kozakiewicz, A.; Guńka, P. A.; Dąbrowski, P.; Skowerski, K. Bis(Cyclic Alkyl Amino Carbene) Ruthenium Complexes: A Versatile, Highly Efficient Tool for Olefin Metathesis. *Angew. Chemie Int. Ed.* **2017**, 56 (4), 981–986.
- (39) Prasanna, N.; Srinivasan, S.; Rajagopal, G.; Athappan, P. R. Synthesis, Spectral and Electrochemical Studies of Ruthenium(II)/(III) Complexes of Alicyclic B-Ketamines.



- Indian J. Chem.* **2001**, 40 (4), 426–429.
- (40) Guironnet, D.; Rünzi, T.; Göttker-Schnetmann, I.; Mecking, S. Control of Molecular Weight in Ni(II)-Catalyzed Polymerization via the Reaction Medium. *Chem. Commun.* **2008**, No. 40, 4965–4967.
- (41) Biswas, S. Mechanistic Understanding of Transition-Metal-Catalyzed Olefin Isomerization: Metal-Hydride Insertion-Elimination vs.  $\pi$ -Allyl Pathways. *Comments Inorg. Chem.* **2015**, 35 (6), 300–330.
- (42) Kuriyama, W. Carbonylchlorohydridotris(Triphenylphosphine)Ruthenium(II). In *Encyclopedia of Reagents for Organic Synthesis*; John Wiley & Sons, Ltd: Chichester, UK, 2014; pp 1–7.
- (43) Colacot, T. J. A Highly Active Palladium(I) Dimer for Pharmaceutical Applications. *Platin. Met. Rev.* **2009**, 53 (4), 183–188.
- (44) Ohlmann, D. M.; Tschauder, N.; Stockis, J.-P.; Gooßen, K.; Dierker, M.; Gooßen, L. J. Isomerizing Olefin Metathesis as a Strategy To Access Defined Distributions of Unsaturated Compounds from Fatty Acids. *J. Am. Chem. Soc.* **2012**, 134 (33), 13716–13729.
- (45) Koley, D.; De, S.; Sivendran, N.; Gooßen, L. J. Isomerization of Functionalized Olefins by Using the Dinuclear Catalyst  $[\text{Pd I}(\mu\text{-Br})(\text{P}^t\text{Bu}_3)]_2$ : A Mechanistic Study. *Chem. – A Eur. J.* **2021**, 27 (61), 15227–15239.

## CHAPTER 5: Tandem Heterogeneous Catalysts for Selective Polyethylene

### Depolymerization

#### 5.1 Introduction

This final chapter contains an anthology of our investigations on several promising heterogeneous catalyst pairings for the selective depolymerization of polyethylene via tandem dehydrogenation, metathesis, and isomerization. In addition to an evaluation of their efficacy, the methodical development of these tandem catalytic systems is provided. Using the insight acquired from these experimental efforts we present guidelines and recommendations for reaction development.

#### 5.2 MoO<sub>x</sub>-SiO<sub>2</sub> (Mo-Si) for Polyethylene Depolymerization

We initiated our screening of heterogeneous catalysts with an investigation of silica-supported molybdate. These materials are known as a model metathesis catalyst due to their well-defined and isolated surface sites.<sup>1-4</sup> MoO<sub>x</sub>(10wt%)-SiO<sub>2</sub> (**Mo-Si**) was synthesized according to literature procedure (see **Appendix D**).<sup>5</sup> The catalyst was initially tested in 1-decene self-metathesis batch reactions, and the success of the synthesis was confirmed by the formation of C<sub>18</sub> product, octadecene (53% substrate conversion after 6 hours, **Figure D1**). The overall products distribution consisted of unreacted starting material (C<sub>10</sub>, 69 mol%) and hydrocarbon products ranging from C<sub>8</sub>-C<sub>9</sub> (8 mol%), C<sub>11</sub>-C<sub>13</sub> (5 mol%) and C<sub>14</sub>-C<sub>18</sub> (18 mol%). These products were indicative of successful isomerization and metathesis of the initial olefin substrate.

Next, we looked to study polyethylene as the primary substrate of interest. We employed our flow reactor setup to continuously replenish ethylene (5 mmol/h) while analyzing the gaseous product formation over time. The flow reactor was loaded with 500 mg of **Mo-Si** and 2500 mg of polyethylene (MW ~ 870 g/mol) which was held under several varying pressures (80-100 PSI) and temperatures (150°C-170°C) to screen reaction conditions (**Figure D2**). The total allotted reaction

time was 50 hours. The reaction of polyethylene with **Mo-Si**, produced propylene and butene as the predominant products at rates ca. 0.0006 and 0.0004 mmol/h, respectively. Notably, the olefin formation rates were very low lying near our GC detection limits. Moreover, no significant changes in product formation rates were detected upon varying reaction pressure or temperature. In addition to an examination of the gaseous phase, we also analyzed the resulting polymer via  $^1\text{H}$  NMR (see Chapter 4 for details on analysis). The catalyst showcased some ability to isomerize the olefinic end-group of polyethylene, in which the fraction of internal double-bonds within the polymer sample increased from 54.5 to 82.8 mol% after reaction. Additionally, the polymer's degree of polymerization increased from 61.2 to 63.8. The slight increase in chain length can be explained by the cross-metathesis of terminally functionalized chain ends to form a molecule of short olefin (gaseous) in addition to a longer polymer molecule.

Next, we postulated that the introduction of the dehydrogenation catalyst would augment the rate of propylene formation as it would increase the number of reactive functional groups along the polyethylene chain; thus, we performed the tandem reaction of **PtRe-Si** and **Mo-Si** with polyethylene. In a second reaction under otherwise identical conditions, 150 mg of **PtRe-Si** (known to catalyze dehydrogenation/isomerization) catalyst was added. Compared to the previous experiment, we noted slightly higher olefin formation rates, suggesting an increase in productive ethenolysis events. However, overall, the rate remained low (ca. 0.0004 mmol/h, **Figure D2**). Furthermore, the addition of **PtRe-Si** to the reaction mixture augmented the isomerization reaction as revealed by the high fraction of internal bonds in the reacted polymer (91.8 mol%, **Table 5.1**). The increasing concentration of internally unsaturated polymer is consistent with a slow ethenolysis step. Considering the apparent gain in molecular weight and the low rate of olefin formation we concluded that this catalyst was not satisfactory. A faster and more stable metathesis

catalyst was necessary for successful tandem depolymerization. Thus, we moved on to identify other metathesis catalysts.

**Table 5.1.**  $^1\text{H}$  NMR analysis of reacted polyethylene using **Mo-Si** as a depolymerization catalyst

Sample Description	T/°C	Time/h	Terminal to Internal C=C	$M_N^a$
Unreacted PE	n/a	n/a	1 to 1.3	$61.2 \pm 0.9$
Heated PE (no catalyst)	150	4	1 to 1.3	$59.8 \pm 1.1$
PE reacted w/ <b>Mo-Si</b>	$150 \pm 20$	50	1 to 4.8	$63.8 \pm 0.8$
PE reacted w/ <b>Mo-Si</b> + <b>PtRe-Si</b>	$150 \pm 20$	50	1 to 11.2	$64.5 \pm 0.3$

<sup>a</sup>Standard deviations were calculated by performing calculations using two distinct proton resonances via  $^1\text{H}$  NMR.

### 5.3 $\text{MoO}_x\text{-Al}_2\text{O}_3$ (**Mo-Al**) for Polyethylene Depolymerization

Alumina-supported molybdate catalysts were also investigated for compatibility with the depolymerization methodology. These catalysts are known to be nearly 10 times faster than their silica-supported counterparts,<sup>1,3,6-9</sup> and they have also been applied in the commercialized Shell Higher Olefin Process (SHOP) the cross-metathesis of long linear  $\alpha$ -olefins.<sup>10</sup> In addition to an investigation on  $\text{MoO}_x(20\text{wt}\%)\text{-Al}_2\text{O}_3$  (**Mo-Al**) we also studied a cobalt-promoted version of the catalyst which was purchased commercially,  $\text{CoO}(4\text{wt}\%)\text{-MoO}_x(15\text{wt}\%)\text{-Al}_2\text{O}_3$  (**CoMo-Al**). **Mo-Al** was synthesized in-house to contain 20wt% molybdenum according to literature procedure (see **Appendix D**).<sup>7</sup>

The metathesis activity of **Mo-Al** was tested in a 1-decene self-metathesis batch experiment. However, after 10 hours of reaction at  $150^\circ\text{C}$ , limited conversion of the substrate (2.8 mol%) to  $\text{C}_{18}$  product was detected. We hypothesized that the low activity of the catalyst was due to poor activation of the molybdenum site. Consequently, we thought to add an alkylating agent to augment catalytic rate. Thus, for subsequent experiments, **CoMo-Al** and **Mo-Al** catalysts were

used in conjunction with an alkyl aluminum promoter ( $\text{Me}_3\text{Al}$ ). We performed an optimization of the alkyl aluminum loading through a series of batch experiments, and an equimolar ratio of  $\text{Me}_3\text{Al}$  to molybdenum was shown to give the highest activity (**Figure D3**). This equimolar ratio was held constant as the desired quantity of  $\text{Me}_3\text{Al}$  for all subsequent reactions. In addition to metathesis, these catalysts are known to be active for isomerization; thus, these two materials (**Mo-Al** and **CoMo-Al**) were used as the sole catalysts for the tandem depolymerization.

To better understand the effect of the cobalt promoter, **Mo-Al** and **CoMo-Al** were studied in 1-decene self-metathesis reactions. Reactions were performed under an inert atmosphere of Ar under standard conditions. A round-bottom flask connected to a reflux condenser and a bubbler was charged with 0.27 mL 1-decene and 100 mg of catalyst (1:1  $\text{Me}_3\text{Al}:\text{Mo}$ ) held at  $150^\circ\text{C}$ . Only the condensed phase was collected for GC analysis. Under identical conditions, the 1-decene conversion rate (per hour) normalized by molybdenum loading for **CoMo-Al** and **Mo-Al** were 133 and  $50 \text{ mmol}_{\text{C}_{10}} \text{ g}_{\text{Mo}}^{-1} \text{ h}^{-1}$ , respectively. In addition to a faster catalytic rate, the cobalt promoted catalyst was also shown to accelerate the isomerization as evidenced by the broadening of the high molecular weight product distribution (**Figure 5.1**).

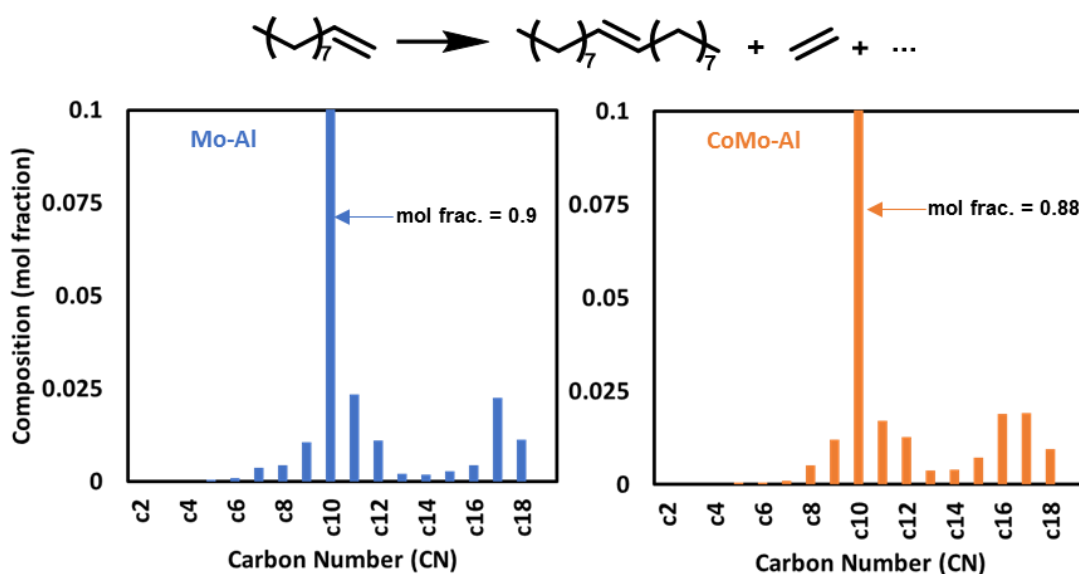


**Figure 5.1.** Pictured on the left in blue is the product distribution for 1-decene metathesis and isomerization reactions

**Figure 5.1 (cont.)** using **Mo-Al** catalyst (10 hours reaction time). Pictured on the right is the distribution produced using **CoMo-Al** catalyst (5 hours reaction time).

Prioritizing the faster catalyst, we further studied the cobalt-promoted system. Using a stainless-steel batch reactor, **CoMo-Al** was tested for ethylene-alkene cross-metathesis activity. The reactor was charged with 2.7 mL of 1-decene, 1000 mg of **CoMo-Al** (1:1 Me<sub>3</sub>Al:Mo), and 220 PSI of ethylene. The mixture was reacted at 200°C for 10 hours. After the desired reaction time and once the reactor was cooled down to room temperature, the vapor phase contents were discharged into a GC sampling valve for analysis. The gaseous distribution showed the formation of propylene (7.9 mol%) and butene (13.8 mol%) as the predominant products (**Figure 5.2**). The larger quantity of butene compared to propylene was concerning, since the tandem isomerization/ethenolysis should always yield a higher mole fraction of propylene. This selectivity toward butene could only be explained by side reactions (ethylene dimerization). In a control reaction, we substituted our alkene substrate with n-decane, and under standard reaction conditions, propylene and butene were formed. The formation of these products in the presence of a saturated alkane indicated that **CoMo-Al** was catalyzing ethylene dimerization (**Figure D4**). The formation of propylene through an initial dimerization step convolutes product formation from productive ethenolysis events (on model alkene or polyethylene). Thus, we must produce evidence beyond an analysis of light olefin formation for proof of depolymerization.

To identify the culprit of the dimerization reaction, we first investigated the alkyl aluminum promoter, which is known to oligomerize ethylene at high temperature and pressure.<sup>11</sup> However, the reaction of Me<sub>3</sub>Al with ethylene (100 PSI) in a batch reactor held at 150°C for 5 hours produced minimal butene (>1 mol% conversion of ethylene to butene), showcasing that the promoter was poorly activity for dimerization under these conditions. This result suggested that the mixture of **CoMo-Al** and Me<sub>3</sub>Al was promoting the side reaction.

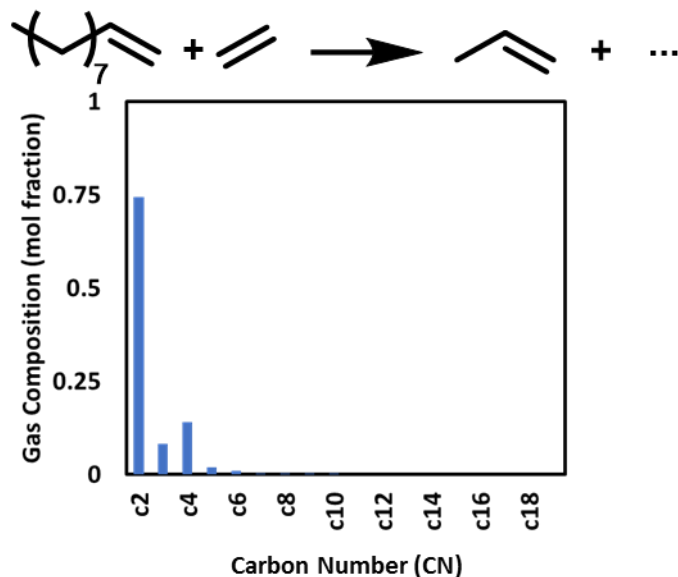


**Figure 5.2.** Gaseous product distribution for an ethylene-alkene cross-metathesis reaction performed in batch using **CoMo-Al**.

Although **CoMo-Al** was shown to mediate ethylene dimerization, the catalyst successfully performed alkene metathesis and isomerization in tandem. Thus, we proceeded to study the catalyst in reactions with polyethylene. We once again employed our flow reactor setup to continuously replenish ethylene (5 mmol/h) while analyzing the gaseous product formation over time. The flow reactor was loaded with 500 mg of **CoMo-Al** (1:1  $\text{Me}_3\text{Al}:\text{Mo}$ ), and 500 mg of polyethylene (MW ~ 870 g/mol) which was held at 100 PSI and heated to 150°C. Data was collected for 74 hours of reaction time. In a second reaction under otherwise identical conditions, 150 mg of **PtRe-Si** was added, and the results of the two experiments were compared.

In each experiment, the formation of multiple olefin products ( $\text{C}_3\text{-C}_{11}$ ) was detected in the outlet stream (**Figure 5.3**). Comparing the cumulative olefin formation rates (see **Appendix D** for calculations), we noted that the dual catalyst system (**PtRe-Si** and **CoMo-Al**) was 4.7 times faster than sole **CoMo-Al**. The dual catalysts produced propylene and butene at a maximum rate of 0.29 mmol/h and 0.2 mmol/h, respectively. However, as showcased previously, the catalyst mixture

was active for ethylene dimerization as evidenced by the high rate of butene formation relative to other olefin products.

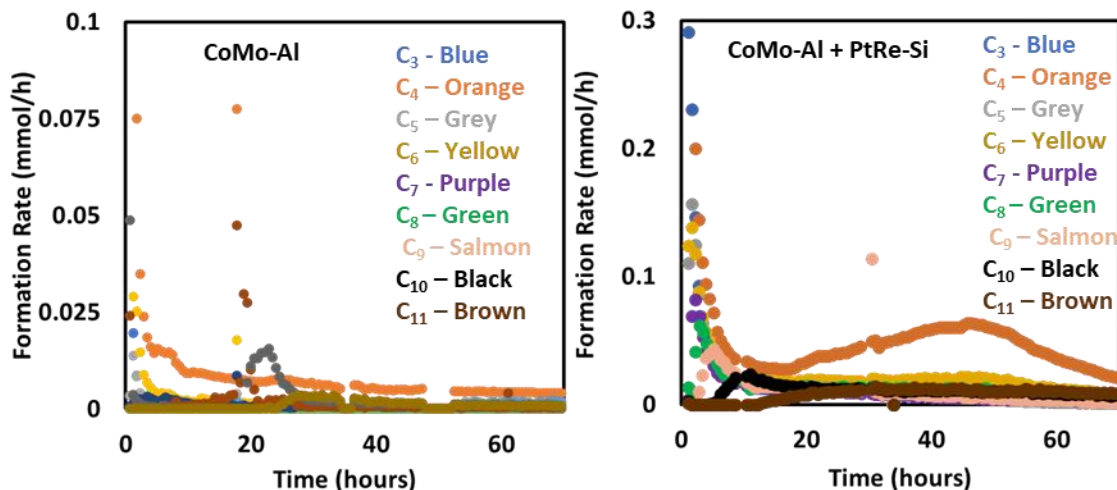


**Figure 5.3.** Gaseous product distribution reported over time for tandem isomerization and metathesis of polyethylene in flow. Pictured on the left, **CoMo-Al** is used as the sole isomerization and metathesis catalyst. On the right **CoMo-Al** is used in conjunction with **PtRe-Si** for dehydrogenation.

To gather more definitive evidence for tandem isomerization and metathesis of polyethylene, the resulting polymer was characterized via  $^1\text{H}$  NMR. This analysis revealed significant isomerization of the starting vinyl terminated polyethylene as well as an apparent reduction in molecular weight with or without the addition of dehydrogenation catalyst (**Table 5.2**). These results were consistent with a successful depolymerization. However, a gravimetric analysis of the resulting solid content post-reaction revealed a 300wt% and 20wt% increase in solid mass for reactions with **CoMo-Al/PtRe-Si** and **CoMo-Al**, respectively. Thus, even if some polyethylene had been depolymerized, new polymer was being formed through oligomerization. Activity for oligomerization is in direct contrast to the goal of our project; and ultimately, this investigation asserted that **Mo-Al** catalyst systems were not suitable for further development.

**Table 5.2.**  $^1\text{H}$  NMR analysis of reacted polyethylene using **CoMo-Al** as a depolymerization catalyst

Sample Description	T/ $^{\circ}\text{C}$	Time/h	Terminal to Internal C=C	$M_N$
Unreacted PE	n/a	n/a	1 to 1.3	$61.2 \pm 0.9^a$



**Table 5.2 (cont.)**

<b>Sample Description</b>	<b>T/°C</b>	<b>Time/h</b>	<b>Terminal to Internal C=C</b>	<b>M<sub>N</sub></b>
PE reacted w/ <b>CoMo-Al</b>	150	74	Terminal n.d.	38.6
PE reacted w/ <b>CoMo-Al</b> + <b>PtRe-Si</b>	150	74	1 to 6.3	48.9

<sup>a</sup>Standard deviations were calculated by performing calculations using two distinct proton resonances via <sup>1</sup>H NMR.

#### 5.4 ReO<sub>x</sub>-Al<sub>2</sub>O<sub>3</sub> (**Re-Al**) for Polyethylene Depolymerization

We next turned our attention to the application of alumina supported rhenium oxide catalysts which are known to be well-suited for ethenolysis.<sup>1,12–15</sup> For this study, we synthesized a ReO<sub>x</sub>(10wt%)-Al<sub>2</sub>O<sub>3</sub> (**Re-Al**) catalyst according to literature procedure (refer to **Appendix D** for synthetic procedures).<sup>13</sup> Basic knowledge of the catalyst's reactivity toward model alkenes had been established by our collaborators (Scott group at UCSB); thus, the work presented here focuses only on the reaction of **Re-Al** with polyethylene (MW ~ 870 g/mol) using our flow device.

The flow reactor was loaded with 140 mg of **Re-Al**, 150 mg of **PtRe-Si** (1:1 Me<sub>3</sub>Al:Re), and 150 mg of polyethylene (MW ~ 870 g/mol). Afterwards, the reactor was pressurized with 100 PSI of ethylene and then heated to 170°C. Under a continuous flow of ethylene gas (5 mmol/h), the effluent stream was sampled, and the volatile product distribution was analyzed.

The reaction of polyethylene with **Re-Al/PtRe-Si** catalysts produced propylene and butene as the predominant products formed at a maximum rate of 0.03 and 0.02 mmol/h, respectively (**Figure 5.4**). In a separate control study, we exchanged polyethylene for silicon oil (to retain a condensed phase). Upon reaction, the formation of butene was detected showcasing ethylene dimerization by **Re-Al/PtReSi**. However, propylene was not detected in significant quantity (**Figure D6**). This observation suggested that most of the propylene formed upon reaction with polyethylene was derived from the depolymerization pathway. Despite the successful formation of propylene from

polyethylene, the catalytic rate was low, and the activity of the catalyst decayed rapidly. The resulting polymer material was submitted to Dow Chemical for further characterization of the molecular weight distribution (MWD).

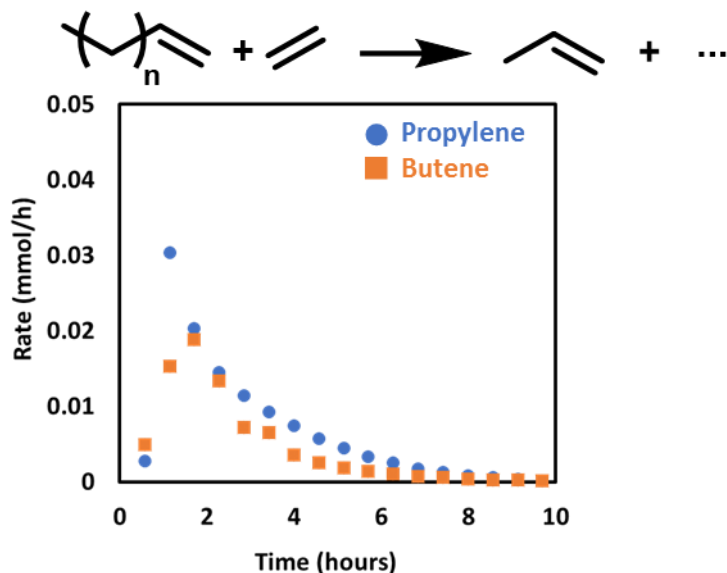


**Figure 5.4.** Flow reactor data showcasing olefin formation over time for a polyethylene depolymerization reaction catalyzed by tandem **Re-Al** and **PtRe-Si**.

In addition to **PtRe-Si**, a “pincer”-ligated iridium dehydrogenation complex ( $[\text{tBuPOCOP}]\text{Ir}[\text{C}_2\text{H}_4]$ , **1-Ir**) was also studied. This iridium catalyst has been used, previously, in tandem with **Re-Al** for alkane dehydrogenation and cross-metathesis reactions.<sup>16</sup> Considering the similarity of these tandem reactions to our methodology, we thought to extend this catalyst system to polyethylene depolymerization. **1-Ir** was adsorbed onto **Re-Al** to afford a bimetallic catalyst (see **Appendix D** for synthetic details), and we reacted the resulting material with polyethylene in our flow reactor (100 PSI, 170°C) under a continuous feed of ethylene gas (5 mmol/h). We detected propylene and butene as the predominant products which were formed at a maximum rate of 0.22 and 0.03 mmol/h, respectively (**Figure 5.5**). In a second experiment, we removed polyethylene from the reaction formulation, and this control study showcased that **1-Ir/Re-Al** was not significantly active for ethylene dimerization (**Figure D7**). Thus, using **1-Ir/Re-Al**, we successfully produced light

olefins from polyethylene with a high selectivity for propylene (7.4  $R_{C3}/R_{C4}$ ). Unfortunately, the activity of the catalyst decayed rapidly after several hours on stream. The resulting polymer material was submitted to Dow Chemical for further characterization of the MWD.

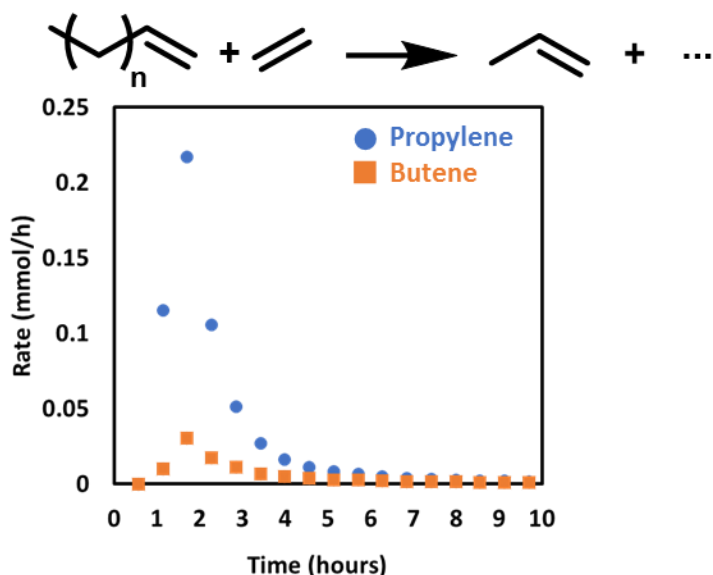


**Figure 5.5.** Flow reactor data showcasing olefin formation over time for a polyethylene depolymerization reaction catalyzed by tandem **1-Ir** supported on **Re-Al**.

## 5.5 Summary of Catalyst Performance for Polyethylene Depolymerization in Continuous Flow

Herein, we summarize the volatile product formation of several catalysts used for continuous flow depolymerization of polyethylene (**Table 5.3**). Because the catalysts were studied under different reaction conditions (e.g., temperature, pressure, etc.), the reported rates could not be directly compared. Nonetheless, the analyses of the polymer samples after reaction and of the volatile product selectivity (propylene to butene ratio) provide metrics to evaluate a catalysts' viability for polyethylene depolymerization.

A high selectivity for butene relative to propylene, generally, correlates with ethylene dimerization. This side reaction is undesired as dimerization appears to coincide with the formation of higher molecular weight polymer. This was illustrated using **CoMo** and **Mo** catalysts activated

by Me<sub>3</sub>Al. Oligomerization activity ruled out the application of these catalysts for polyethylene depolymerization. Importantly, a high selectivity for propylene relative to butene is not sufficient proof of successful tandem depolymerization; thus, a control study or other experimentation (i.e., isotope labeling) are essential to determining the origin of light olefin formation.

A mixture of **1-Ir** and **Re-Al** only showed minor activity for ethylene dimerization. Furthermore, the catalyst showed a high selectivity for propylene (7.4 R<sub>C3</sub>/R<sub>C4</sub>). However, the catalytic rate decayed quickly under the reaction conditions. Unfortunately, the poor temperature stability of these catalysts makes them incompatible for commercial application. Future work should look towards identifying or developing catalysts with higher activity and improved stability.

**Table 5.3.** Summary of flow investigations for polymer depolymerization reactions.

Catalyst(s)	T/°C	Ethylene P/ $\dot{n}$ (PSI/mmole h <sup>-1</sup> )	R <sub>C3,max</sub> <sup>a</sup> (mmole <sub>C3</sub> g <sub>cat</sub> <sup>-1</sup> h <sup>-1</sup> )	R <sub>C4,max</sub> <sup>a</sup> (mmole <sub>C4</sub> g <sub>cat</sub> <sup>-1</sup> h <sup>-1</sup> )	S <sub>@C3,max</sub> <sup>b</sup> (R <sub>C3,max</sub> /R <sub>C4</sub> )
Mo-Si PtRe-Si	150	80/5	0.02	0.006	3.3
CoMo-Al PtRe-Si <sup>c</sup>	150	100/5	3.9	2.7	1.4
Re-Al PtRe-Si	170	100/5	2.1	1.4	1.8
1-Ir Re-Al	150	100/5	14.7	2.0	7.4

Red colored cells highlight poorly performing catalysts for PE depolymerization (dimerization side reactions and/or low rates). Green colored cells highlight catalysts that successfully formed propylene from PE. <sup>a</sup>Rates are calculated by normalizing the maximum formation rate for the olefin of interest by the concentration of metathesis catalyst. <sup>b</sup>Selectivity is defined as the ratio of propylene to butene, and it is evaluated at the maximum rate of propylene formation. <sup>c</sup>Data reported for **CoMo-Al/PtRe-Si** are convoluted by the oligomerization of ethylene.

## 5.6 Conclusions and Outlook

In this chapter, we have showcased the depolymerization of polyethylene to light olefin products, propylene and butene. The analysis of plausible catalytic materials was performed in our continuous flow reactor, and the implementation of this reactor system allowed for the rapid screening of catalytic rate and stability. Within this summary, we provide the evaluation of several promising metathesis and dehydrogenation catalyst pairings.

Unfortunately, the catalytic rate of **Mo-Si** proved to be far too sluggish, and the side reactions (i.e., ethylene oligomerization) catalyzed by **CoMo-Al** and **Mo-Al** activated by Me<sub>3</sub>Al were undesired. However, using two different heterogeneous rhenium systems, **Re-Al/PtRe-Si** and **1-Ir/Re-Al**, we successfully demonstrated the formation of light olefins from polyethylene. Looking towards future advances, efforts must be made to identify faster and more stable tandem catalysts as the activity of the materials presented are not sufficient.

## 5.7 References

- (1) Lwin, S.; Wachs, I. E. Olefin Metathesis by Supported Metal Oxide Catalysts. *ACS Catal.* **2014**, *4* (8), 2505–2520.
- (2) Zhang, B.; Li, Y.; Lin, Q.; Jin, D. A Study of MoO<sub>3</sub>/SiO<sub>2</sub> Metathesis Catalyst Break-in: Active Site Formation and Characterisation. *J. Mol. Catal.* **1988**, *46* (1–3), 229–241.
- (3) Chakrabarti, A.; Wachs, I. E. Molecular Structure-Reactivity Relationships for Olefin Metathesis by Al<sub>2</sub>O<sub>3</sub>-Supported Surface MoO<sub>x</sub> Sites. *ACS Catal.* **2018**, *8* (2), 949–959.
- (4) Debecker, D. P.; Stoyanova, M.; Rodemerck, U.; Gaigneaux, E. M. Preparation of MoO<sub>3</sub>/SiO<sub>2</sub>–Al<sub>2</sub>O<sub>3</sub> Metathesis Catalysts via Wet Impregnation with Different Mo Precursors. *J. Mol. Catal. A Chem.* **2011**, *340* (1–2), 65–76.
- (5) Andrei, R. D.; Popa, M. I.; Cammarano, C.; Hulea, V. Nickel and Molybdenum Containing Mesoporous Catalysts for Ethylene Oligomerization and Metathesis. *New J. Chem.* **2016**, *40* (5), 4146–4152.
- (6) Grünert, W.; Stakheev, A. Y.; Feldhaus, R.; Anders, K.; Shpiro, E. S.; Minachev, K. M. Reduction and Metathesis Activity of MoO<sub>3</sub>/Al<sub>2</sub>O<sub>3</sub> Catalysts II. The Activation of MoO<sub>3</sub>/Al<sub>2</sub>O<sub>3</sub> Catalysts. *J. Catal.* **1992**, *135* (1), 287–299.
- (7) Chakrabarti, A.; Wachs, I. E. Activation Mechanism and Surface Intermediates during

- Olefin Metathesis by Supported MoO<sub>x</sub>/Al<sub>2</sub>O<sub>3</sub> Catalysts. *J. Phys. Chem. C* **2019**, *123* (19), 12367–12375.
- (8) Bradshaw, C. P. C.; Howman, E. J.; Turner, L. Olefin Dismutation: Reactions of Olefins on Cobalt Oxide-Molybdenum Oxide-Alumina. *J. Catal.* **1967**, *7* (3), 269–276.
  - (9) LIPSCH, J. The CoO-MoO<sub>3</sub>-Al<sub>2</sub>O<sub>3</sub> Catalyst I. Cobalt Molybdate and the Cobalt Oxide Molybdenum Oxide System. *J. Catal.* **1969**, *15* (2), 163–173.
  - (10) Keim, W. Oligomerization of Ethylene to  $\alpha$ -Olefins: Discovery and Development of the Shell Higher Olefin Process (SHOP). *Angew. Chemie - Int. Ed.* **2013**, *52* (48), 12492–12496.
  - (11) Da Rosa, R. G.; De Souza, M. O.; De Souza, R. F. Oligomerization and Co-Oligomerization of  $\alpha$ -Olefins Catalyzed by Nickel(II)/Alkylaluminum Systems. *J. Mol. Catal. A Chem.* **1997**, *120* (1–3), 55–62.
  - (12) Lutz. United States Patent: 5672802. **1997**.
  - (13) Sharkey, B. E.; Denning, A. L.; Jentoft, F. C.; Gangadhara, R.; Gopaladasu, T. V.; Nicholas, K. M. New Solid Oxo-Rhenium and Oxo-Molybdenum Catalysts for the Deoxydehydration of Glycols to Olefins. *Catal. Today* **2018**, *310*, 86–93.
  - (14) Mol, J. C. Olefin Metathesis over Supported Rhenium Oxide Catalysts. *Catal. Today* **1999**, *51* (2), 289–299.
  - (15) Lwin, S.; Keturakis, C.; Handzlik, J.; Sautet, P.; Li, Y.; Frenkel, A. I.; Wachs, I. E. Surface ReO<sub>x</sub> Sites on Al<sub>2</sub>O<sub>3</sub> and Their Molecular Structure–Reactivity Relationships for Olefin Metathesis. *ACS Catal.* **2015**, *5* (3), 1432–1444.
  - (16) Jia, X. et al. Efficient and Selective Degradation of Polyethylenes into Liquid Fuels and Waxes under Mild Conditions. *Sci. Adv.* **2016**, *2* (6), 1–8.

# Appendix A: Liquid Immobilized Guerbet Catalyst in a Tank Reactor for Mechanistic Investigation

By Nicholas Wang

## Table of Contents

1. **Reactor Setup and Equipment**  
Figure A1. Depiction and image of continuously stirred tank reactor setup.
2. **Catalyst Synthesis and Stability with Polymer**  
Figure A2. Stability of catalyst in batch with PEG (Polyethylene glycol).  
Figure A3.  $^{31}\text{P}$  NMR studies for catalyst stability in polymer.
3. **Mass Balance for Ethanol Coupling Reaction**  
Figure A4. Mass Balance Over Time for Ethanol Coupling Experiment.
4. **Sample Calculation for Residence Time**
5. **Rate Calculations for 1-Ru**  
Figure A5. Species Calibration Curves for 1-Ru.
6. **CSTR Mass Transport**  
Figure A6. Product profile produced using the flow reactor while varying the stir-rate of the catalyst solution and the stir-bar size.
7. **Modeling of Guerbet Reaction in the CSTR**  
Figure A7. Reactions Considered for Guerbet Model.  
Figure A8. Parameterized Reaction Equations for Each Chemical Species.  
Figure A9. Combined/Parameterized Reaction and CSTR Design Equations.  
Figure A10. Experimental Setup and Data for Determining  $C_{T,L}$ .  
Figure A11. Simulated Profile for Ethanol Coupling Reaction.
8. **Random Coupling Model (Flory's Equal Reactivity Principle)**  
Figure A12. Butanol Selectivity as a Function of Ethanol Conversion.  
Figure A13. Butanol Formation as a Function of Ethanol Conversion.
9. **Cannizzaro and Tishchenko Side Products – Batch Condensation Reactions**  
Table A1. Composition for identified/detected products in the presence of sodium ethoxide.
10. **Gas-Phase analysis of Transfer Hydrogenations for Unsaturated  $C_4$  Intermediates**  
Figure A14. Butyraldehyde Hydrogenation.  
Figure A15. Crotyl Alcohol Hydrogenation.  
Figure A16. Crotonaldehyde Hydrogenation.
11. **Comparison of Acetone and Butanol Formation Rates**  
Figure A17.  $i\text{PrOH}$  and Butyraldehyde Transfer Hydrogenation.  
Figure A18.  $i\text{PrOH}$  and Crotyl Alcohol Transfer Hydrogenation.  
Figure A19.  $i\text{PrOH}$  and Crotonaldehyde Transfer Hydrogenation.  
Figure A20. Acetone Formation Rates in the Presence of Various Intermediates.
12. **Hydrogen Solubility Under Reaction Conditions**  
Figure A21. Schematic for Thermodynamic Model.  
Table A2. Stream Table for Flash Separation of a PEG, Ethanol and Hydrogen Mixture.
13. **Product Identification**  
Table A3. GC species retention time for Guerbet reaction (Restek column).  
Table A4. GC species retention time for Guerbet reaction (DB-Wax column).
14. **Materials, Equipment, and Supplies Summary**
15. **Preparation of chemicals**
16. **Notes and references**

## 1. Reactor Setup and Equipment

### Continuously Stirred Tank Reactor Configuration

For ethanol coupling reactions in our continuously stirred tank reactor setup (CSTR), the catalyst and co-catalyst (sodium ethoxide) were dissolved in a polymer solvent and placed within a stainless-steel reactor that was fitted with an aluminum heating jacket. The temperature of the heating jacket was controlled by a hotplate and thermocouple (IKA C-MAG HS7 digital). Ethanol was delivered using a Kd Scientific Legato 100 Syringe Pump, and nitrogen carrier gas was supplied from a pressurized tank whose flow was set by an Alicat mass flow controller (MCS series). Pressurized tubing and fittings were purchased from McMaster-Carr and Swagelok. Attached to this reactor setup, an Agilent 6850 gas chromatograph equipped with an FID was used to analyze the gaseous products. A Restek rxi-1ms column was used for the analysis of ethanol coupling reactions and a J&W DB-Wax column was used for the analysis of transfer hydrogenation reactions.

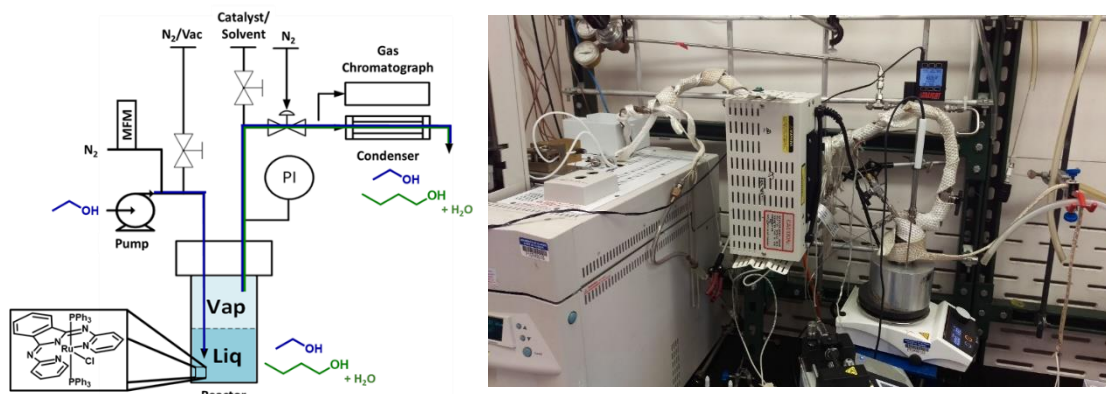


Figure A1. Continuously Stirred Tank Reactor Configuration.

## 2. Catalyst Synthesis and Stability with Polymer

### Ru(bpi)(PPh<sub>3</sub>)<sub>2</sub>Cl Synthesis:

Synthesis of the ruthenium complex was taken from literature.<sup>1-3</sup> Confirmation of complex synthesis was performed by <sup>1</sup>HNMR and <sup>31</sup>PNMR using benzene-d<sub>6</sub> as an internal standard.

1.74 mmol (80 mg) of EtOH was placed in a sealed vessel with 2 mmol (1000 mg) of monomethoxy PEG<sub>500</sub>, 0.88 mmol (60 mg) of sodium ethoxide, and 5.5e<sup>-3</sup> mmol (5.5 mg) of ruthenium catalyst. The reaction was carried out at 120°C over 10 hours. The data shows that the catalyst maintains a stable rate even after multiple hours on stream. The conversion throughout the experiment is kept below 7%.

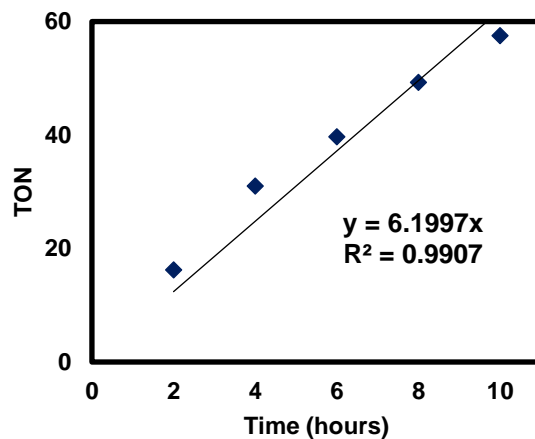


Figure A2. Stability of Catalysts in Batch with PEG (polyethylene glycol).



$3 \times 10^{-4}$  mmol (3 mg) of **1-Ru** was dissolved in 8.7 mmol (400 mg) of ethanol and 0.8 mmol (400 mg) of PEG<sub>500</sub>. These mixtures were then heated to 120°C for 30 minutes. Afterwards, the samples were cooled, and 0.5 mL of benzene- $d_6$  was added. The resulting solutions were analyzed using  $^{31}\text{P}$  NMR, and the stability of the catalysts was compared. **1-Ru** can be identified by the peak at 25.89 ppm. Additionally, some  $\text{PPh}_3$  dissociation was observed (-6 ppm). After heating, an unidentified complex (24.95 ppm) was observed in the catalyst-PEG mixture. However, this species was only detected in small quantities (6%), showcasing that the catalyst remains largely inert to the polymer under the reaction conditions.

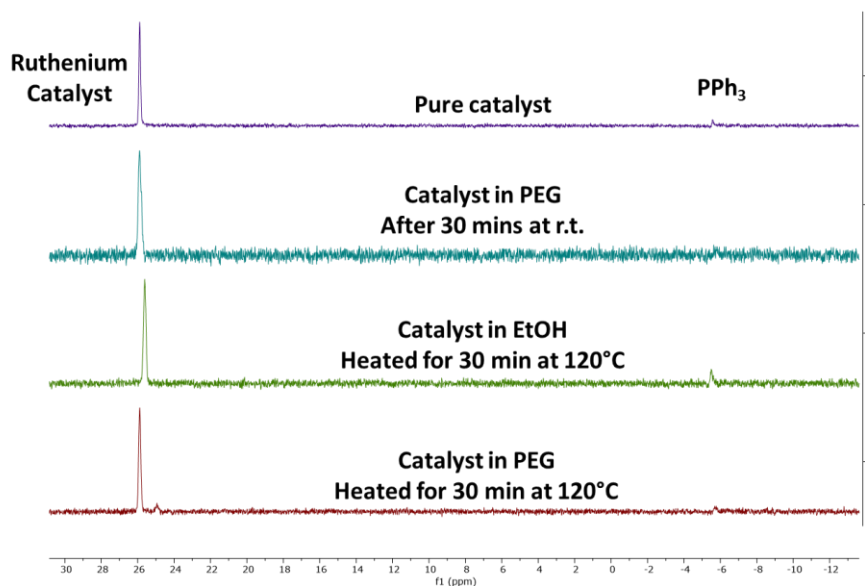


Figure A3.  $^{31}\text{P}$  NMR studies for catalyst stability in polymer.

### 3. Mass Balance for Ethanol Coupling Reaction

The mass balance is depicted below for an ethanol coupling experiment performed at 120°C under standard catalyst loadings. Notably, the mass balance does not close initially, due to the transient accumulation of butanol. After 5 hours on stream, we attain a quasi-steady condition, and the mass balance fully closes. The mass balance is calculated by comparing the initial ethanol flow rate to the sum of all volatilized product and substrate formation rates ( $\text{C}_2\text{-C}_6$ ).

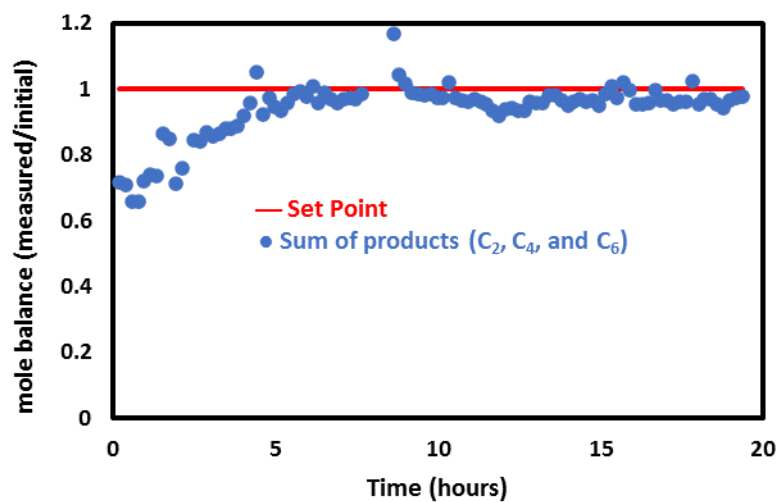


Figure A4. Mass Balance Over Time for Ethanol Coupling Experiment.

#### 4. Sample Calculation for Residence Time

Residence times were calculated by dividing the total reaction volume by the total volumetric flowrate. For the CSTR setup, the reactor volume was calculated using the volume of polymer solvent. These residence times are only an approximation, since the calculation of the exact residence time would require knowledge of the ethanol quantity dissolved within the polymer.

##### Relevant Parameters

$$n_{Ru} = \text{moles of catalyst (mmol)}$$

$$\dot{n}_{EtOH} = \text{molar flowrate of ethanol} \left( \frac{\text{mmol}}{\text{h}} \right)$$

$$\dot{n}_{Tol} = \text{molar flowrate of ethanol} \left( \frac{\text{mmol}}{\text{h}} \right)$$

$$x_{Tol} = \text{mole fraction of toluene}$$

$$\dot{v}_{EtOH}(l) = \text{liquid volumetric rate of ethanol} \left( \frac{\text{mL}}{\text{min}} \right)$$

$$\dot{v}_{EtOH}(g) = \text{gaseous volumetric rate of ethanol} \left( \frac{\text{mL}}{\text{min}} \right)$$

$$\dot{v}_{N_2}(g) = \text{gaseous volumetric rate of nitrogen} \left( \frac{\text{mL}}{\text{min}} \right)$$

$$\rho_{EtOH} = \text{density of ethanol} \left( \frac{\text{g}}{\text{mL}} \right)$$

$$\rho_{Al} = \text{density of alumina} \left( \frac{\text{g}}{\text{mL}} \right)$$

$$MW_{EtOH} = \text{molecular weight of ethanol} \left( \frac{\text{g}}{\text{mol}} \right)$$

$$M_{Al} = \text{mass of alumina (g)}$$

$$R = \text{ideal gas constant} \left( \frac{\text{L atm}}{\text{mol K}} \right)$$

$$T = \text{temperature (K)}$$

$$V = \text{reaction volume (mL)}$$

$$\tau = \text{residence time (s)}$$

##### Convert liquid volumetric rate of ethanol to a molar flowrate of ethanol:

$$\dot{n}_{EtOH} = \left( 0.00125 \frac{\text{mL (l)}}{\text{min}} \right) * \left( 0.789 \frac{\text{g}}{\text{mL}} \right) * \left( \frac{1 \text{ mol}}{46 \text{ g}} \right) * \left( 1000 \frac{\text{mmol}}{\text{mol}} \right) * \left( 60 \frac{\text{min}}{\text{h}} \right) = 1.286 \frac{\text{mmol EtOH}}{\text{h}}$$

##### Convert the molar rate of ethanol to a gaseous volumetric flowrate:

Note, temperature and pressure are taken from reaction operating conditions.

$$\dot{v}_{EtOH}(g) = \dot{n}_{EtOH} * MW_{EtOH} * \frac{1}{\rho_{EtOH,gas@120^{\circ}C}}$$

$$\dot{v}_{EtOH} = \left( 1.286 \frac{\text{mmol EtOH}}{\text{h}} \right) * \left( 46 \frac{\text{mg}}{\text{mmol}} \right) * \left( \frac{1 \text{ mL}}{0.001409 \text{ g}} \right) * \left( \frac{1 \text{ g}}{1000 \text{ mg}} \right) * \left( \frac{1 \text{ h}}{60 \text{ min}} \right) = 0.7 \frac{\text{mL}}{\text{min}} \text{ of EtOH (g)}$$

Calculate residence time:

CSTR: Reactor volume is calculated using the volume of PEG used for the reaction.

Ex. for a sample with a 6 g loading of PEG

$$V = \frac{m}{\rho_{PEG}} = \frac{6}{1.12} \text{ mL} \sim 5.38 \text{ mL}$$

Nitrogen flowrate is set by mass flow controller. Ethanol flowrate was calculated above.

$$\tau = \frac{V}{\dot{v}_{EtOH}(g) + \dot{v}_{N_2}(g)} = \frac{5.38 \text{ mL}}{0.7 + 8.5 \frac{\text{mL}}{\text{min}}} * 60 \frac{\text{s}}{\text{min}} \sim 35 \text{ s}$$

## 5. Example Rate Calculations

Toluene was used as an internal standard (1 mol% in the ethanol feed) to precisely quantify the rate of product formation during catalysis. The rate of formation was then normalized by the catalyst quantity to calculate the turnover frequencies.

Example calculation for ethanol coupling rate calculations using 1-Ru:

Convert volumetric liquid injection flowrates of ethanol (substrate) and toluene (1 mol%) feed to molar flowrates.

$$\dot{n}_{EtOH} = \dot{v}_{EtOH}(L) * \rho_{EtOH} * \frac{1}{MW_{EtOH}} = 4.11 \frac{\text{mmol EtOH}}{h}$$

$$\dot{n}_{Tol} = x_{Tol} * \dot{n}_{EtOH} = 0.1 * 4.11 = 0.411 \frac{\text{mmol Tol}}{h}$$

Calibration curve: mixtures of ethanol butanol and toluene are measured in known quantities and run through the gas chromatograph to produce intensities (areas). Similar calibration curves were created for other species (not shown).

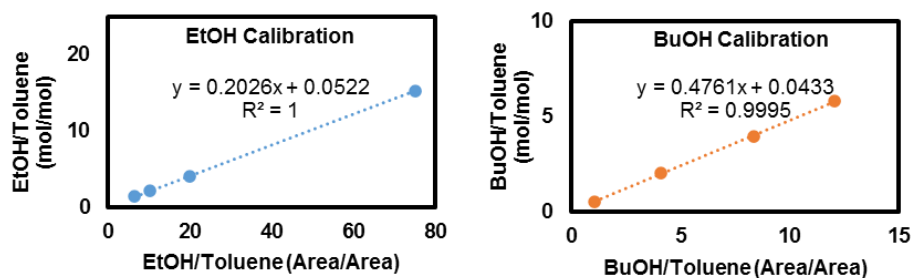


Figure A5. Species Calibration Curves.

Use response factor from calibration curves with areas obtained from the gas chromatograph during catalysis to calculate the rate of product formation based upon the molar flowrate of toluene. Finally, normalize by catalyst loading to get turnover rate.

$$\dot{n}_{BuOH} = \frac{Area \text{ BuOH}}{Area \text{ Toluene}} * \dot{n}_{Tol} * \frac{1}{Response \text{ Factor}}$$

$$\dot{n}_{BuOH} = \frac{100}{4500} \left( \frac{Area \text{ BuOH}}{Area \text{ Toluene}} \right) * 0.411 \left( \frac{\text{mmol Tol}}{h} \right) * \frac{1}{0.4761 \left( \frac{Area \text{ Toluene}}{Area \text{ BuOH}} * \frac{\text{mmol BuOH}}{\text{mmol Tol}} \right)}$$

$$= 0.00192 \frac{\text{mmole BuOH}}{h}$$

$$TOF = \frac{\dot{n}_{BuOH}}{n_{Ru}} = \frac{0.00192 \frac{\text{mol BuOH}}{h}}{0.0016 \text{ mol Ru}} = 1.2 \text{ h}^{-1}$$

## 6. CSTR Mass Transport

EtOH and N<sub>2</sub> were fed into our flow reactor at 1.25  $\mu\text{L}/\text{min}$  (l) and 8.4 mL/min (g), respectively. The reactor is held at 120°C and 15.5 psi and is charged with a solution of PEG (4 mL) and EtONa (385 mM). After pre-heating (1-hour), **1-Ru** (0.66 mM) is injected into the system, and the volatile product formation rate is analyzed over time via GC. The stir-rate and stir-bar dimensions were altered to perturb the transfer surface between the ethanol (solvated in PEG) and the reactor headspace. No discontinuity of alcohol formation rate detected upon increasing the stir-rate of the catalyst solution. Moreover, the two near-identical profiles shown below depict no augmentation to alcohol formation rate despite an increase in stir-bar size. These observations suggest that the catalysis performed in our flow reactor is not mass transfer limited.

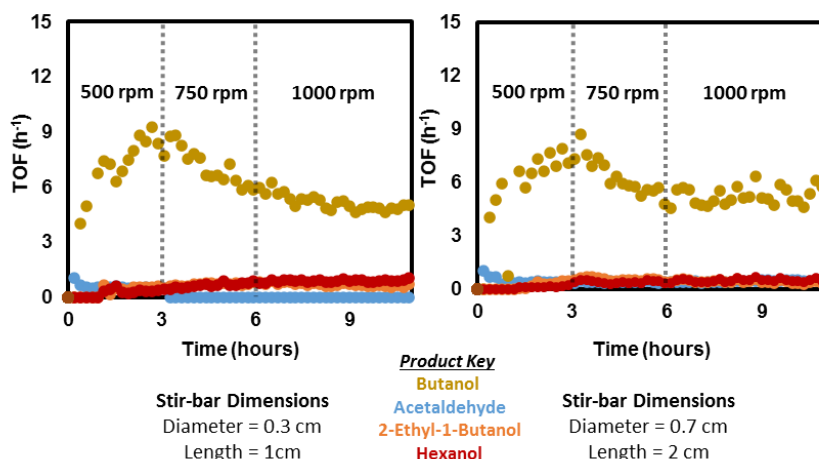


**Figure A6.** Product profile produced using the flow reactor while varying the stir-rate of the catalyst solution and the stir-bar size.

## 7. Modeling of Guerbet Reaction in the CSTR

To further validate our mechanistic understanding, we developed a qualitative kinetic model for the reaction in our CSTR. First, several chemical reactions including elimination ( $k_1$  and  $k_{-4}$ ), condensation ( $k_2$ ,  $k_5$ ), and transfer hydrogenation ( $k_3$ ,  $k_4$ ,  $k_6$ , and  $k_7$ ) were selected to describe the proposed pathway. Elimination was considered the slowest step for the reaction network, and first order dependencies were assumed for all chemical species. Next, a set of differential equations was developed describing their rates of formation, and these differential rate expressions were coupled with CSTR design equations while assuming that evaporation rate was directly proportional to the concentration in the liquid phase (instantaneous equilibrium i.e., no mass transfer limitation). Paired with experimental data, the combined reaction and reactor equations were solved simultaneously using Matlab(ODE45) to produce reaction profiles describing the formation rate of products in the gas-phase. Examination of the simulated experiment validated the non-linear reaction profile generated experimentally. First, the initial accumulation of butanol was observed; whereafter, butanol was consumed to produce hexanol, which also slowly collected in the reactor. After the transient accumulation of the various products, steady state was attained.

### Relevant Parameters

$$N_A = \text{Moles in the CSTR (mole)}$$

$$F_{A, \text{in or out}} = \text{Molar flow in or out of the reactor} \left( \frac{\text{mole}}{\text{time}} \right)$$

$$R_A = \text{Reaction rate} \left( \frac{\text{mol}}{\text{volume time}} \right)$$

$$C_{A,L} = \text{Liquid phase concentration (M)}$$

$$C_{A,V} = \text{Gas phase concentration (M)}$$

$$q = \text{Volumetric flowrate} \left( \frac{\text{volume}}{\text{time}} \right)$$

$x_A = \text{Liquid mole fraction}$

$y_A = \text{Gas mole fraction}$

$P = \text{Overall pressure}$

$P_A^* = \text{Saturation pressure for species A}$

$C_{T,L} = \text{Total liquid phase concentration}(M)$

$C_{T,V} = \text{Total gas phase concentration}(M)$

$G_A = \text{Lumped parameter}$

#### Derived Reaction Equations ( $R_A$ )

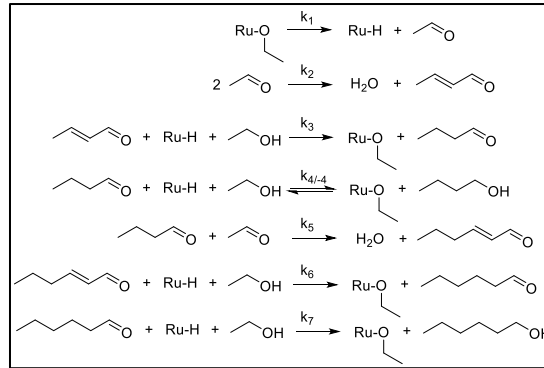


**Figure A7.** Reactions Considered for Guerbet Model.

Parameterized Species	Equations for Each Reaction Species
$y_1$ - Ethanol	$dy_1/dt = 0;$
$y_2$ - Acetaldehyde	$dy_2/dt = k_1 y_9 - k_2 y_2^2 - k_5 y_2 y_4$
$y_3$ - Crotonaldehyde	$dy_3/dt = k_2 y_2^2 - k_3 y_3 y_1 y_{10}$
$y_4$ - Butanal	$dy_4/dt = k_3 y_3 y_1 y_{10} - k_4 y_4 y_{10} y_1 + k_4 y_5 y_9 - k_5 y_4 y_2$
$y_5$ - Butanol	$dy_5/dt = k_4 y_4 y_{10} y_1 - k_4 y_5 y_9$
$y_6$ - 2-hexenal	$dy_6/dt = k_5 y_4 y_2 - k_6 y_6 y_{10} y_1$
$y_7$ - Hexenal	$dy_7/dt = k_6 y_6 y_{10} y_1 - k_7 y_7 y_{10} y_1$
$y_8$ - Hexanol	$dy_8/dt = k_7 y_7 y_{10} y_1$
$y_9$ - RuOEt	
$y_{10}$ - RuH	
	<b>Equations for Catalyst Concentration</b>
	$dy_9/dt = -k_1 y_9 + k_3 y_3 y_{10} y_1 + k_4 y_4 y_{10} y_1$
	$-k_4 y_5 y_9 + k_6 y_6 y_{10} y_1 + k_7 y_7 y_{10} y_1 + k_0 y_{10} y_1$
	$dy_{10}/dt = k_1 y_9 - k_3 y_3 y_{10} y_1 - k_4 y_4 y_{10} y_1 + k_4 y_5 y_9 - k_6 y_6 y_{10} y_1$
	$-k_7 y_7 y_{10} y_1 - k_0 y_{10} y_1$

**Figure A8.** Parameterized Reaction Equations for Each Chemical Species.

#### CSTR Design Equations

The CSTR design equation describes the accumulation in the CSTR as a function of inlet flow, outlet flow, and chemical reaction.

$$\frac{dN_A}{dt} = F_{A,in} - F_{A,out} + R_A$$

Next, we rewrite the design equation to be in terms of concentration. Assuming that the concentration of ethanol is constant in the polymer (low conversion) and considering that ethanol is the only feed, inlet flows are not considered for other reaction species. Thus the accumulation in the liquid polymer ( $C_{A,L}$ ) is a function of the evaporation in the gas phase  $[(q/V_L) * C_{A,V}]$  and the reaction rate.

$$\frac{dC_{A,L}}{dt} = -\frac{qC_{A,V}}{V_L} + R_A$$

### Relating liquid phase concentration ( $C_L$ ) to gas phase concentration ( $C_V$ )

Next a relationship is developed to relate concentration in the liquid phase to the gas phase. Assuming an instantaneous equilibrium, Raoult's law can be rewritten in terms of concentration. The total concentration in the liquid and gas-phase is presumed to be constant since ethanol is the predominant substrate (low conversion assumption).

$$y_A P = x_A P_A^*$$

$$\left(\frac{C_{A,V}}{C_{T,V}}\right) P = \left(\frac{C_{A,L}}{C_{T,L}}\right) P_A^*$$

### Combining reactor design equations and reaction equations

Combining reaction equations with CSTR design equations while assuming an instantaneous evaporation results in the following expression for each volatile reaction species where the lumped parameter  $G_A$  includes the residence time ( $q/V_L$ ) and volatility of the substrate ( $P^*/P$ ). Combining the reaction and reactor equations results in the final parameterized differential equations which describe the liquid concentration in the CSTR.

$$\frac{dC_{A,L}}{dt} = -\left[\left(\frac{q}{V_L}\right)\left(\frac{C_{T,V}}{C_{T,L}}\right)\left(\frac{P_A^*}{P}\right)\right] C_{A,L} + R_A = -G_A C_{A,L} + R_A$$

Parameterized Species	Initial Conditions	Combined differential equations that describe concentration (y) in the CSTR
$y_1$ - Ethanol	$y_1 = 0.04$ M	$dy_1/dt = 0$ ;
$y_2$ - Acetaldehyde	$y_2 = 0$	$dy_2/dt = -G_2 y_2 + k_1 y_9 - k_2 y_2^2 - k_5 y_2 y_4$
$y_3$ - Crotonaldehyde	$y_3 = 0$	$dy_3/dt = -G_3 y_3 + k_2 y_2^2 - k_3 y_3 y_1 y_{10}$
$y_4$ - Butanal	$y_4 = 0$	$dy_4/dt = -G_4 y_4 + k_3 y_3 y_1 y_{10} - k_4 y_4 y_{10} y_1 + k_4 y_5 y_9 - k_5 y_4 y_2$
$y_5$ - Butanol	$y_5 = 0$	$dy_5/dt = -G_5 y_5 + k_4 y_4 y_{10} y_1 - k_4 y_5 y_9$
$y_6$ - 2-Hexenal	$y_6 = 0$	$dy_6/dt = -G_6 y_6 + k_5 y_4 y_2 - k_6 y_6 y_{10} y_1$
$y_7$ - Hexenal	$y_7 = 0$	$dy_7/dt = -G_7 y_7 + k_6 y_6 y_{10} y_1 - k_7 y_7 y_{10} y_1$
$y_8$ - Hexanol	$y_8 = 0$	$dy_8/dt = -G_8 y_8 + k_7 y_7 y_{10} y_1$
$y_9$ - RuOEt	$y_9 = 6.6 \times 10^{-4}$ M	
$y_{10}$ - RuH	$y_{10} = 0$	
<b>Equations for Catalyst Concentration</b>		
$dy_9/dt = -k_1 y_9 + k_3 y_3 y_{10} y_1 + k_4 y_4 y_{10} y_1 - k_4 y_5 y_9 + k_6 y_6 y_{10} y_1 + k_7 y_7 y_{10} y_1 - k_8 y_{10} y_1$		
$dy_{10}/dt = k_1 y_9 - k_3 y_3 y_{10} y_1 - k_4 y_4 y_{10} y_1 + k_4 y_5 y_9 - k_6 y_6 y_{10} y_1 - k_7 y_7 y_{10} y_1 - k_8 y_{10} y_1$		

**Figure A9.** Combined/Parameterized Reaction and CSTR Design Equations.

### Estimating $C_{T,L}$ and $C_{T,V}$

( $C_{T,L}$ ) An experiment was designed to determine the concentration of ethanol in the liquid phase at elevated temperatures. A solution of PEG was placed into our stainless-steel flow reactor where ethanol and nitrogen are fed into the heated reactor at rates of 4  $\mu$ L/min and 8 mL/min, respectively. After 5 hours on stream, the reactor was sealed and cooled. Once the reactor reached room temperature a sample of the reactor solution was analyzed using an external standard (toluene) to calculate the concentration of ethanol in the PEG. The loading of PEG (which correlates to the excess headspace) was varied to determine the impact of condensation on the experiment. The experiment provided an estimate for the concentration of ethanol in the liquid phase to initialize our set of differential equations.

$$C_{T,L} = \frac{\left(\frac{10 \text{ mg EtOH}}{46 \frac{\text{mg}}{\text{mmol}}}\right)}{5.33 \frac{\text{mL}}{\text{min}}} = 0.0417 \text{ M}$$

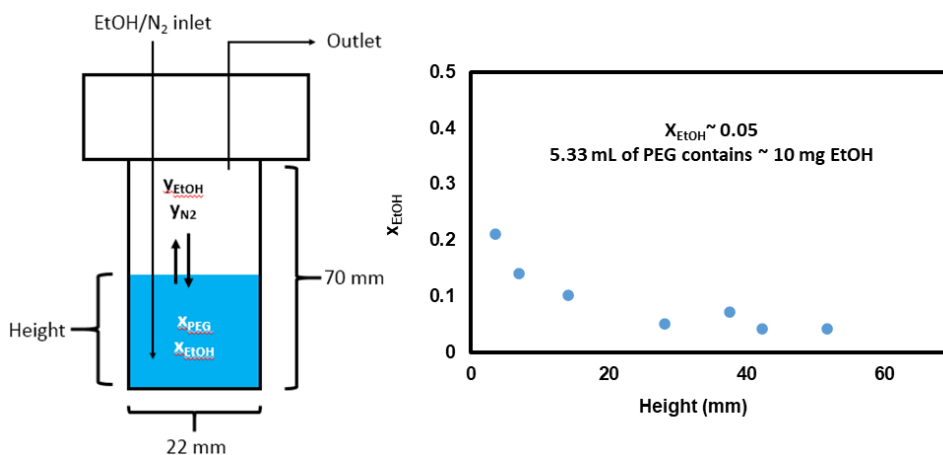


**Figure A10.** Experimental Setup and Data for Determining  $C_{T,L}$ .

( $C_{T,V}$  and  $q$ ) The total moles of gas in the headspace was estimated using the ideal gas law (1 atm, 120°C). Afterwards the composition of the headspace was calculated based on the molar feed ratios considering ethanol and nitrogen feed rates of 4  $\mu\text{L}/\text{min}$  (l) and 8 mL/min (g), respectively. Assuming ethanol concentration remains constant, the gaseous volumetric flowrate ( $q$ ) of all Guerbet products was set to 4 mL/h (g). This was calculated using the density of ethanol vapor at 120°. Note the solubility of nitrogen gas was not considered.

$$n_T \sim \frac{PV_V}{RT} = \frac{(1 \text{ atm}) \left( \frac{35}{1000} \text{ L} \right) \left( 1000 \frac{\text{mmol}}{\text{mol}} \right)}{\left( 0.082 \frac{\text{L atm}}{\text{mol K}} \right) (120 + 273 \text{ K})} = 1 \text{ mmol}$$

$$x_{EtOH,V} = \frac{\dot{n}_{EtOH}}{\dot{n}_{N_2} + \dot{n}_{EtOH}} = \frac{6.86e^{-5} \frac{\text{mol}}{\text{min}}}{7.14e^{-4} \frac{\text{mol}}{\text{min}} + 6.86e^{-5} \frac{\text{mol}}{\text{min}}} = 0.088$$

$$C_{T,V} = n_{EtOH,V} * V_V = \frac{0.088 \text{ mmol}}{35 \text{ mL}} = 0.0025 \text{ M}$$

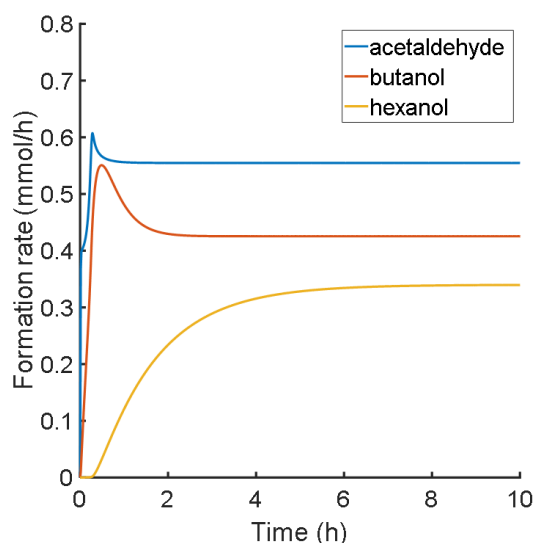


**Figure A11.** Simulated profile for ethanol coupling reaction in the CSTR flow system. Calculations were based upon ethanol and nitrogen flowrates set at 4  $\mu\text{L}/\text{min}$  (l) and 8 mL/min, respectively. Rate constants [elimination:  $k_1 = k_4 = 75 \text{ h}^{-1}$ ; condensation:  $k_2 = k_5 = 1.2e^5 \text{ M}^{-1}\text{h}^{-1}$ ; hydrogenation:  $k_3 = k_4 = k_6 = k_7 = 4e^8 \text{ M}^{-2}\text{h}^{-1}$ ]. Initial Conditions [EtOH] = 0.04 M and [RuOEt] =  $6.6e^{-4}$  M.

## 8. Random Coupling Model (Flory's Equal Reactivity Principle)

### Step-growth condensation equation

$$x_i = (1 - p)p^{i-1}$$

### Relevant Parameters

$x_i$  = mole fraction

$p$  = extent of reaction (conversion)

$i$  = number of repeat units

### Composition of a random coupling reaction at 2.5 mol% ethanol conversion

$$x_{EtOH} = x_1 = (1 - 0.025)0.025^{1-1} = 0.975$$

$$x_{BuOH} = x_2 = (1 - 0.025)0.025^{2-1} = 0.0244$$

$$x_{HexOH} = x_3 = (1 - 0.025)0.025^{3-1} = 0.00060$$

$$\frac{C_4}{C_6} = \frac{x_{BuOH}}{x_{HexOH}} = \frac{0.0244}{0.0006} = 40.67$$

For the following data, an ethanol coupling reaction was modeled using the step-growth condensation equation shown above. For a specified ethanol conversion, the mol fraction of coupling products ranging from  $C_2$  to  $C_{28}$  was calculated. Selectivity is described as the mol fraction of butanol relative to the total formation of other carbon products [ $S_{C_4} = C_4/\sum(C_i)$ ].

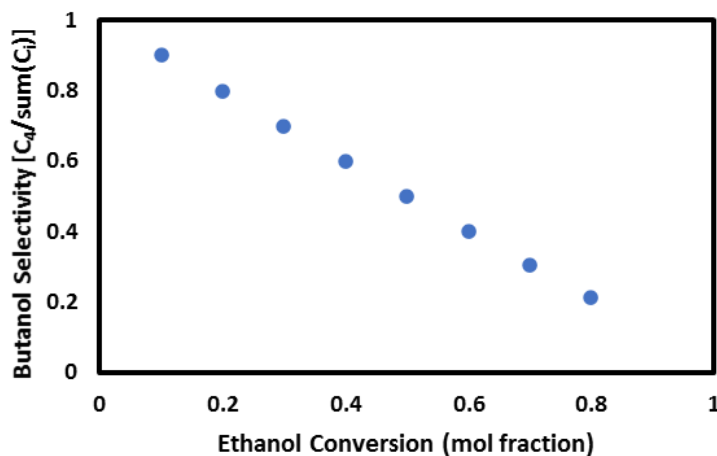


Figure A12. Butanol Selectivity as a Function of Ethanol Conversion.



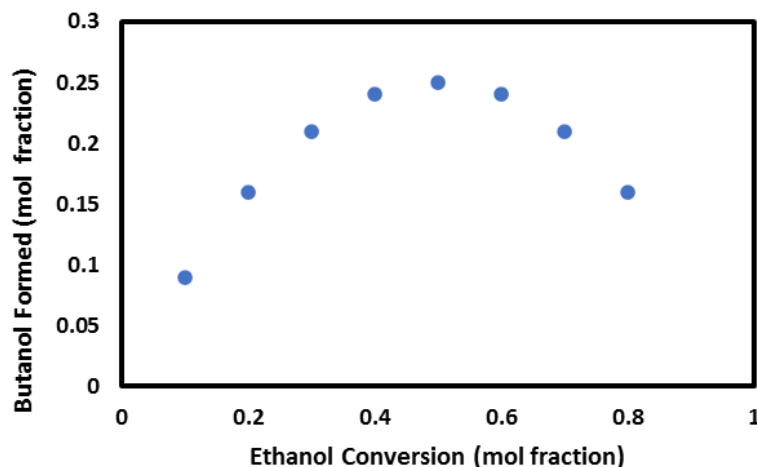


Figure A13. Butanol Formation as a Function of Ethanol Conversion.

#### 9. Cannizzaro and Tishchenko Side Products – Batch Condensation Reactions

Diglyme (1 mL), acetaldehyde and butyraldehyde (1:1 molar mixture totaling 1 mL) were reacted in the presence of sodium ethoxide (330 mM) at 120°C in a sealed glass vessel for 1 hour. The resulting product mixture revealed the presence of aldehydes, acids, and esters whose relative compositions have been tabulated below. The range of products showcases competition amongst aldol condensation, Cannizzaro and Tishchenko reactions.

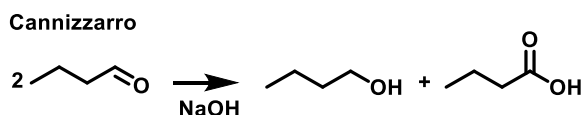


Table A1. Composition for identified/detected products in the presence of sodium ethoxide.

Species	mol%
Acetaldehyde	35.24
Butyraldehyde	53.39
Butanol	0.41
Crotonaldehyde	0.2
2-ethyl-butanol	0.85
2-ethyl-hexanol	1.42
Butyl Butyrate	0.41
Acetic Acid	7.26
Butyric Acid	0.82

#### 10. Gas-Phase analysis of Transfer Hydrogenations for Unsaturated C<sub>4</sub> Intermediates

<sup>i</sup>PrOH (spiked with 1 mol% of unsaturated C<sub>4</sub>) and He are fed into our flow device at 20 μL/min (l) and 100 mL/min (g), respectively. The reactor is held at 120°C and 15.5 psi. After 3 hours, a solution of PEG (4.9 mL) and EtONa (420 mM) are injected into the reactor where we observe poor mass balance closure in the gas phase for experiments involving butyraldehyde and crotonaldehyde. For aldehyde substrates in the presence of sodium ethoxide, some formation of butanol is observed which is derived from aldehyde disproportionation side reactions (Cannizzaro), which takes two molecules of the corresponding aldehyde and converts it into an acid and an alcohol. Crotyl alcohol which has a carbon-carbon double bond cannot participate in aldehyde side reactions where no side-products are observed in the presence of sodium. After an additional 3 hours on stream, a solution

of PEG (0.45 mL) and **1-Ru** (15 mM) are injected into the reactor and mixed with the sodium ethoxide co-catalyst, where high to moderate conversion of unsaturated substrates to butanol is observed.

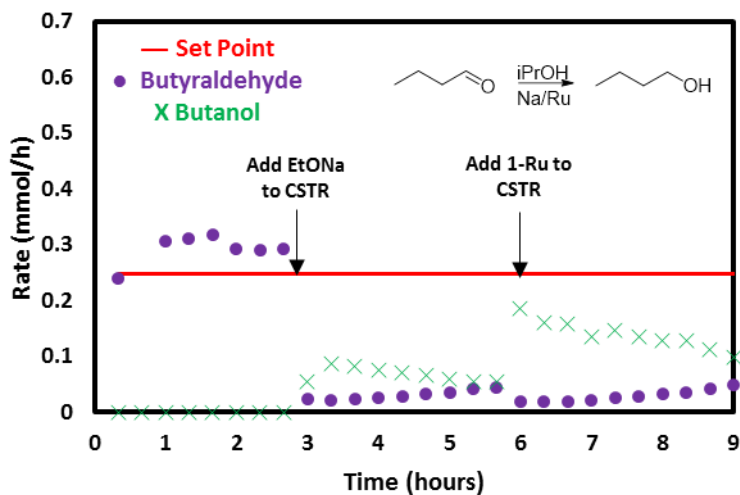


Figure A14. Butyraldehyde Hydrogenation.

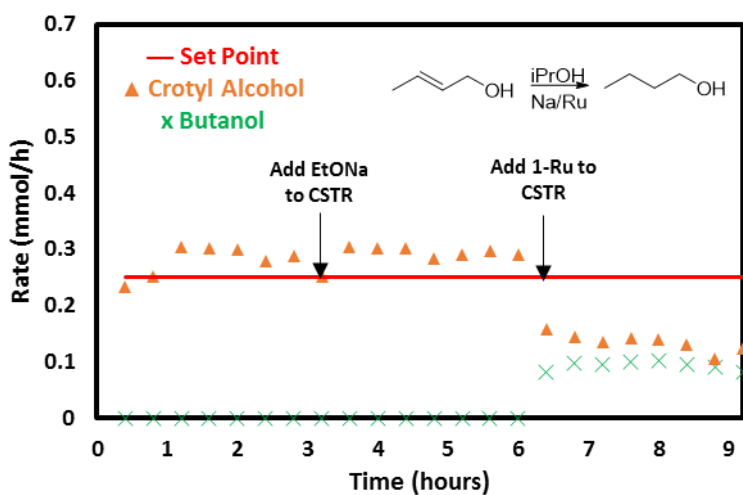


Figure A15. Crotyl Alcohol Hydrogenation.

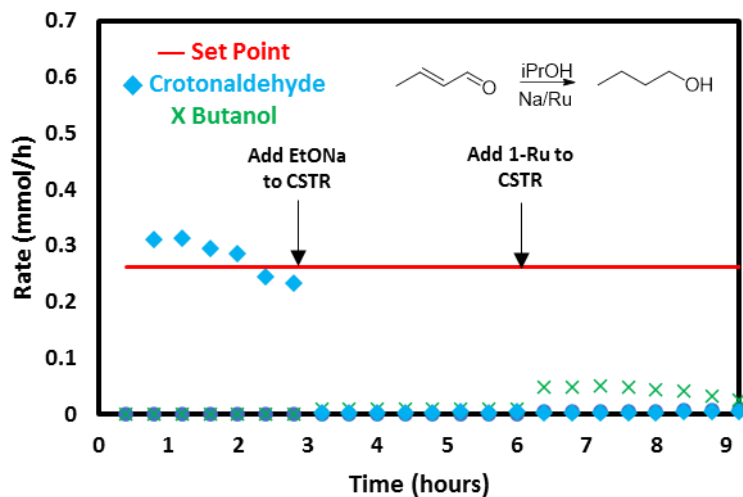


Figure A16. Crotonaldehyde Hydrogenation.

#### 11. Comparison of Acetone and Butanol Formation Rates

<sup>i</sup>PrOH (spiked with 1 mol% of unsaturated C<sub>4</sub>) and He are fed into our flow device at 20  $\mu$ L/min (l) and 100 mL/min (g), respectively. The reactor is held at 120°C and 15.5 psi. After 3 hours, a solution of PEG (4.9 mL) and EtONa (420 mM) are injected into the reactor where no acetone formation is observed. After an additional 3 hours on stream, a solution of PEG (0.45 mL) and **1-Ru** (15 mM) are injected into the reactor and mixed with the sodium ethoxide co-catalyst, whereafter the formation of acetone is detected.

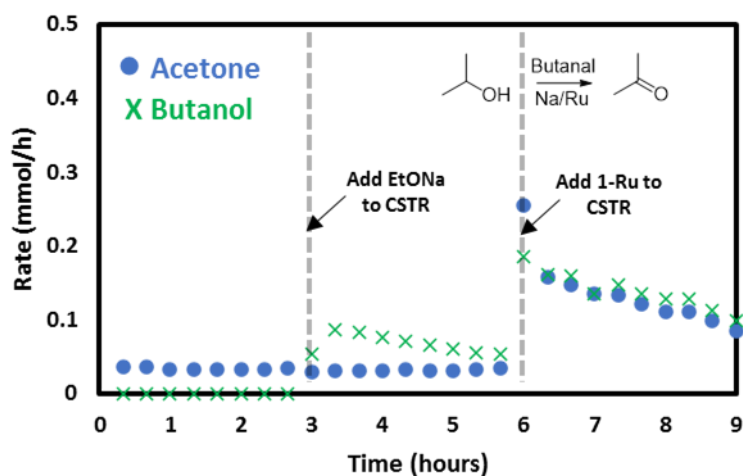


Figure A17. <sup>i</sup>PrOH and Butyraldehyde Transfer Hydrogenation.

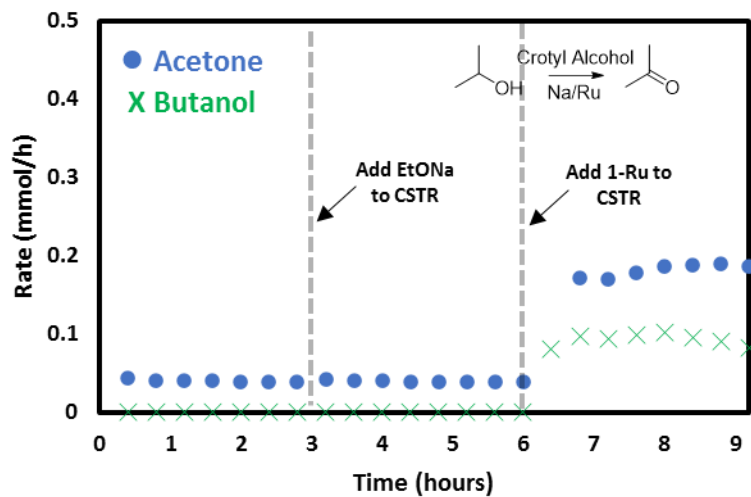


Figure A18. *i*PrOH and Crotyl Alcohol Transfer Hydrogenation.

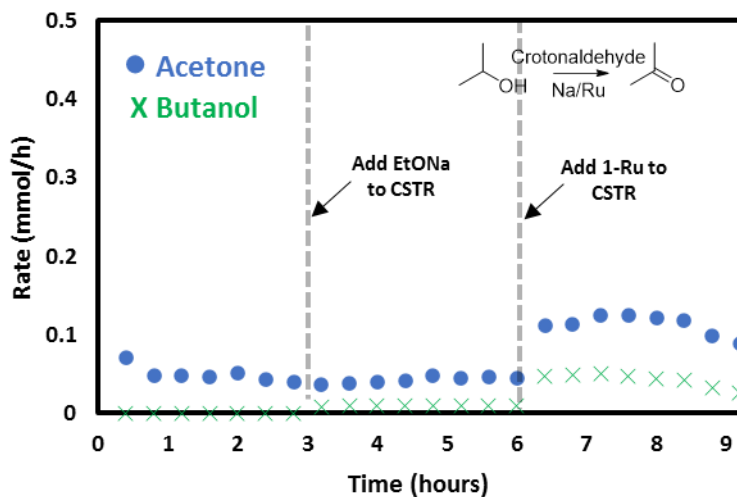


Figure A19. *i*PrOH and Crotonaldehyde Transfer Hydrogenation.

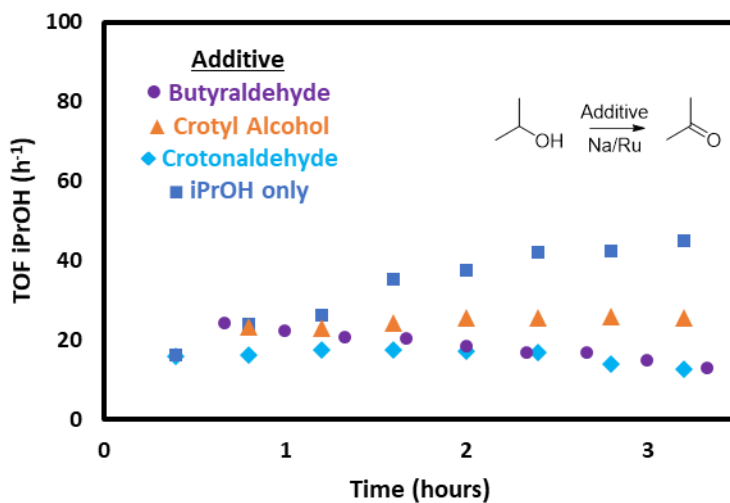


Figure A20. Acetone Formation Rates in the Presence of Various Intermediates.

## 12. Hydrogen Solubility Under Reaction Conditions

A thermodynamic simulation was developed in ChemCad using the SRK equation of state. The solubility of hydrogen gas relative to ethanol in a dimethyl ether PEG (Selexol™) was determined using a simple flash column held at 120°C and 1 atm. Inlet rates were selected to approximate the flowrates into our CSTR. The flowrate of hydrogen gas was selected assuming a maximum hydrogen formation rate which corresponds to the maximum dehydrogenation of ethanol (~10 mol%).

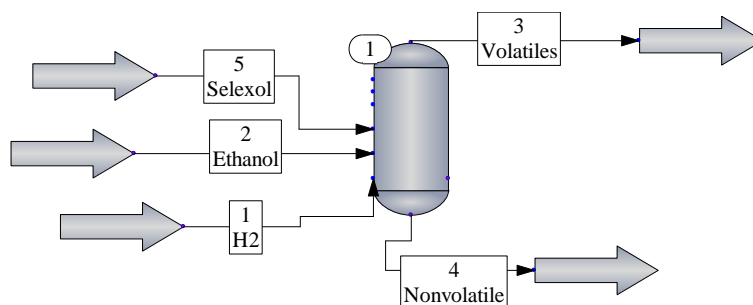


Figure A21. Schematic for Thermodynamic Model.

Table A2. Stream Table for Flash Separation of a PEG, Ethanol and Hydrogen Mixture.

Species	Inlet Flow (mol/h)	Non-volatiles (mol/h)
Selexol™	10	10
Ethanol	10	2.5
Hydrogen (gas)	1	0.001

## 13. Product Identification

Retention times for product species were identified using reagents purchased commercially. Analysis is performed using an Agilent 6850 gas chromatograph equipped with either a Restek rxi-1ms column (30m x 0.25mm x 0.5 µm film thickness) for ethanol coupling reactions or a J&W DB-WAX GC Column (30m x 0.25 mm x 0.25 µm film thickness) for hydrogen transfer reactions and an FID.

Table A3. GC species retention time for Restek rxi-1ms column. Temperature ramp starts at 50°C and ends at 135°C (15°C/min) with 7psi inlet pressure (helium carrier gas).

Commercially Purchased Product	Retention Time (min)
Acetaldehyde	2.347
Ethanol	2.411
Butanal	2.945
Ethyl acetate	2.979
Butanol	3.389
Crotyl alcohol	3.519
Crotonaldehyde	3.655
2-Ethyl Butanol	7.118
Hexanol	7.775

Table A4. GC species retention time for J&W DB-WAX GC Column. Temperature ramp starts at 50°C and ends at 150°C (15°C/min) with 15psi inlet pressure (helium carrier gas).

Commercially Purchased Product	Retention time (min)
Ethanol	3.825
Acetaldehyde	2.1

**Table A4 (cont.)**

Acetone	2.579
Isopropyl Alcohol	3.7
Acetic Acid	15.911
Butyraldehyde	3.034
Crotyl Alcohol	10.808 and 11.3
Crotonaldehyde	5.8
Butanol	9.21
Butyric Acid	18.862
n-hexane	1.9
2-Ethyl butyraldehyde	4.949
Ethyl butyrate	5.929
Butyl acetate	7.29
Hexanal	7.396
Trans-2-hexenal	10.742
2-Ethyl-butanol	12.874
Hexanol	14.027
Butyl Butyrate	10.886
2-Ethyl-Hexanol	16.589
Octanol	17.668

**14. Materials, Equipment, and Supplies Summary****Equipment:**

Kd Scientific Legato 100 syringe pump  
 Alicat mass flow controller (MCS series)  
 IKA C-MAG HS7 digital hotplate  
 Agilent gas chromatograph 6850

Restek rxi-1ms column 30m, 0.25 mmID 0.25  $\mu$ m film thickness

Column Conditions: Temperature ramp starts at 50°C and ends at 135°C (15°C/min) with 7psi inlet pressure (helium carrier gas).

J&W DB-WAX GC Column 30m, 0.25 mmID, 0.25  $\mu$ m film thickness

Column Conditions: Temperature ramp starts at 50°C and ends at 150°C (15°C/min) with 15psi inlet pressure (helium carrier gas).

Stainless steel tubing (1/4<sup>th</sup> and 1/8<sup>th</sup> inch) and compression fittings purchased from Swagelok and McMaster-Carr

NMR spectra were recorded at room temperature on a Varian spectrometer operating at 500 MHz and referenced to C<sub>6</sub>D<sub>6</sub>. IR spectra were collected at room temperature using a Bruker Alpha ATR Infrared Spectrometer.

**Chemicals:**Sigma Aldrich

acetaldehyde, butyraldehyde, crotyl alcohol, crotonaldehyde 2-ethylbutyraldehyde, 2-ethyl-hexanol, butyric acid, acetic acid, ethyl butyrate, butyl acetate, hexanal, trans-2-hexenal, octanol, PEG<sub>500</sub>, 1,4 dicyanobenzene, 2-aminopyridine, diglyme

Fischer Chemicals

Toluene, iso-propyl alcohol

Alfa Aesar

2-ethyl butanol, hexanol, octanol

Decon labs

Ethanol

TCI Chemicals

Butanol

Acros Organics

Triphenyl Phosphine

J&J Materials

Ru(III) Chloride Hydrate

#### 15. Preparation of chemicals

Solvents were commercially available and purchased from their respective vendors (see above). All chemicals and materials were stored under argon. Ethanol and toluene were dried using 2Å molecular sieves. Polyethylene glycol was sparged with argon prior to storage in a glovebox. Sodium ethoxide was prepared in-house by reacting sodium metal with an excess of dried and degassed ethanol.

#### 16. Notes and References

- (1) Fox, M. A.; Harris, J. E.; Heider, S.; Pérez-gregorio, V.; Zakrzewska, M. E.; Farmer, J. D.; Yufit, D. S.; Howard, J. A. K.; Low, P. J. A Simple Synthesis of Trans -RuCl ( C <sub>6</sub>H<sub>5</sub> )<sub>2</sub> ( Dppe )<sub>2</sub> Complexes and Representative Molecular Structures. *J. Organomet. Chem.* **2009**, 694 (15), 2350–2358.
- (2) Siegl, W. Metal Ion Activation of Nitriles . Syntheses of 1, 3-Bis ( Arylimino ) Isoindolines. *J. Org. Chem.* **1977**, 42 (11), 1872–1878.
- (3) Zhang, D. Bin; Wang, J. Y.; Wen, H. M.; Chen, Z. N. Electrochemical, Spectroscopic, and Theoretical Studies on Diethynyl Ligand Bridged Ruthenium Complexes with 1,3-Bis(2-Pyridylimino)Isoindolate. *Organometallics* **2014**, 33 (18), 4738–4746.

# **APPENDIX B: Study and Immobilization of Homogeneous Catalysts in a Packed Bed Reactor**

By Nicholas Wang

## **Table of Contents**

- 1. Reactor Setup and Equipment**
  - Figure B1.** Schematic of reactor setup for ethanol coupling reactions.
  - Figure B2.** Schematic of modified reactor setup for hydrogenation reactions.
- 2. 1-Ru Stability with Inorganic Support**
  - Figure B3.** Stability of catalyst in batch with basic alumina.
  - Figure B4.** IR studies of catalyst on alumina.
- 3. Supported Liquid Phase Catalyst: Synthesis and Heterogenization**
  - Figure B5.** Heterogenization of ruthenium complex.
  - Figure B6.** NMR analysis of immobilized 1-Ru.
- 4. Sample Calculation for Residence Time**
- 5. Rate Calculations for 1-Ru**
  - Figure B7.** Species calibration curves for 1-Ru.
- 6. GC Product Characterization**
  - Figure B8.** GC spectra for Guerbet products.
  - Table B1.** GC species retention time for Guerbet reaction.
- 7. Calculations and Data for Mass Transfer Studies**
  - Figure B9.** Integration of activity profiles.
  - Table B2.** Experimental data for PBR intraparticle studies.
  - Table B3.** Experimental data for PBR channeling studies.
  - Table B4.** Experimental data for PBR interparticle studies.
- 8. Catalyst Stability: 1-Ru w/triphenylphosphine (TPP)**
  - Figure B10.** Temperature variance.
  - Figure B11.** Acetaldehyde Co-feed (PBR).
  - Figure B12.** Catalyst stability with PPh<sub>3</sub>.
- 9. Rate Calculations for 2-Ir**
  - Figure B13.** Calibration for 1-hexene and Hexane.
- 10. Materials, Equipment, and Supplies Summary**
- 11. Preparation of chemicals**
- 12. Notes and references**



## 1. Reactor Setup and Equipment

### Packed Bed Reactor Configuration

For ethanol coupling reactions in our packed bed reactor (PBR), the SLPC was loaded into a tubular glass reactor fitted with glass frits and Teflon caps. This tubular reactor was then placed within a stainless-steel tube which was heated by a Supelco gas-purification heating jacket. A temperature control system was fashioned using a pt100 rtd in conjunction with a Supelco gas purification jacket. The rtd probe was placed around the tubing that housed the packed bed. Control experiments performed in absence of catalyst were used to correlate the outside temperature of the tubular reactor with the temperature of the catalyst bed under operating conditions. A syringe pump for the ethanol feed was purchased from KD-scientific, and a Hamilton airtight glass syringe was used to deliver the liquid feed that is vaporized upon entering a heated tee. A mass flow controller for the nitrogen carrier gas was purchased from Alicat. All the gases were delivered from pressure tanks equipped with regulators. An Agilent 6850 Gas Chromatograph was used for analysis. Pressurized tubing and fittings were purchased from McMaster-Carr and Swagelok. The entry tee and tubing throughout the reactor were wrapped in heat tape to assist with the vaporization of ethanol. Ethanol is fed through a syringe pump into the heated inlet. The vaporized feed is then swept by the carrier gas through the reaction bed and to the GC for analysis.

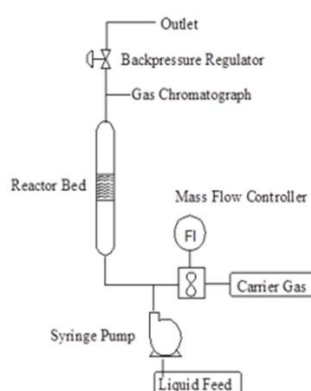


**Figure B1.** Schematic of reactor setup for ethanol coupling reactions.

For hydrogenation reactions, the flowrate of nitrogen was regulated by an Alicat flowmeter. The syringe pump for liquid delivery was removed, and a container of hexene was sparged using nitrogen which created a hexene-saturated vapor. This saturated gas is then swept over the reaction bed using a carrier gas. A second Alicat flowmeter was installed to also regulate the co-flow of hydrogen from a compressed tank. All other equipment and materials remained identical between systems.

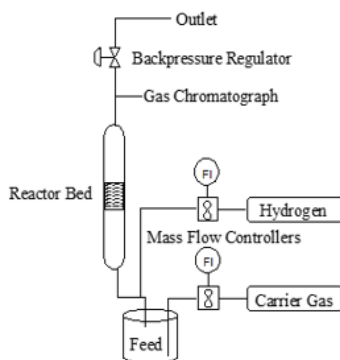


**Figure B2.** Schematic of modified reactor setup for hydrogenation reactions.

## 2. 1-Ru Stability with Inorganic Support

*1-Ru stability with SiO<sub>2</sub> support.* 6.9 mmol (318 mg) of EtOH was placed in a vessel with 3.3 mmol (200 mg of SiO<sub>2</sub>), 0.69 mmol (47 mg) of sodium ethoxide, and 3.45e<sup>-3</sup> mmol (3.5 mg) of ruthenium catalyst. The ethanol coupling reaction was carried out at 150°C for 4 hours. No catalytic activity was detected, suggesting that silica heavily inhibited the reaction.

**1-Ru stability with basic  $\text{Al}_2\text{O}_3$  support.** 17.4 mmol (800 mg) of EtOH was placed in a sealed vessel with 3.9 mmol (400 mg) of basic  $\text{Al}_2\text{O}_3$ , 0.8 mmol (60 mg) of sodium ethoxide, and  $6 \times 10^{-3}$  mmol (6 mg) of ruthenium catalyst. The reaction was carried out at  $120^\circ\text{C}$  over 10 hours. The data shows that the catalyst maintains a stable rate even after multiple hours on stream.

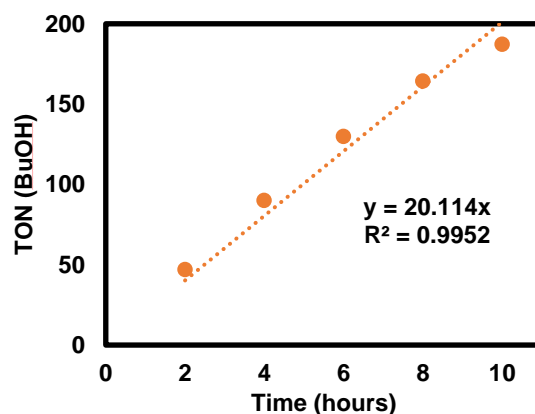


**Figure B3.** Stability of Catalyst in Batch with Basic  $\text{Al}_2\text{O}_3$ .

Infrared spectroscopy was used to show that the catalyst structure remains intact even when absorbed onto alumina ( $3 \times 10^{-3}$  mmol of **1-Ru** on 3.9 mmol of basic-alumina). Characteristic stretches were identified for the isoindoline functionality present on **1-Ru** between  $1450 - 1600 \text{ cm}^{-1}$ , and the same functional group was identified after the catalyst was deposited onto alumina. This observation suggests that the ligand structure remains intact. An additional spectrum was taken of the bis(pyridylimino)isoindoline ligand (BPI), and analysis of the ligand reveals similar features with the addition of a strong absorption in the range of  $1600-1650 \text{ cm}^{-1}$ , which is indicative of the non-deprotonated form of the ligand.<sup>1</sup> To confirm that the support would not deprotonate the ligand, an IR spectrum was taken of BPI-doped alumina. The IR spectrum showcased the same features which indicate the presence of a protonated isoindoline structure.

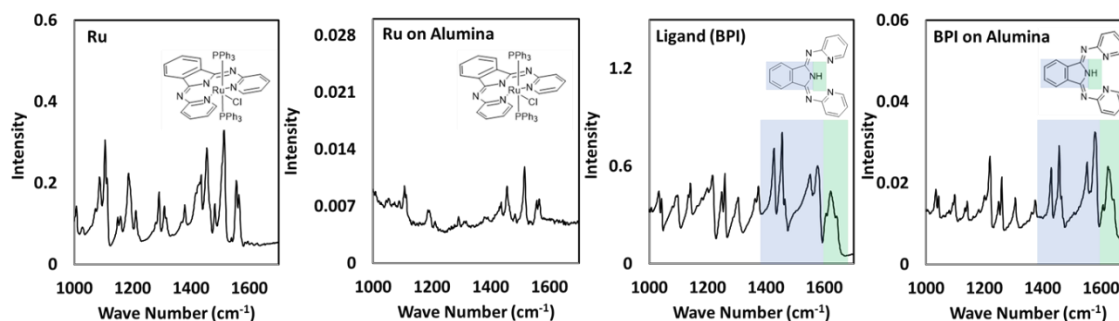


**Figure B4.** IR study of **1-Ru** and BPI on alumina.

### 3. Supported Liquid Phase Catalyst: Synthesis and Heterogenization

#### $\text{Ru}(\text{bpi})(\text{PPh}_3)_2\text{Cl}$ Synthesis:

Synthesis of the ruthenium complex was taken from literature.<sup>2-4</sup> Confirmation of complex synthesis was performed by  $^1\text{H}$ NMR and  $^{31}\text{P}$ NMR using benzene- $\text{d}_6$  as an internal standard.

#### $[\text{Ir}(\text{C}_8\text{H}_{12})\{\text{PC}_6\text{H}_{11}\}_3](\text{C}_5\text{H}_5\text{N})[\text{PF}_6]$ (Crabtree's) synthesis:

Synthesis of Crabtree's catalyst was taken from literature.<sup>5</sup> Confirmation of complex synthesis was performed by  $^1\text{H}$ NMR.

#### Heterogenization procedure:

For a single batch of SLPC, basic alumina oxide ( $\text{Al}_2\text{O}_3$ ) is first dried in a heated oven ( $150^\circ\text{C}$ ). Afterwards 7.85 mmol (800 mg) of  $\text{Al}_2\text{O}_3$  is taken and stirred with 1.03 mmol (70 mg) of sodium ethoxide in an ethanol solution for 1 hour. This material is dried, using schlenk techniques, overnight to remove any trapped ethanol. Next the heterogenized material is mixed with 70 mg of PEG and a desired quantity ( $3 \times 10^{-7} - 7 \times 10^{-7}$  mmol) of the Ruthenium catalyst within a solution of diethyl ether for 1 hour. The quantity of

PEG was determined to fill no more than 30% of the alumina pore volume. This solution containing our heterogenized material is then dried using schlenk techniques for four hours, affording our final immobilized material. The composition of the supported catalyst used in the PBR is described using weight percent (wt%), and this is calculated by dividing the component mass by the total mass of the heterogenized catalyst.

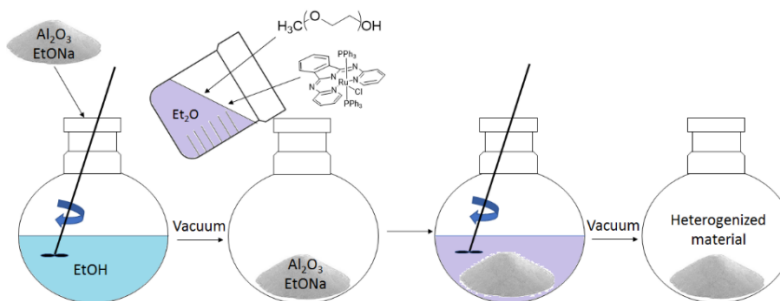


Figure B5. Heterogenization Process.

The stability of the ruthenium catalyst during the immobilization was illustrated by the following leaching experiment. 1.5 mL of benzene- $d_6$  was added to some SLPC and a  $^{31}\text{P}$  NMR was taken. The phosphorous signal of the leached catalyst remained unchanged. Some free  $\text{PPh}_3$  was detected in this experiment. This  $\text{PPh}_3$  release is likely the result of the reaction between **1-Ru** and the sodium ethoxide co-catalyst as previously proposed in the literature.<sup>6</sup>

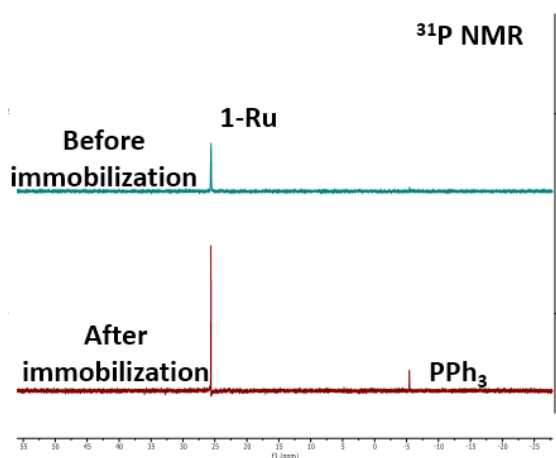


Figure B6.  $^{31}\text{P}$  NMR of 1-SLPC for **1-Ru**.

#### 4. Sample Calculation for Residence Time

Residence times were calculated by dividing the total reaction volume by the total volumetric flowrate. For the PBR setup, the reactor volume was calculated using the volume of supported material. These residence times are only an approximation, since the calculation of the exact residence time would require knowledge of the ethanol quantity dissolved within the polymer.

##### Relevant Parameters

$$n_{\text{Ru}} = \text{moles of catalyst (mmol)}$$

$$\dot{n}_{\text{EtOH}} = \text{molar flowrate of ethanol} \left( \frac{\text{mmol}}{\text{h}} \right)$$

$$\dot{n}_{\text{Tol}} = \text{molar flowrate of ethanol} \left( \frac{\text{mmol}}{\text{h}} \right)$$

$x_{Tol}$  = mole fraction of toluene

$\dot{v}_{EtOH}(l)$  = liquid volumetric rate of ethanol  $\left(\frac{mL}{min}\right)$

$\dot{v}_{EtOH}(g)$  = gaseous volumetric rate of ethanol  $\left(\frac{mL}{min}\right)$

$\dot{v}_{N_2}(g)$  = gaseous volumetric rate of nitrogen  $\left(\frac{mL}{min}\right)$

$\rho_{EtOH}$  = density of ethanol  $\left(\frac{g}{mL}\right)$

$\rho_{Al}$  = density of alumina  $\left(\frac{g}{mL}\right)$

$MW_{EtOH}$  = molecular weight of ethanol  $\left(\frac{g}{mol}\right)$

$M_{Al}$  = mass of alumina (g)

$R$  = ideal gas constant  $\left(\frac{L \text{ atm}}{mol \text{ K}}\right)$

$T$  = temperature (K)

$V$  = reaction volume (mL)

$\tau$  = residence time (s)

Convert liquid volumetric rate of ethanol to a molar flowrate of ethanol:

$$\dot{n}_{EtOH} = \dot{v}_{EtOH}(l) * \rho_{EtOH} * \frac{1}{MW_{EtOH}}$$

Convert the molar rate of ethanol to a gaseous volumetric flowrate:

Note, temperature and pressure are taken from reaction operating conditions.

$$\dot{v}_{EtOH}(g) = \dot{n}_{EtOH} * MW_{EtOH} * \frac{1}{\rho_{EtOH,gas@120^\circ C}}$$

Calculate residence time:

PBR: Reactor volume is calculated using the bed height and diameter of the reaction bed, measured using precision calipers. This measurement is performed for every change in catalyst loading.

Ex. for a sample with a 100 mg loading of supported catalyst

$$V(PFR \text{ bed}) = \frac{\pi d^2 h}{4} = \frac{3.14 * 0.007^2 * 0.003}{4} m^3 \sim 0.115 \text{ mL}$$

Nitrogen flowrate is set by mass flow controller. Ethanol flowrate was calculated above.

$$\tau = \frac{V}{\dot{v}_{EtOH}(g) + \dot{v}_{N_2}(g)} = \frac{0.115 \frac{mL}{min}}{2.2 + 8.5 \frac{mL}{min}} \sim 0.64 \text{ s}$$

## 5. Example Rate Calculations

Toluene was used as an internal standard (1 mol% in the ethanol feed) to precisely quantify the rate of product formation during catalysis. The rate of formation was then normalized by the catalyst quantity to calculate the turnover frequencies.

Example calculation for ethanol coupling rate calculations using 1-Ru:

Convert volumetric liquid injection flowrates of ethanol (substrate) and toluene (1 mol%) feed to molar flowrates.

$$\dot{n}_{EtOH} = \dot{v}_{EtOH}(l) * \rho_{EtOH} * \frac{1}{MW_{EtOH}}$$

$$\dot{n}_{Tol} = x_{Tol} * \dot{n}_{EtOH}$$

Calibration curve: mixtures of ethanol butanol and toluene are measured in known quantities and run through the gas chromatograph to produce intensities (areas). Response factors were generated using the method of internal standards. Similar calibration curves were created for other species (not shown).

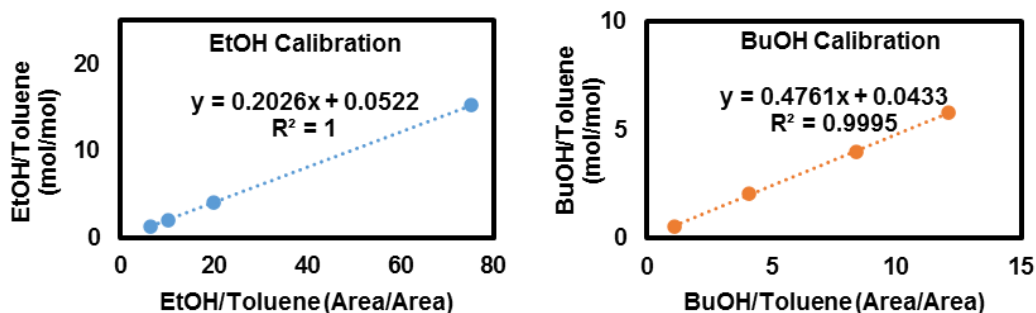


Figure B7. Species calibration curves.

Use response factor from calibration curves with areas obtained from the gas chromatograph during catalysis to calculate the rate of product formation based upon the molar flowrate of toluene. Finally, normalize by catalyst loading to get turnover rate.

$$\dot{n}_{BuOH} = \frac{Area\ BuOH}{Area\ Toluene} * \dot{n}_{Tol} * \frac{1}{Response\ Factor}$$

$$TOF = \frac{\dot{n}_{BuOH}}{n_{Ru}}$$

## 6. GC Spectra and Product Identification

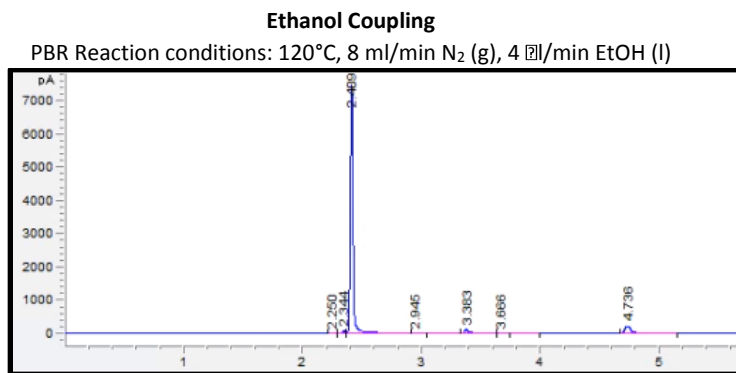


Figure B8. Sample GC spectra for Guerbet products produced in flow systems (PBR data shown above).

For ethanol coupling, retention times for product species were identified using reagents purchased commercially. Analysis is performed using an Agilent 6850 gas chromatograph equipped with a Supelco FUSED SILICA capillary column (30m x 0.25mm x 0.5 μm film thickness) and an FID. Temperature ramp starts at 50°C and ends at 135°C (15°C/min) with 7psi inlet pressure (helium carrier gas).

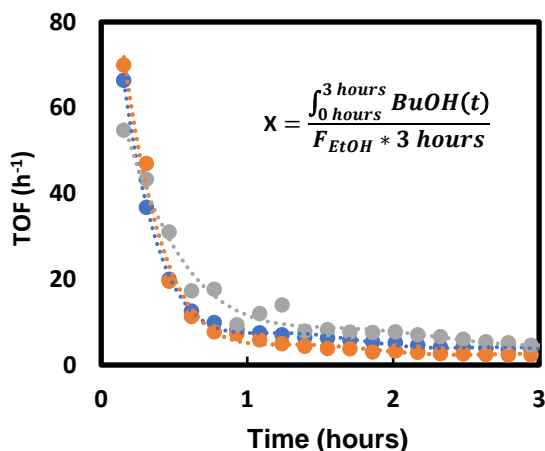
For 1-hexene hydrogenation, retention times for 1-hexene and n-hexane were identified using reagents purchased from Sigma Aldrich (purity > 97%). Analysis is performed using an Agilent 6850 gas chromatograph equipped with a Supelco FUSED SILICA capillary column (100m x 0.25mm x 0.5 μm film thickness) and an FID. Temperature in the column remains at 85°C with 45 psi inlet pressure (helium carrier gas). Some hexane isomers were identified (feed impurity).

**Table B1.** GC species retention time for Guerbet reaction.

For ethanol coupling reactions	
Component	Retention time – 30m Supelco Column
Acetaldehyde	2.347
Ethanol	2.411
Butanal	2.945
Ethyl acetate	2.979
Butanol	3.389
Crotyl alcohol	3.519
Crotonaldehyde	3.655
2-Ethyl Butanol	7.118
Hexanol	7.775
For hydrogenation reactions	
Component	Retention time – 100m Supelco Column
1-hexene	9.968
n-hexane	10.126
hexane isomer	10.175

## 7. Calculations and Data for Mass Transfer Studies

Conversion was calculated by integrating (trapezoidal rule) over the total amount of butanol formed by the catalyst and dividing by the total ethanol flow over a 3-hour reaction period. Turnovers are converted to moles of butanol using toluene as an internal standard.

**Figure B9.** Integration of activity profiles.

**For intraparticle studies:** Three different batches of SLPC with varying ruthenium loadings were loaded into a packed bed reactor at 120°C with an ethanol flow rate of 4 mL/min (l) and a nitrogen flowrate of 8 ml/min (g). Activity was monitored using an in-line gas chromatograph.

**Table B2.** Experimental data for intraparticle studies.

Al <sub>2</sub> O <sub>3</sub> (mmol)	EtONa (mmol)	PEG <sub>500</sub> (mmol)	Ru (e <sup>-3</sup> mmol)	Conversion (%)
1.67	0.22	0.03	0.68	0.18
1.67	0.22	0.03	0.5	0.11
1.67	0.22	0.03	0.37	0.08
0	0	0	0	0

**Channeling Studies:** One batch of SLPC with constant ruthenium content was synthesized. Afterwards three different experiments where the total quantity of catalyst material was varied (100, 200 and 300 mg) was performed. The catalyst was

loaded into a packed bed flow reactor at 120°C with an ethanol flow rate of 4 mL/min (l) and a nitrogen flowrate of 8 ml/min (g). Activity was monitored using an in-line gas chromatograph.

**Table B3.** Experimental data for channeling studies.

Al <sub>2</sub> O <sub>3</sub> (mmol)	EtONa (mmol)	PEG (mmol)	Ru (e <sup>-3</sup> mmol)	Conversion (%)
255	0.32	0.044	1.02	0.32
170	0.22	0.03	0.68	0.19
87.5	0.1	0.014	0.34	0.09
0	0	0	0	0

**For interparticle studies:** Two different batches of SLPC were synthesized and loaded into a packed bed flow reactor at 120°C. Flowrates were varied for each experiment while maintaining a constant ethanol partial pressure (constant flow ratio of ethanol to nitrogen). The volumetric flow of ethanol is calculated using the ideal gas law to obtain the total volumetric flow (nitrogen + ethanol). Residence times are calculated by dividing the total bed volume by the gas-phase volumetric flow for a reactor cell with an inner diameter of 0.007 meters (see calculations above).

**Table B4.** Experimental data for interparticle studies.

\*\*The catalyst material used below is 7.4wt% polymer and base. The remaining mass is alumina.

N <sub>2</sub> (g) (ml/min)	EtOH (g) (ml/min)	Bed Volume (ml)	Residence time (s)	SLPC (mg)	[Ru] (mmol)	Conversion (%)	TON
0	0	0	0	0	0	0	0
8	2.2	0.225	1.34	300	1.90e <sup>-3</sup>	0.82	17.7
10	2.75	0.225	1.06	300	1.90e <sup>-3</sup>	0.61	16
12	3.3	0.225	0.88	300	1.90e <sup>-3</sup>	0.48	17.8
8	2.2	0.15	0.88	200	7.60e <sup>-4</sup>	0.22	21.3
10	2.75	0.15	0.71	200	7.60e <sup>-4</sup>	0.15	20.4
12	3.3	0.15	0.59	200	7.60e <sup>-4</sup>	0.11	16.7

## 8. 1-Ru Stabilization Studies

### Temperature Variance:

EtOH and N<sub>2</sub> are fed into the reactor at 4 mL/min (l) and 8 mL/min (g) respectively at 120° and a pressure of 16 psi (P<sub>EtOH</sub> = 1.4 psi). The vaporized feed is flown over 200 mg of SLPC (7wt% base, 7wt% PEG, and 0.63wt% 1-Ru). The turnover frequencies denote the rate of butanol formation over time.

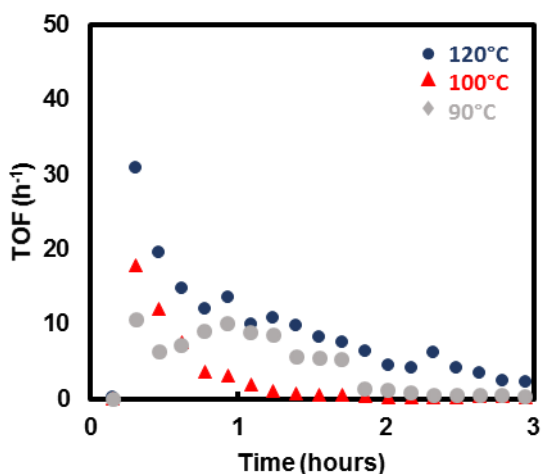


**Figure B10.** Butanol formation rate vs time under varying temperatures.

#### Acetaldehyde Co-feed (PBR):

For this experiment, 100 mg of SLPC (7wt% base, 7wt% PEG, and 0.68wt% **1-Ru**) was used, and an acetaldehyde-ethanol mixture (15 mol% acetaldehyde) and nitrogen were fed into our reactor at 4 mL/min (l) and 8 mL/min (g) respectively. The reactor was held at a temperature of 120°C and a pressure of 16 psi. **Figure B11**, below, depicts the formation of the various product species observed during catalysis. In addition to butanol, significant formation of butanal and crotonaldehyde were observed.

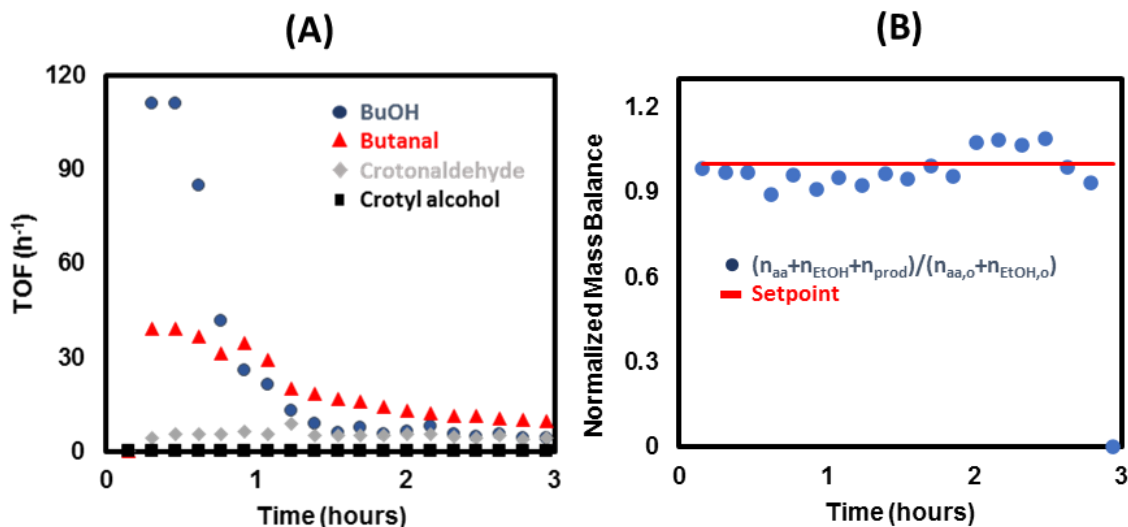


**Figure B11.** Product formation rate vs time when using an acetaldehyde co-feed. (A) showcases the rate profile. (B) showcases the mass balance. The blue circles show the summation of all products and unreacted reagent species normalized by the initial feed rate. The red line depicts unity (mass balance closure).

#### Batch Experiments:

**1-Ru** and sodium ethoxide (0.016M and 0.4M respectively) were added to a solution of dilute ethanol in PEG (9.1wt% ethanol). Two different batches of this reaction mixture were then loaded with varying triphenylphosphine concentrations (0.028 and 0.25M). Aliquots were taken to monitor reaction progress over time. Analysis is performed by gas chromatography. Further evidence was collected in batch experiments which also suggest an inverse relationship between triphenylphosphine and butanol formation. **1-Ru** and sodium ethoxide (0.016M and 0.4M respectively) were added to a solution of dilute ethanol in PEG (9.1wt% ethanol). Two different batches of this reaction mixture were then loaded with varying triphenylphosphine quantities (0.028 and 0.25M). The two mixtures were sealed and heated to 120°C. Aliquots were taken and analyzed through gas chromatography to monitor the activity over time. In the absence of triphenylphosphine, the reaction proceeds at a stable rate of 4.7 TOF ( $\text{h}^{-1}$ ) over 10 hours. Under low concentrations of triphenyl phosphine (0.028M), a similar rate of butanol formation is observed, 6.2 TOF ( $\text{h}^{-1}$ ). However, upon increasing the concentration of triphenylphosphine to match the conditions in our flow system (0.25M), minimal butanol formation was detected over 10 hours of reaction time. This observation suggests that there is an inverse relationship between butanol formation and triphenylphosphine concentration under our flow reactor conditions. Nevertheless, with the addition of excess ligand we successfully observed increased stability. As depicted by the data below, at low concentrations of triphenylphosphine we observe a minimal effect on the activity of the catalyst; however, as the ligand concentration increases, we see a significant decrease in the rate of butanol formation.



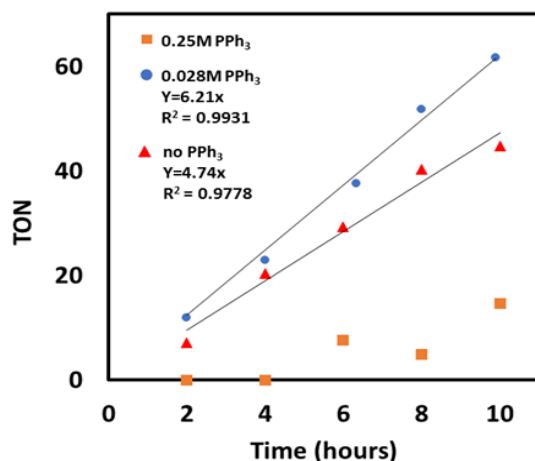


Figure B12. Catalyst stability w/PPh<sub>3</sub>.

### 9. Rate Calculations for 2-Ir

Composition of SLPC: 800 mg AlO<sub>3</sub>, 80 mg PEG, and 6 mg Ir-Cat

Using the method of internal standards (IS), the response factor for 1-hexene and n-hexane were determined (methanol as the IS). Since the response factors for 1-hexene and n-hexane via gas chromatography were nearly identical, activity and conversions are calculated based upon the ratio of the relative areas for each chromatography peak.

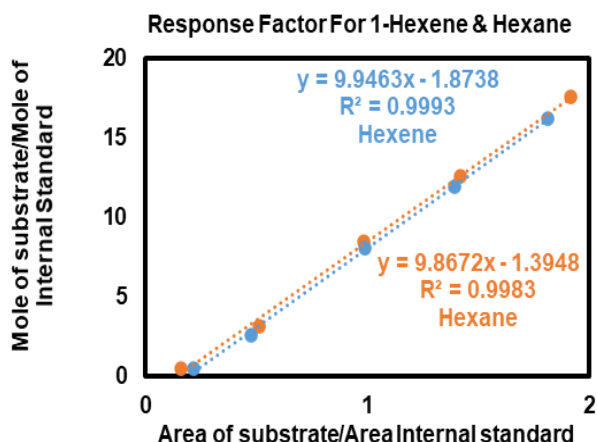


Figure B13. Calibration for 1-hexene and Hexane.

Conversion is calculated by taking the ratios of the GC signal for hexene (A1) and hexane (A2). This conversion is then used to calculate the molar flowrate of hexane produced. This rate is normalized by the quantity of catalyst to calculate turnover rate. The flow of 1-hexene is determined experimentally by sparging a container of 1-hexene for two hours and calculating the mass change before and after.

$$\text{Conversion} = X = \frac{A_2}{A_1 + A_2}$$

$$\text{Flowrate of hexane produced} = \dot{n}_{\text{Hexane}} = X * \dot{n}_{\text{Hexene},0}$$

### 10. Materials, Equipment, and Supplies Summary

Equipment:

- Kd Scientific Legato 100 syringe pump
- Alicat mass flow controller
- Agilent gas chromatograph 6850
- Restek rxi-1ms column 30m, 0.25 mmID 0.25 μm film thickness

Column Conditions: Temperature ramp starts at 50°C and ends at 135°C (15°C/min) with 7psi inlet pressure (helium carrier gas).

Stainless steel tubing (1/4<sup>th</sup> and 1/9<sup>th</sup> inch) and compression fittings purchased from Swagelok  
NMR spectra were recorded at room temperature on a Varian spectrometer operating at 500 MHz and referenced to C<sub>6</sub>D<sub>6</sub>. IR spectra were collected at room temperature using a Bruker Alpha ATR Infrared Spectrometer.

#### Chemicals:

Toluene – Fischer Chemicals  
Ethanol – Decon Labs  
Butanol – TCI Chemicals  
Acetaldehyde – Sigma Aldrich  
Crotonaldehyde – Sigma Aldrich  
Butanal – Sigma Aldrich  
Crotyl alcohol – Sigma Aldrich  
Diethyl Ether – Sigma Aldrich  
1,4 Dicyanobenzene – Sigma Aldrich  
2-aminopyridine – Sigma Aldrich  
1-hexene – Sigma Aldrich  
hexane – Sigma Aldrich  
Hydrogen - Airgas  
Nitrogen - Airgas  
Polyethylene Glycol 500 MW monomethyl ether -Sigma Aldrich  
Polyethylene Glycol 500 MW dimethyl ether – Sigma Aldrich  
Hexanol - Alfa Aesar  
2-ethyl-butanol – Alfa Aesar  
Neutral Alumina – Alfa Aesar 60 mesh  
Basic Alumina – Alfa Aesar 60 mesh  
Triphenyl Phosphine – Acros Organics  
Ru(II) Chloride Hydrate – J&J Materials

#### 11. Preparation of chemicals

Solvents were commercially available and purchased from Fischer Chemicals, Sigma Aldrich, Alfa Aesar, J&J Materials, TCI, Cambridge Isotope Labs, or Decon Labs. All chemicals and materials were also stored under argon. Ethanol and toluene were dried using 2Å molecular sieves. Solid support materials were dried in an oven held at 150°C. Polyethylene glycol was sparged with argon prior to storage. Sodium ethoxide was prepared by reacting sodium metal with an excess of dried and degassed ethanol.

#### 12. Notes and References

- 1 R. R. Gagne and D. N. Marks, *Inorg. Chem.*, 1984, **23**, 65–74.
- 2 M. A. Fox, J. E. Harris, S. Heider, V. Pérez-gregorio, M. E. Zakrzewska, J. D. Farmer, D. S. Yufit, J. A. K. Howard and P. J. Low, *J. Organomet. Chem.*, 2009, **694**, 2350–2358.
- 3 W. Siegl, *J. Org. Chem.*, 1977, **42**, 1872–1878.
- 4 D. Bin Zhang, J. Y. Wang, H. M. Wen and Z. N. Chen, *Organometallics*, 2014, **33**, 4738–4746.
- 5 R. Crabtree and S. Morehouse, *Inorg. Synth.*, 1979, **24**, 173–176.
- 6 K. N. T. Tseng, J. W. Kampf and N. K. Szymczak, *ACS Catal.*, 2015, **5**, 5468–5485.

# Appendix C: Tandem Homogeneous Flow Catalysis for Selective Polyethylene Depolymerization

By Nicholas Wang

## Table of Contents

1. **Flow Reactor Build and Setup**
  - Figure C1.** Tabulated response GC factors used for quantitative analysis.
  - Table C1.** Column conditions for flow experiments.
  - Table C2.** Column conditions for batch experiments.
2. **Synthetic Procedures and Calculations**
  - Figure C2.**  $^1\text{H}$  NMR analysis of polyethylene.
3. **bis-CAAC-Ru (Ultracat) and  $\text{Ru}[\text{PPh}_3]_3[\text{CO}][\text{Cl}]\text{H}$  (2-Ru) in batch**
  - Figure C3.** Reaction conversion profile for homogeneous catalysts.
  - Figure C4.** Product distribution profile for homogeneous catalysts.
4. **bis-CAAC-Ru (Ultracat) and PtRe-Si**
  - Figure C5.** Product profile for a reaction of polyethylene with **Ultracat** and **PtRe-Si** under a catalyst feed rate of 0.01 mL/min.
  - Figure C6.** Product profile for a reaction of polyethylene with **Ultracat** and **PtRe-Si** under a catalyst feed rate of 0.005 mL/min.
5. **bis-CAAC-Ru (Ultracat) and  $\text{Ru}[\text{PPh}_3]_3[\text{CO}][\text{Cl}]\text{H}$  (2-Ru) in flow.**
  - Figure C7.** Product profile for a co-flow of **Ultracat** and **2-Ru** fed at 0.01 mL/min.
  - Figure C8.** Product profile for a co-flow of **Ultracat** and **2-Ru** fed at 0.01 mL/min on virgin and recycled PE.
6. **Chemicals and Equipment Summary**
7. **Notes and References**

## 1. Flow Reactor Build and Setup

### a. Reactor Build and Equipment

For tandem reactions in our stirred tank reactor setup (CSTR), the catalyst and relevant substrate were placed within a stainless-steel reactor (Parr) that was fitted with an aluminum heating jacket. The temperature of the heating jacket was controlled by a hotplate and thermocouple (IKA C-MAG HS7 digital). An Alicat flowmeter is used to deliver ethylene, and a KD Scientific syringe pump is used to delivery liquid feeds. Attached to this reactor setup, is an equilibar back pressure regulator and an Agilent 6850 gas chromatograph (GC). The GC is equipped with an FID, and a Petrocol® DH Capillary GC Column (L × I.D. 100 m × 0.25 mm, d<sub>i</sub> 0.50 μm) was used to analyze the gaseous products. Stainless steel tubing and other connectors were purchased from Swagelok and McMaster-Carr (a mixture of 1/4" and 1/8" tubing and fittings).

**Table C1.** Column conditions for flow experiments.

Oven Ramp	°C/min	Next °C	Hold min
Initial		50	8
Ramp1	15	100	1
Ramp2	15	150	15.00

**Table C2.** Column conditions for batch experiments.

Oven Ramp	°C/min	Next °C	Hold min
Initial		50	8
Ramp1	15	100	1
Ramp2	15	150	90.00
Ramp 3	15	170	30.00

### b. Species Calibration – GC Response Factors (RF)

The sample concentration is related to the GC response (A) using the method of internal standards. Liquid substrates, (C<sub>5</sub>-C<sub>10</sub> unsaturated hydrocarbons), are combined to form a stock solution (20 mL) where the concentration of each species is known. To several samples of this hydrocarbon solution (a known and measured amount), toluene is added in varying quantities (100 – 500 mg), and the resulting mixture is fed into the gas chromatograph to extrapolate column response factors, which are tabulated below. For gaseous substrates (ethylene, propylene, and butene), the calibration is performed by co-feeding vaporized toluene (0.025 mmol/min, molar flow controlled via syringe pump) with the product gasses (variable flowrates) whose flows are controlled using an Alicat MFC (Series MCS). This gaseous stream is sampled using an in-line Agilent GC equipped with a rotating valve. Response factors for this study are also tabulated below within the figure. A power law fit is used to extrapolate the sampling space to higher carbon number products.

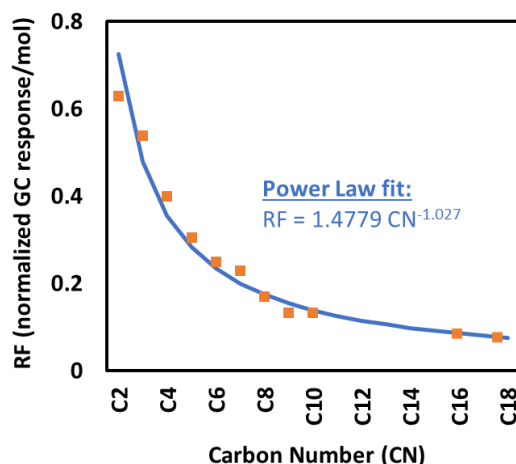


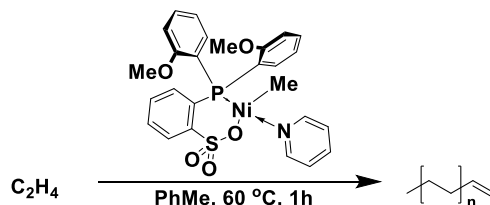
**Figure C1.** Tabulated response GC factors used for quantitative analysis.

## 2. Synthetic Procedures

\*Refer to chemicals and equipment section for materials sourcing

- Synthesis of  $\text{Ru}[\text{PPh}_3]_3[\text{CO}][\text{Cl}]\text{H}$  (2-Ru)  
The synthesis procedure was taken directly from literature.<sup>1</sup>

- Synthesis of low MW Polyethylene ( $\sim 800$  g/mol)



For the synthesis of polyethylene, a 300 ml Parr HP 5500 Compact reactor equipped with an overhead stirrer was evacuated under vacuum for 1h. This evacuation was followed by three Vacuum/Argon backfill cycles. After thoroughly degassing the reactor, 100 ml of anhydrous, anaerobic toluene, purified by a MBRAUN solvent delivery system, was transferred into it via cannula. After this the reactor was heated to 60°C Inside an Ar-filled glovebox 2.8 mg (5  $\mu\text{Mol}$ ) of  $\{\kappa 2 \text{-P,O-2-[Di(2-methoxyphenyl)phosphino]benzenesulphonato}\}$ nickel(II)-methyl pyridine were weighed into a dry 7-mL glass vial and dissolved in 1 mL of anhydrous toluene. This solution was loaded into a dry 5-mL plastic syringe and removed from the glove box. The reactor was vented under positive Ar pressure, and the catalyst was injected. The syringe was pumped several times with the reactor solvent to ensure complete catalyst transfer. The reactor was the closed and charged with a constant pressure of 35 bar of ultra-high purity ethylene. The polymerization was allowed to proceed for 60 min, after which the reactor was vented and cooled to room temperature. The reaction mixture was poured into a large excess of methanol and stirred for 30 min to precipitate the polymer. The polyethylene was collected via vacuum filtration, washed several times with methanol, and dried *in vacuo* at 43°C. Total yield: 12.2g.

Catalyst synthesis and isolation procedure was taken from the literature.<sup>2,3</sup>

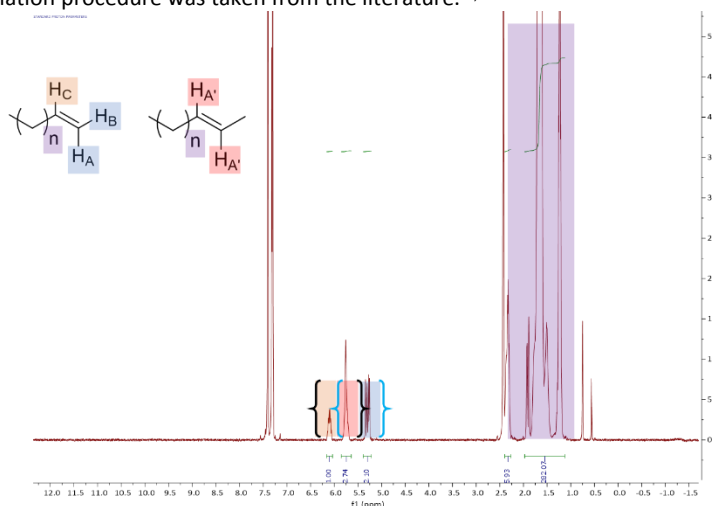


Figure C2.  $^1\text{H}$  NMR analysis of polyethylene.

- End group analysis for internal to terminal ratio and  $M_N$

The synthesized polyethylene contains one functional group per chain. Thus,  $M_N$  was calculated using two different proton pairs (blue and black brackets in **Figure C2**). First, the ratio of olefinic to vinylic PE was calculated. Afterwards, the  $-\text{CH}_2-$  protons on polyethylene were normalized by the allylic protons to determine the number of saturated to unsaturated carbons (equivalent to  $M_N$ ).

## 3. bis-CAAC-Ru (Ultracat) and $\text{Ru}[\text{PPh}_3]_3[\text{CO}][\text{Cl}]\text{H}$ (2-Ru) in batch

#### 1-decene metathesis and isomerization

Reactions were performed under an inert atmosphere of Ar under standard conditions. A round-bottom flask connected to a reflux condenser and a bubbler was charged with 24 mL 1-decene, 1.57 mM of **Ultracat**, and 3.5 mM of **2-Ru** held at 50°C. Product analysis was only performed on the condensed phase (GC) as the evaporated volatiles were not captured.

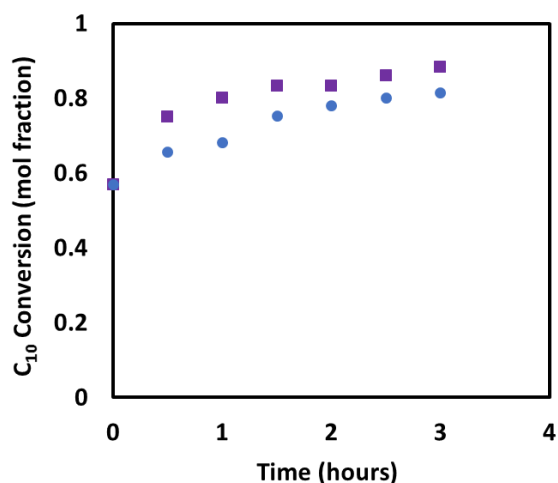


Figure C3. Reaction conversion profile for homogeneous catalysts.

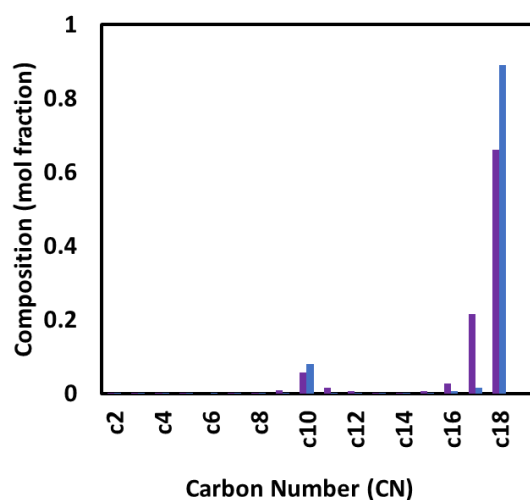
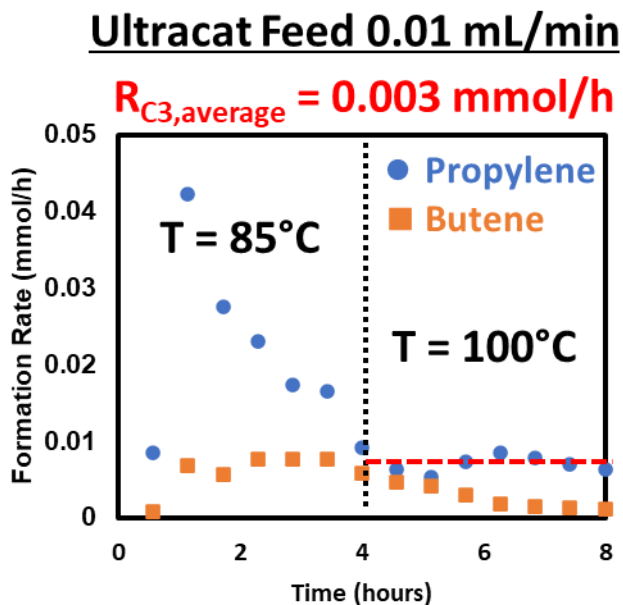


Figure C4. Product distribution profile for homogeneous catalysts.

#### 4. bis-CAAC-Ru (**Ultracat**) and PtRe-Si

A 0.01 M solution of **Ultracat** in toluene (variable flowrates) was co-fed with ethylene (15 mmol/h) into our CSTR setup held at 60 PSI. The reactor contained 150 mg of polyethylene and 100 mg of Pt(5wt%)-Re(5wt%)-SiO<sub>2</sub> (**PtRe-Si**) dehydrogenation catalyst supplied by Dow Chemical.<sup>4</sup> Metal oxide supports are known to be active for the isomerization of olefins. Thus, **PtRe-Si** was employed to simultaneously catalyze isomerization and dehydrogenation of polyethylene. In these reactions, the rate of olefin formation was shown to be invariant to that of the catalyst flow, showcasing that the reaction was not limited by the rate of metathesis.



**Figure C5.** Product profile for a reaction of polyethylene with Ultracat and PtRe-Si under a catalyst feed rate of 0.01 mL/min.

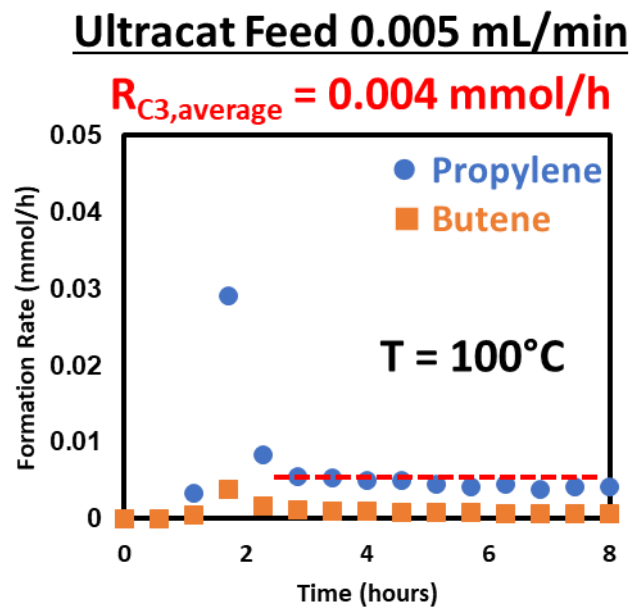


**Figure C6.** Product profile for a reaction of polyethylene with Ultracat and PtRe-Si under a catalyst feed rate of 0.005 mL/min.

##### 5. bis-CAAC-Ru (Ultracat) and Ru[PPh<sub>3</sub>]<sub>3</sub>[CO][Cl]H (2-Ru) in flow.

A solution of **Ultracat** (0.01 M) and **2-Ru** (0.004 M) in toluene (0.01 mL/min) was co-fed with ethylene (5 mmol/h) into our CSTR held at 100°C under atmospheric conditions. The reactor contained 250 mg of polyethylene.

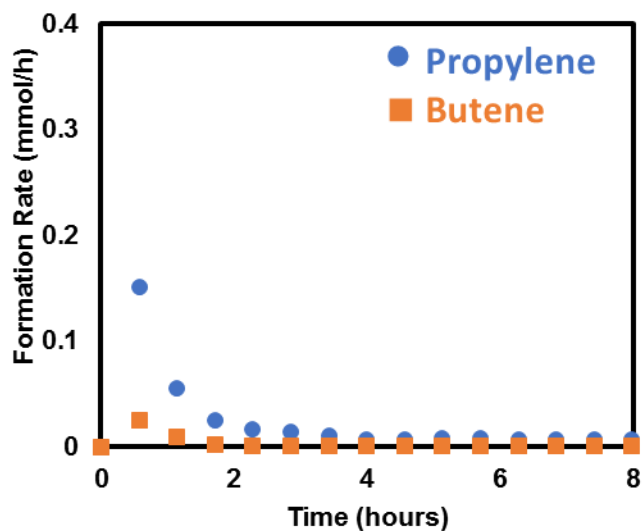


**Figure C7.** Product profile for a co-flow of Ultracat and 2-Ru fed at 0.01 mL/min.

A solution of **Ultracat** (0.01 M) and **2-Ru** (0.004 M) in toluene (0.01 mL/min) was co-fed with ethylene (5 mmol/h) into our CSTR held at 70°C under atmospheric conditions. The reactor contained 250 mg of polyethylene. After an 8-hour reaction, the CSTR was cooled, and the polymer-catalyst solution was left in the CSTR for 2-days at room temperature. Afterwards, a fresh and identical catalyst feed was installed to further react with the “recycled” polymer under otherwise identical conditions.

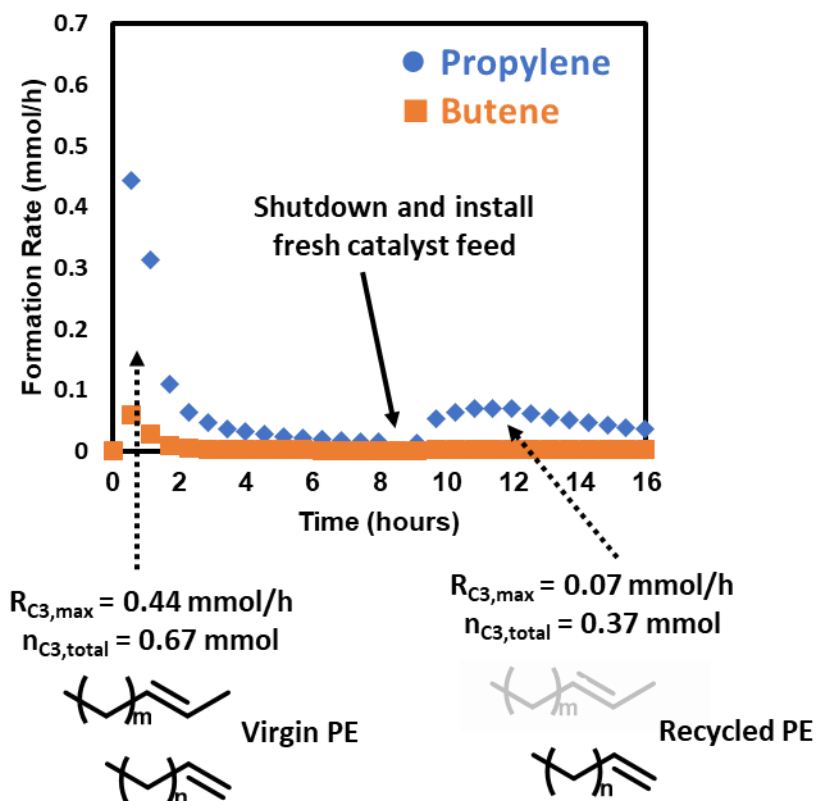


**Figure C8.** Product profile for a co-flow of Ultracat and 2-Ru fed at 0.01 mL/min on virgin and recycled PE.

## 6. Chemicals and Equipment Summary

### a. Materials, Equipment, and Supplies Summary



#### Equipment:

Alicat mass flow controller (MCS series)

Agilent gas chromatograph 6850

Petrocol® DH Capillary GC Column

Parr HP 5500 Compact Reactor

IKA C-MAG HS7 digital

Stainless steel tubing (1/4<sup>th</sup> and 1/9<sup>th</sup> inch) and compression fittings purchased from Swagelok and McMaster-Carr

NMR spectra were recorded at room temperature on a Varian spectrometer operating at 500 MHz and referenced to C<sub>6</sub>D<sub>6</sub>. IR spectra were collected at room temperature using a Bruker Alpha ATR Infrared Spectrometer.

Elemental analysis was performed using an Exeter Analytical - Model CE440 CHN Analyzer

#### Chemicals:

Sigma Aldrich

Ru(PPh<sub>3</sub>)<sub>3</sub>(CO)(Cl)H

1-decene

1-butene

2-butene

Butadiene

Benzene sulfonic acid

1-bromo-2-methoxy benzene

N,N,N',N'-Tetramethylethylenediamine

Strem

Ultracat

Cobalt molybdate on gamma alumina

[PdI(μ-Br)tBu<sub>3</sub>P]<sub>2</sub>

Airgas

Propylene

Matheson

Ethylene

Fischer Chemicals

Toluene

Alfa Aesar

Gamma alumina

#### Preparation of chemicals

Solvents were commercially available and purchased from their respective vendors (see above). All chemicals and materials were degassed and stored under argon. 1-decene was dried using 2 Å molecular sieves.

#### 7. Notes and References

- (1) Prasanna, N.; Srinivasan, S.; Rajagopal, G.; Athappan, P. R. Synthesis, Spectral and Electrochemical Studies of Ruthenium(II)/(III) Complexes of Alicyclic B-Ketamines. *Indian J. Chem.* **2001**, 40 (4), 426–429.
- (2) Guironnet, D.; Rünzi, T.; Göttker-Schnetmann, I.; Mecking, S. Control of Molecular Weight in Ni(II)-Catalyzed Polymerization via the Reaction Medium. *Chem. Commun.* **2008**, No. 40, 4965–4967.
- (3) Göttker-Schnetmann, I.; Mecking, S. A Practical Synthesis of [(Tmeda)Ni(CH<sub>3</sub>)<sub>2</sub>], Isotopically Labeled [(Tmeda)Ni(<sup>13</sup>CH<sub>3</sub>)<sub>2</sub>], and Neutral Chelated-Nickel Methyl Complexes. *Organometallics* **2020**, 39 (18), 3433–3440.
- (4) Ertem, S. P.; Onuoha, C. E.; Wang, H.; Hillmyer, M. A.; Reineke, T. M.; Lodge, T. P.; Bates, F. S. Hydrogenolysis of Linear Low-Density Polyethylene during Heterogeneous Catalytic Hydrogen-Deuterium Exchange. *Macromolecules* **2020**.

# Appendix D: Tandem Heterogeneous Catalysts for Selective Polyethylene Depolymerization

By Nicholas Wang

## Table of Contents

1. Synthetic Procedures
2. **MoOx-SiO<sub>2</sub> (Mo-Si)**
  - Figure D1.** Non-volatiles product distribution for 1-decene metathesis and isomerization at 50°C using **Mo-Si** catalyst.
  - Figure D2.** Volatile product distribution for polyethylene metathesis and isomerization using **Mo-Si** catalyst within our flow reactor configuration.
3. **MoOx-Al<sub>2</sub>O<sub>3</sub> (Mo-Al)**
  - Figure D3.** Liquid product distribution for self-metathesis reactions in the presence of Me<sub>3</sub>Al.
  - Figure D4.** Gaseous product distribution for the pressurized batch reaction of **CoMo-Al** with ethylene using n-decane as an inert solvent.
  - Figure D5.** Gaseous product distribution reported over time for tandem flow depolymerization.
4. **ReOx-Al<sub>2</sub>O<sub>3</sub> (Re-Al)**
  - Figure D6.** Olefin formation rate in the absence of polyethylene reported over time for tandem **PtRe-Si** and **Re-Al** catalysts.
  - Figure D7.** Olefin formation rate in the absence of polyethylene reported over time for tandem **1-Ir** and **Re-Al** catalysts.
5. Chemicals and Equipment Summary
6. Notes and References

## 1. Synthetic Procedures

\*Refer to chemicals and equipment section for materials sourcing

### a. Synthesis of $\text{MoO}_x\text{-SiO}_2$ (Mo-Si)

The catalyst was synthesized using a wet impregnation technique according to literature procedure.<sup>2</sup> Metal was dissolved in DI water and added to silica in a round bottom flask. The mixture was dried under air for 24 hours. The catalyst was then heated to 100 °C by submerging the flask into a stirred hot oil bath for 12 hours. Afterwards, the catalyst was evenly spread in a quartz boat and placed inside of a glass sleeve which is inserted into a furnace for calcination (1.5 °C/min up to 600 °C for 10 hours in air). The furnace is cooled to room temperature, and the glass sleeve is sealed using Swagelok caps. The catalyst is then transferred into a glovebox for storage.

### b. Synthesis of $\text{MoO}_x\text{-Al}_2\text{O}_3$ (Mo-Al)

The catalyst was synthesized using an incipient wet impregnation technique according to literature procedure.<sup>3</sup> In a round bottom flask, DI water is used to dissolve ammonium molybdate, and the solution is mixed with gamma alumina. Next, the mixture is dried overnight while open to air. The catalyst is then heated to 100 °C by submerging the flask into a stirred hot oil bath for 12 hours. Afterwards, the catalyst was evenly spread in a quartz boat and placed inside of a glass sleeve which is inserted into a furnace for calcination (1.5 °C/min up to 600 °C for 10 hours in air). The furnace is cooled to room temperature, and the glass sleeve is sealed using Swagelok caps. The catalyst is then transferred into a glovebox for storage.

### c. Synthesis of $\text{ReO}_x\text{-Al}_2\text{O}_3$ (Re-Al) and $[(^t\text{BuPOCOP})\text{Ir}(\text{C}_2\text{H}_4)]$ (1-Ir) deposition procedure

The catalyst was synthesized using a wet impregnation technique according to literature procedure.<sup>4</sup> Gamma alumina was placed into a round-bottom flask with a stir bar and dried at 110 °C for 24 hours using a hot oil bath. Ammonium perrhenate was mixed in 5 mL of DI water then added to the dried support at room temperature. The catalyst was stirred in the round bottom flask heated to 80 °C, overnight. Afterwards, the catalyst was evenly spread in a quartz boat and placed inside of a glass sleeve which is inserted into a furnace for calcination (5 °C/min up to 650 °C for 8 hours in air). The furnace is gradually cooled to room temperature while flowing helium over the calcined catalyst. The ends of the glass sleeve were then sealed with Swagelok caps, and the material was transferred into a glovebox for storage.

The synthesis of **1-Ir** was performed according to literature procedure.<sup>5</sup> The desired quantity of **1-Ir** was adsorbed onto **Re-Al** using pentane as the solvent. After adsorption of **1-Ir**, the solid catalyst appeared a reddish-brown in color. The catalyst was dried under vacuum overnight.

## 2. $\text{MoO}_x\text{-SiO}_2$ (Mo-Si)

### a. 1-decene metathesis and isomerization

Reactions were performed under an inert atmosphere of Ar under standard conditions. A round-bottom flask connected to a reflux condenser and a bubbler was charged with 0.075 mL 1-decene and 660 mg of **Mo-Si**. Afterwards, the vessel was heated to 120°C for 6 hours. Product analysis was only performed on the condensed phase (GC) as the evaporated volatiles were not captured.

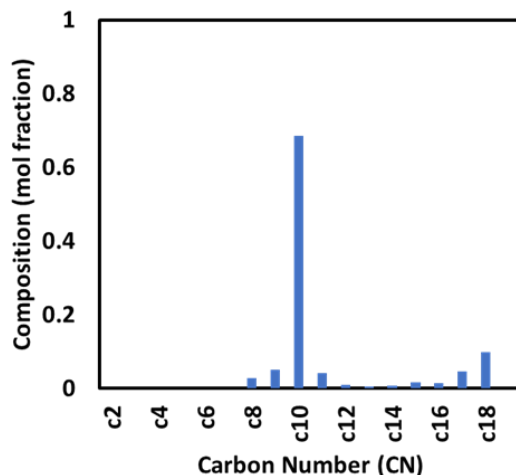


**Figure D1.** Non-volatiles product distribution for 1-decene metathesis and isomerization at 50°C using Mo-Si catalyst.

b. Polymer-Ethylene Flow Reactions

The flow reactor was loaded with 500 mg of **Mo-Si** and 2500 mg of polyethylene (MW ~ 870 g/mol) which was held at variable pressure (80-100 PSI) and temperatures (150°C-170°C) to screen reaction conditions (see below). The total allotted reaction time was 50 hours. In a second reaction under otherwise identical conditions, 150 mg of Pt(5wt%)-Re(5wt%)-SiO<sub>2</sub> (**PtRe-Si**) dehydrogenation catalyst was added, and the results of the two experiments were analyzed. Data below is truncated after 8 hours of reaction time as no significant deviations to catalyst rate were detected upon varying temperature or pressure.

Condition screening in flow reactor:

Regime A - 80 PSI and 150°C for 6 hours

Regime B - 80 PSI and 170°C for 12 hours

Regime C - 100 psi and 120°C for 32 hours

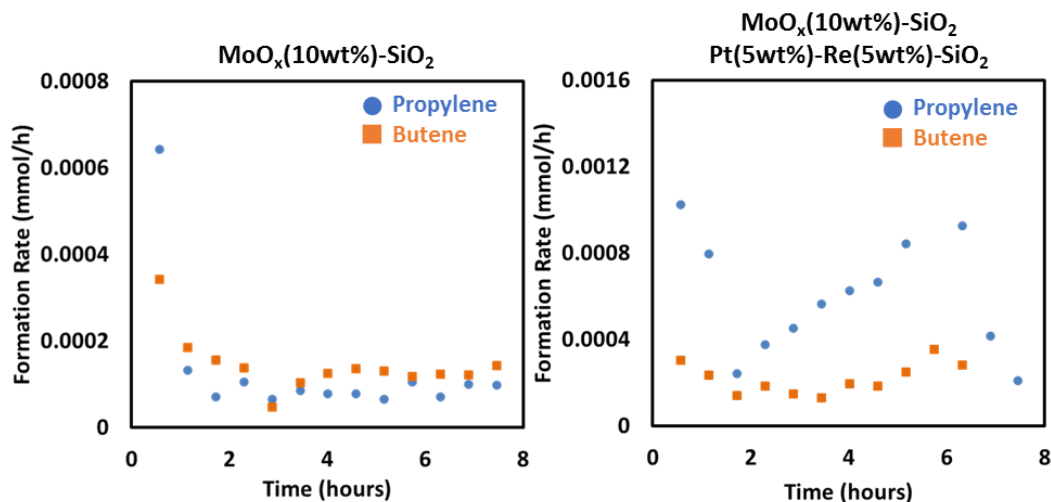


**Figure D2.** Volatile product distribution for polyethylene metathesis and isomerization using Mo-Si catalyst within our flow reactor configuration. Pictured on the left is a reaction using Mo-Si as the sole catalyst, on the right is the products distribution upon the addition of PtRe-Si.

### 3. MoO<sub>x</sub>-Al<sub>2</sub>O<sub>3</sub> (Mo-Al)

a. Optimization of Promoter (Me<sub>3</sub>Al) Loading

The desired quantity of trimethyl aluminum (2M in toluene) is added to the metathesis catalyst of interest. After 15 minutes of stirring, the excess toluene is removed under vacuum. Reactions were performed in a round bottom flask that was equipped with

a reflux condenser. The reaction system was left open to the atmosphere (bubbler), and only the condensed phase was collected for analysis (GC). For each reaction, 0.27 mL of 1-decene and 100 mg of catalyst were reacted at 150°C.

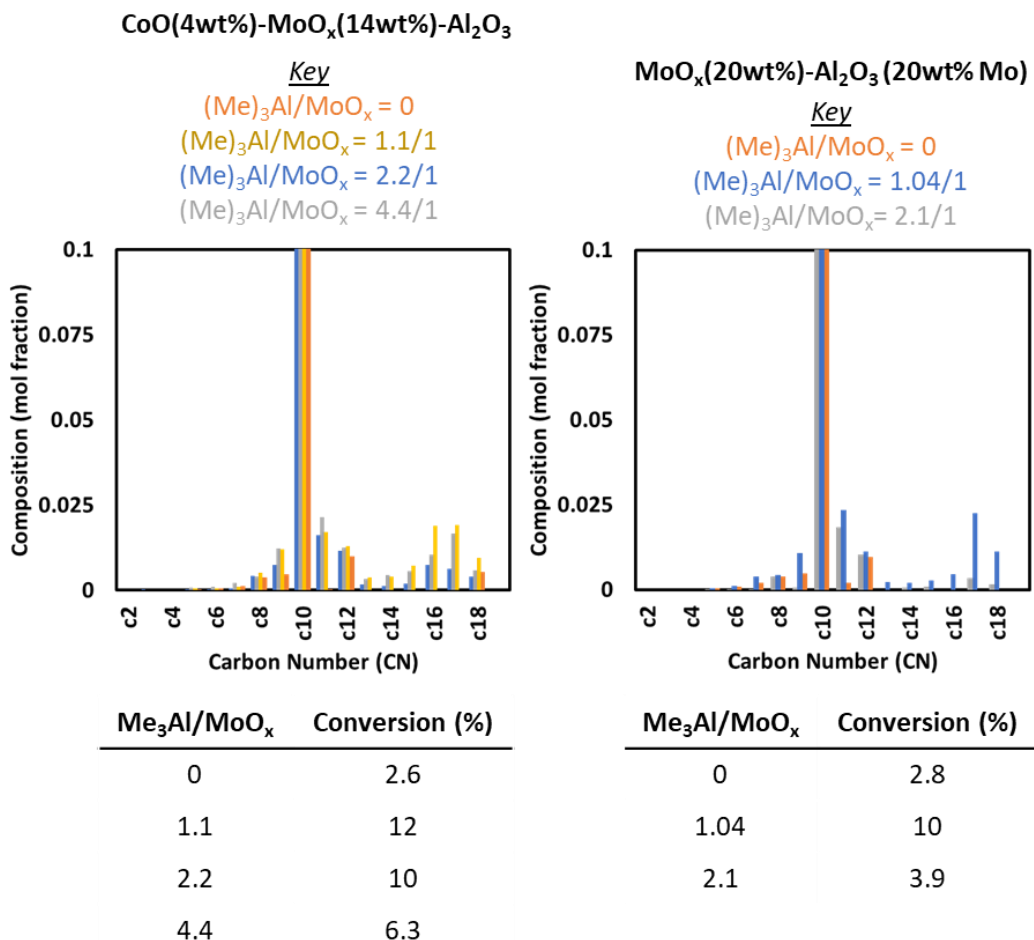


**Figure D3.** Liquid product distribution for self-metathesis reactions in the presence of Me<sub>3</sub>Al. On the left is the product distribution for 1-decene self-metathesis reactions using a commercially purchased CoO(4wt%)-MoO<sub>x</sub>(14wt%)-Al<sub>2</sub>O<sub>3</sub> (CoMo-Al) catalyst (5-hour reaction time). On the right is data from 10-hour reactions using a synthesized MoO<sub>x</sub>(20wt%)-Al<sub>2</sub>O<sub>3</sub> (Mo-Al).

**b. Dimerization Control Reaction (n-Decane)**

Using a stainless-steel batch reactor, **CoMo-Al** was tested for ethylene dimerization activity. The reactor was charged with 2.7 mL of n-decane, 1000 mg of **CoMo-Al**, the desired quantity of Me<sub>3</sub>Al, and 220 PSI of ethylene. The mixture was reacted at 200°C for 10 hours. After the reaction, the vapor phase contents were discharged into a GC sampling valve for analysis. The data below showcases short-olefin formation in the absence of alkene, suggesting that the propylene and butene formed are a result of ethylene dimerization to butene followed by ethenolysis of butene to propylene. No consumption of n-decane was detected.

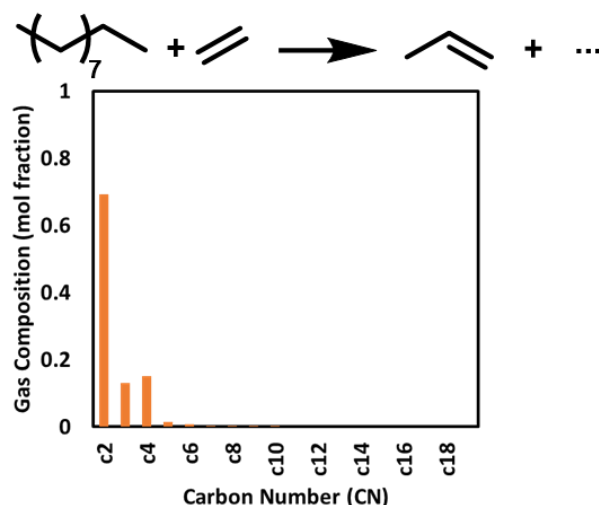


**Figure D4.** Gaseous product distribution for the pressurized batch reaction of CoMo-Al with ethylene using n-decane as an inert solvent.

#### c. Polymer-Ethylene Flow Reactions

**CoMo-Al** (500 mg), the desired quantity of  $\text{Me}_3\text{Al}$ , and polyethylene (MW  $\sim 870$  g/mol, 500 mg) were loaded into the flow reactor which was heated to  $150^\circ\text{C}$  and held at 100 PSI (5 mmol/h ethylene). Data was collected for 74 hours of reaction time. In a second reaction under otherwise identical conditions, 150 mg of Pt(5wt%)-Re(5wt%)- $\text{SiO}_2$  (**PtRe-Si**) dehydrogenation catalyst was added. All olefin formation rates were summed and averaged over the reaction time.

$\Sigma[\text{Avg}(R_{i,t})]$  –Cumulative olefin formation rates averaged over 74 hours of reaction time

$\Sigma[\text{Avg}(R_{i,t})]$  (**CoMo-Al**) = 0.0039 mmol/h

$\Sigma[\text{Avg}(R_{i,t})]$  (**CoMo-Al** + **PtRe-Si**) = 0.0183 mmol/h

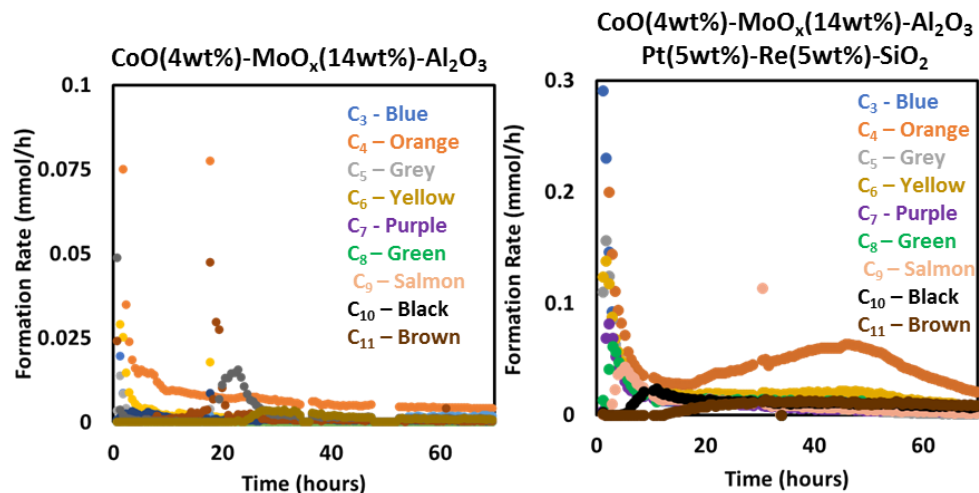


**Figure D5.** Gaseous product distribution reported over time for tandem flow depolymerization. Pictured on the left, CoMo-Al is used as the sole isomerization and metathesis catalyst. On the right CoMo-Al is used in conjunction with PtRe-Si for dehydrogenation.

#### 4. $\text{ReO}_x\text{-Al}_2\text{O}_3$ (Re-Al)

##### a. Dimerization Control Reactions

For control reactions in the absence of polyethylene, **Re-Al** (140 mg), **PtRe-Si** (150 mg), and the desired quantity of  $\text{Me}_3\text{Al}$  were loaded into the flow reactor which was heated to  $170^\circ\text{C}$  and held at 100 PSI of ethylene (flowrate 5 mmol/h). Data was collected for 10 hours of reaction time. In a second reaction under otherwise identical conditions, silicon oil (2 mL) was added to serve as

a reaction solvent. Butene formation was detected in significant quantity (ca. 0.15 mmol/h at maximum rate); however, propylene formation (0.002 mmol/h) was shown to be very low as compared to reactions in the presence of polyethylene.

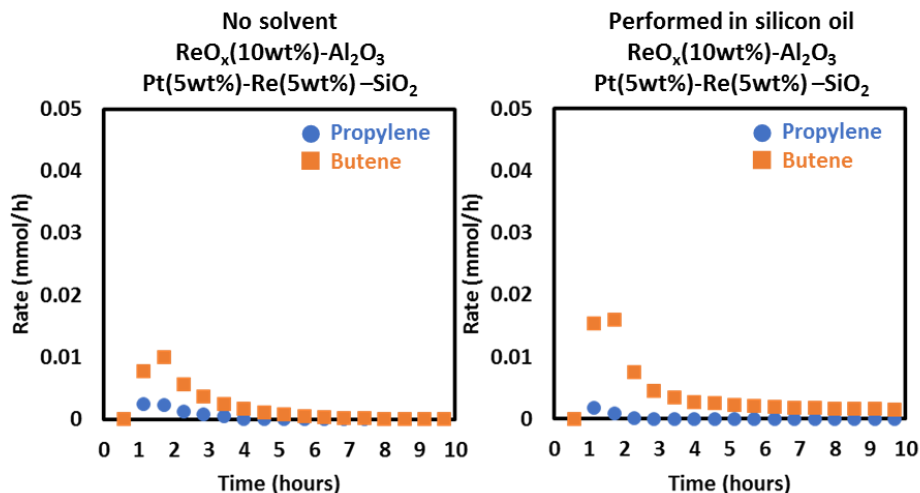


**Figure D6.** Olefin formation rate in the absence of polyethylene reported over time for tandem PtRe-Si and Re-Al catalysts. Pictured on the left, Re-Al is used for isomerization and metathesis in conjunction with PtRe-Si for dehydrogenation. On the right under otherwise identical conditions, silicon oil is added as a non-reactive solvent.

For control reactions in the absence of polyethylene, **1-Ir** (3 mg) was adsorbed onto **Re-Al** (140 mg) to create a bimetallic-supported catalyst. The resulting material was loaded into the flow reactor which was heated to 170°C and held at 100 PSI of ethylene (flowrate 5 mmol/h). Data was collected for 10 hours of reaction time. In a second reaction under otherwise identical conditions, silicon oil (2 mL) was added to serve as a reaction solvent. Butene formation was low (>0.002 mmol/h) relative to reactions with polyethylene, and no propylene formation was detected.

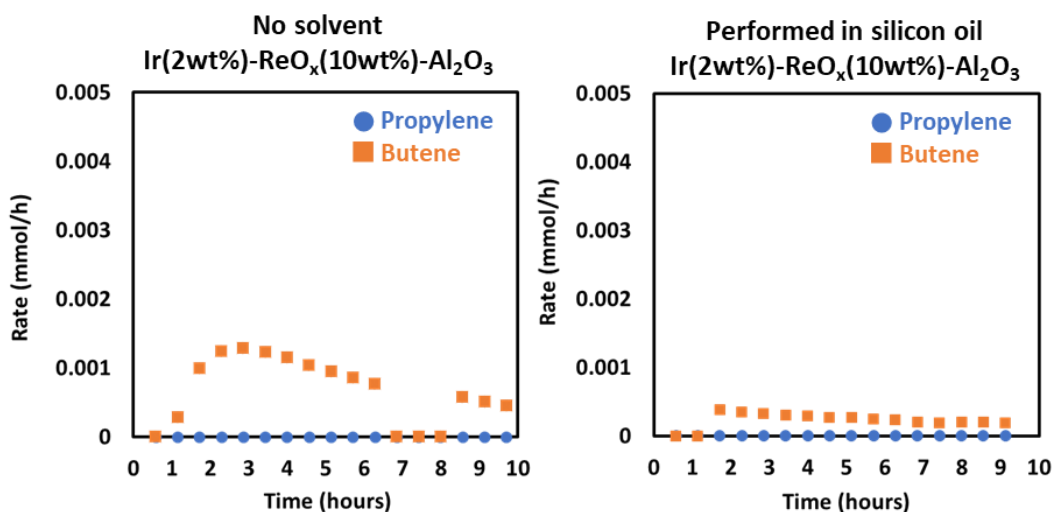


**Figure D7.** Olefin formation rate in the absence of polyethylene reported over time for tandem 1-Ir and Re-Al catalysts. Pictured on the left, a bimetallic catalyst (Re-Al and 1-Ir) is reacted directly with ethylene in the absence of polymer. On the right under otherwise identical conditions, silicon oil is added as a non-reactive solvent.

## 5. Chemicals and Equipment Summary

### b. Materials, Equipment, and Supplies Summary

Equipment:

- Alicat mass flow controller (MCS series)
- Agilent gas chromatograph 6850
- Petrocol® DH Capillary GC Column
- Parr HP 5500 Compact Reactor

IKA C-MAG HS7 digital

Stainless steel tubing (1/4<sup>th</sup> and 1/9<sup>th</sup> inch) and compression fittings purchased from Swagelok and McMaster-Carr  
NMR spectra were recorded at room temperature on a Varian spectrometer operating at 500 MHz and referenced to C<sub>6</sub>D<sub>6</sub>. IR spectra were collected at room temperature using a Bruker Alpha ATR Infrared Spectrometer.

Elemental analysis was performed using an Exeter Analytical - Model CE440 CHN Analyzer

#### Chemicals:

Sigma Aldrich

Ru(PPh<sub>3</sub>)<sub>3</sub>(CO)(Cl)H

1-decene

1-butene

2-butene

Butadiene

Trimethyl aluminum (2M in toluene)

Silica

Ammonium molybdate

Rhenium perrhenate

Benzene sulfonic acid

1-bromo-2-methoxy benzene

N,N,N',N'-Tetramethylethylenediamine

Strem

Ultracat

Cobalt molybdate on gamma alumina

Airgas

Propylene

Matheson

Ethylene

Fischer Chemicals

Toluene

Alfa Aesar

Gamma alumina

#### Preparation of chemicals

Solvents were commercially available and purchased from their respective vendors (see above). All chemicals and materials were degassed and stored under argon. 1-decene was dried using 2Å molecular sieves.

#### 6. Notes and References

- (1) Prasanna, N.; Srinivasan, S.; Rajagopal, G.; Athappan, P. R. Synthesis, Spectral and Electrochemical Studies of Ruthenium(II)/(III) Complexes of Alicyclic B-Ketamines. *Indian J. Chem.* **2001**, *40* (4), 426–429.
- (2) Andrei, R. D.; Popa, M. I.; Cammarano, C.; Hulea, V. Nickel and Molybdenum Containing Mesoporous Catalysts for Ethylene Oligomerization and Metathesis. *New J. Chem.* **2016**, *40* (5), 4146–4152.
- (3) Chakrabarti, A.; Wachs, I. E. Activation Mechanism and Surface Intermediates during Olefin Metathesis by Supported MoO<sub>x</sub>/Al<sub>2</sub>O<sub>3</sub> Catalysts. *J. Phys. Chem. C* **2019**, *123* (19), 12367–12375.
- (4) Sharkey, B. E.; Denning, A. L.; Jentoft, F. C.; Gangadhara, R.; Gopaladasu, T. V.; Nicholas, K. M. New Solid Oxo-Rhenium and Oxo-Molybdenum Catalysts for the Deoxydehydration of Glycols to Olefins. *Catal. Today* **2018**, *310* (June 2017), 86–93.
- (5) Goldman, A. S.; Roy, A. H.; Huang, Z.; Ahuja, R.; Schinski, W.; Brookhart, M. Catalytic Alkane Metathesis by Tandem Alkane Dehydrogenation-Olefin Metathesis. *Science* (80-. ). **2006**, *312* (5771), 257–261.
- (6) Guironnet, D.; Rünzi, T.; Göttker-Schnetmann, I.; Mecking, S. Control of Molecular Weight in Ni(II)-Catalyzed Polymerization via the Reaction Medium. *Chem. Commun.* **2008**, No. 40, 4965–4967.
- (7) Göttker-Schnetmann, I.; Mecking, S. A Practical Synthesis of [(Tmeda)Ni(CH<sub>3</sub>)<sub>2</sub>], Isotopically Labeled [(Tmeda)Ni(<sup>13</sup>CH<sub>3</sub>)<sub>2</sub>], and Neutral Chelated-Nickel Methyl Complexes. *Organometallics* **2020**, *39* (18), 3433–3440.